Contents

1 Introduction

In the 20th century, nanotechnologies have had a great impact on the scientific world, as the material properties in nanometer scale are quite different from the bulk material. What scientists has discovered is that at the 1-100 nm scale, every material starts to act in unimaginable ways, for instance, very large surface-to-volume ratio and quantum effect. They have permitted to develop increasingly small devices used in a wide range of areas such as materials science, electronics and biomedical sciences. Therefore, highly advanced nanomaterials have been fabricated to meet the demands of our daily life such as tiny medical device that repair clogged arteries, new filters to clean water pollution, and also biomedical applications such as biosensors.

So far, rapid detection and accurate identification of pathogen bacteria remains an extremely important issue for medicine, food quality and environmental monitoring. However, the traditional microbiology technologies are time consuming and lack the ability to detect bacteria in “real-time” or outside the laboratory environment. To meet these challenges, various biosensors have been reported for rapid detection of bacteria due to their selective, sensitive and “real-time” measurement of bacteria.

Porous silicon is a nanostructured material like a quantum sponge, containing a web like structure consisting of nanocrystallites and pores [1]. Porous silicon was first observed by Arthur Uhlir in 1956, but there were less than 200 papers published on porous silicon in the following 35 years [2]. Arguably, 1990 was a significant year for the development of porous silicon as strong visible photoluminescence of porous silicon was observed by Leigh Canham, attracting great interest to this material for sensing application.

The development of nanotechnology provides the ability to observe and construct this material. Microscopy techniques were applied to provide some of the most detailed information on the internal structure of porous silicon while nanofabrication techniques were used to construct porous silicon with various nanostructure. Now porous silicon is typically fabricated by electrochemical etching from crystalline silicon. The resulting pore morphology, such as porosity, pore size and thickness, can be controlled by adjusting the etching parameters.

In recent years, porous silicon has attracted much attention as a platform for the fabrication of biosensors due to its high surface area, easy-fabrication and convenient surface modification. Label-free porous silicon-based biosensors have been designed for detection of different targets such as DNA, protein and bacteria, by converting specific biological events into either an optical (photoluminescence, refractive spectrum) or electrochemical (current, potential, impedance) signal. However, the use of porous silicon as a biosensor

platform for detection of bacteria with the help of lysostaphin which lyse the bacteria during the measurement has not been reported.

In this work, porous silicon is used as an optical sensor for bacteria detection. The tunable pore morphology with increasing current densities is first studied by SEM and optical characterization methods, then the size of *S.epidermidis* bacteria and their lysate are measured. Porous silicon samples with appropriate pore size are chosen for biosensing experiments. When the bacteria suspension is flowing onto the sensor surface, the reflected light is scattered by the bacteria cells so the intensity of reflect spectra decreased. After that, lysostaphin is injected into the sensor, thus the bacteria on the sensor surface were lysed and the lysate penetrate into the pores, resulting in an increase of refractive index of the porous layer. Bacteria solutions with different concentration are detected and the reflect spectra during these processes are monitored. Therefore, we hypothesized that the change of reflective spectra can indicate the bacteria number on the porous silicon surface.

What's important, lysostaphin, one kind of lytic enzyme which can react with Gram positive bacteria cell wall such as *S.epidermidis* selectively and then burst the bacteria, is introduced into the biosensing application for the selective detection of *S.epidermidis*. The bacteria cells adhering on the sensor surface can be digested by the lysostaphin so the lysate can penetrate into the nanopores, corresponding to an increase in index of refraction of the porous layer as the lysate displaces buffer solution in the pores. This penetration results in a shift of the Fabry-Pérot fringes, and turn to a shift of EOT after FFT, allowing for a "real-time" detection of bacteria.

2 State of the art

Over the past decade, porous silicon has become a promising platform for biosensing applications, benefiting from easy-fabrication process, adjustable pore morphology, and convenient surface chemistry. Various porous silicon-based structures, such as double layer, microcavities, and photonic crystals, have been reported and biosensing of various biomolecules, such as DNA, proteins, as well as bacterial cells, have already been successfully demonstrated. However, rapid detection and identification of bacteria remains a challenge for real-time detection outside the laboratory environment.

2.1 Porous silicon

Porous silicon (PSi) is a nanostructured material with high surface area, which is formed by the corrosion of crystalline silicon. Owing to its tunable pore dimensions from 1 nm to 100 μm, microporous domains with a high surface area (~ 500 m^2cm^{-3}), convenient surface chemistry, electrical conductivity, variable optical structures and luminescent properties at room temperature, PSi has been extensively exploited [1]. Various PSi structures with these advantages were designed and fabricated, as shown in Figure 2.1.

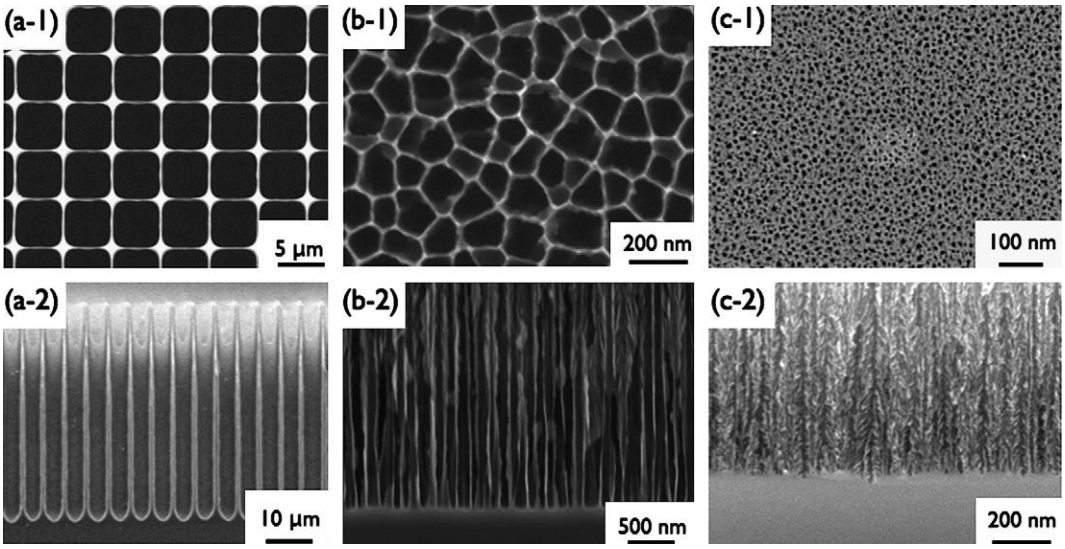

Figure 2.1 Top-view (-1) and Cross-sectional (-2) SEM images of porous silicon layer. (a) 5 μm pores are formed by electrochemical etching after standard photolithography is applied to create ordered etch pits. (b) 120 nm pores are fabricated by electrochemical etching. (c) 20 nm pores are formed [2].

According to the IUPAC (International Union of Pure and Applied Chemistry) guidelines, different categories of PSi with different ranges of pore size exhibiting characteristic adsorption properties could be classified in general, as shown in Table 2.1.

Table 2.1 Pore size classification [3].

Type of porous Si	Corresponding size regime for dominant porosity (nm)
Microporous	≤2
Mesoporous	2-50
Macroporous	＞50

2.1.1 History of porous silicon

Porous silicon was first accidentally observed by Arthur and Ingeborg Uhlir at Bell Labs in 1956, during their studies of the electropolishing of Si in aqueous hydrofluoric acid (HF) based solutions. Under certain conditions, they observed that the surfaces often developed "a matte black, brown or red deposit." However, these deposits were suppose to originate from Si suboxide [4]. One year later, Fuller and Ditzenberger observed that similar films could also be fabricated in HF-HNO_3 solutions without applying any electrical bias to the Si wafer [5].

The porous nature of these films wasn't found until 1975 by Watanabe et al. in Japan [6], who also reported the possible conversion of such layers into thick oxide films and making use of this property as insulator [7]. In the 1970s, the Japanese utilized the porous silicon for dielectric isolation of active Si devices, and then this so-called full isolation by porous oxidized Si process was developed in 1980s.

In 1990, strong visible photoluminescence (PL) at room temperature of PSi was observed by Leigh Canham at the Defense Research Agency in England, a property not found in bulk Si that attracted great interest towards this material [8]. Lehmann and Goesele reported that the band gap of PSi widens compared with bulk Si and they attributed the photoluminescent emission to quantum confinement effects from the nanostructured porous silicon [9]. The quantum confinement effects arise when the pores become extensive enough to overlap with each other, generating nanometer scale silicon filaments. Within one year, the emission wavelength throughout the visible and infrared ranges was observed by adjusting the fabrication parameters [10].

Soon after, electroluminescent (EL) emission of similar characteristics during the formation of porous silicon was reported [11, 12], and the successful fabrication of solid-state EL devices based on this material was developed [13]. The discovery of both PL and EL of porous silicon opened the way to develop optoelectronic devices based on silicon. Examples of porous silicon emitting light under PL and EL conditions are shown in Figure 2.2.

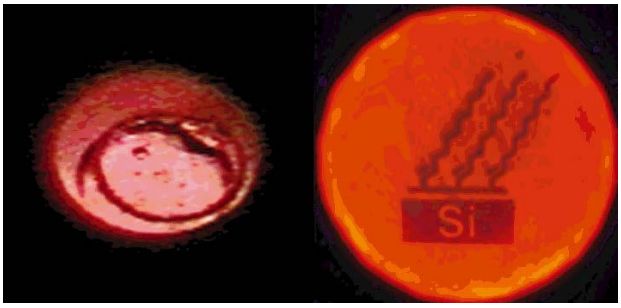

Figure 2.2 Photographs of porous silicon emitting light. Left: a 1 cm diameter porous silicon sample in a Teflon electrochemical cell, under EL conditions. Right: a 1 cm diameter porous silicon irradiated with UV light which induces PL emission [14].

Because of its full compatibility with standard CMOS (Complementary Metal Oxide Semiconductor) processes [14], PSi developed rapidly while the insufficient chemical and mechanical stability and its low EL efficiency remain big challenges. In consideration of the unique features of porous silicon, such as large surface area, controllable pore sizes, convenient surface modification, and conventional fabrication methods, scientists pay attention to fields far outside electronics. Since then, various biomedical sensor, optics, and electronics applications have emerged.

2.1.2 Pore morphology

The morphological characteristics of PSi are porosity, thickness, pore size, and pore wall thickness, which are controlled by the fabrication parameters.

The IUPAC defines porosity as such [15]:

"Porosity: ratio of total pore volume V_p to the apparent volume V.
The meaning of the term "total pore volume" is dependent on the method. We must distinguish between "open porosity," "closed porosity", and "total porosity":

Open porosity: the volume of pores accessible to a given probe molecule

Closed porosity: the volume of pores that are inaccessible to the probe molecule

Total porosity: open porosity + closed porosity; the volume of pores accessible to a given probe molecule plus the volume of pores that are inaccessible to probe"

Different ranges of porosities can be obtained by selecting different Si wafer parameters which include Si doping type, doping density, wafer resistivity, wafer crystallographic orientation, and tuning the etching parameters which include electrolyte composition, HF concentration, current density, etching time etc [16]. Thus, it is important to determine both the wafer and etching parameters as many independent factors are to be mooted [1].

After the fabrication of porous silicon, the porous layer can be oxidized. Because of the volume increase associated with conversion of Si to SiO_2, it is possible that a porous silicon sample will develop closed, inaccessible pores. A similar situation could derive from chemical modification of the inner pore walls of a PSi sample. In addition, the term "open porosity" is dependent on the size of the probe molecule; for instance small pores may not accommodate large molecules. This is particularly true in biosensor and drug delivery applications, where the molecules of interest tend to be large [15].

Many methods could be applied to calculate the porosity, such as gravimetric determination and SLIM (Spectroscopic Liquid Infiltration Method) where usually ethanol is used as probe molecule. So when reporting the results, the method used to measure pore volume and apparent volume should be stated.

Fabrication of porous p-type silicon with pore size ranging from 5-1200 nm was presented by Andreas Janshoff [17], and the effect of variant etching parameters, such as electrolyte composition, HF concentration and current density were studied by Farid A. Harraz [18]. It was found that current density is a decisive factor during the electrochemical etching. As seen in Figure 2.3, increased pore size results from increasing the current density from 5 to 25 mA/cm^2 [19].

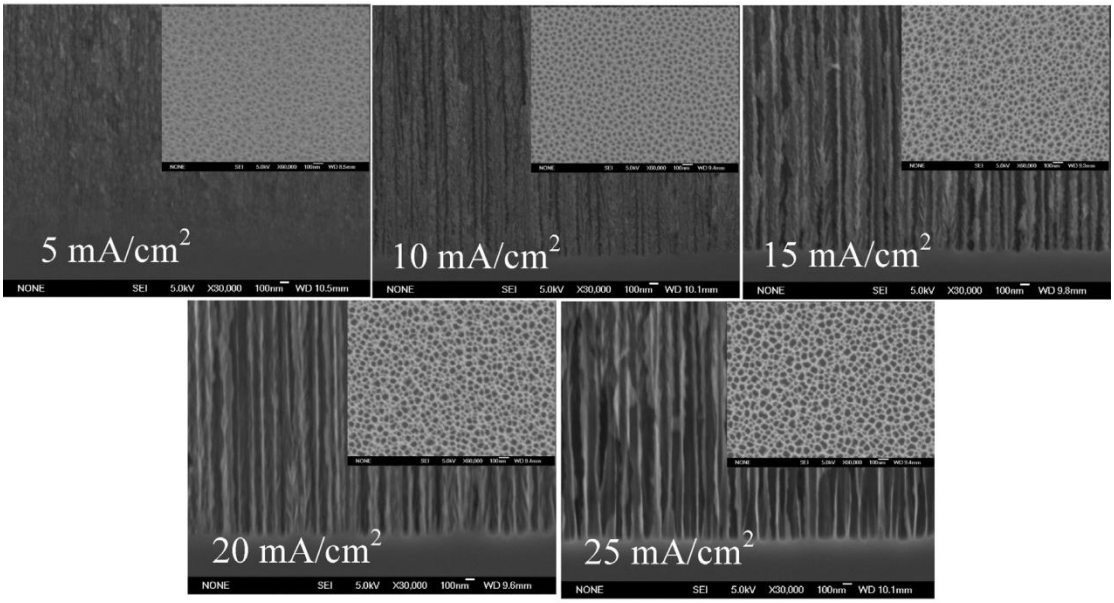

Figure 2.3 Top-view and cross-sectional view SEM images showing the dependence of pore size on applied current density. All samples were anodized using 0.010-0.018 Ω cm n-type Si in 6wt% aqueous HF+8mM $KMnO_4$+3000ppm NCW-1001 [19].

The last main characteristic of porous silicon is the thickness of the porous layer, which is considered to be proportional to the total etching time. The layer thickness can be obtained using SLIM and SEM characterization.

2.1.3 Spatially modulated porous silicon

Since the pore formation or corrosion of silicon only occurs at the pore/silicon interface during the electrochemical etching, the already etched porous layer stays intact during the further process [20]. Thus the porosity and pore size of the produced porous array at any instantaneous point can be modulated by adjusting the applied current. That means, by varying the current-time relationship, it is possible control the relationship between porosity, pore size and depth in the porous layer. This way, all kinds of porosity modulated structures, like double layer, Bragg stack, microcavity, rugate can be fabricated conveniently. Various current waveforms and the corresponding optical spectrum are summarized in Table 2.2.

Table 2.2 Examples of porosity modulated nanostructures prepared with porous silicon. The idealized structures, current density waveform, and reflectance spectra are given [15].

structure	waveform	Spectrum
Double layer	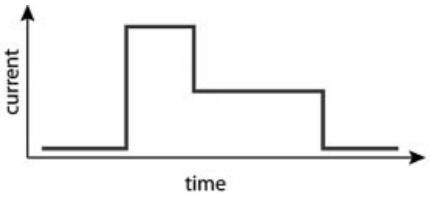	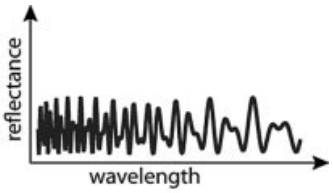
Bragg stack	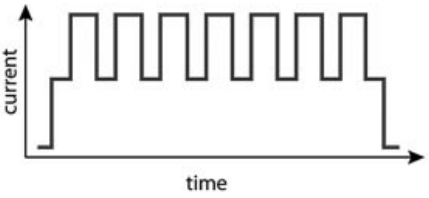	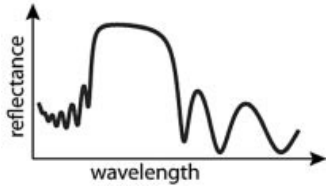
microcavity	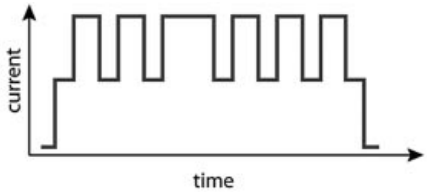	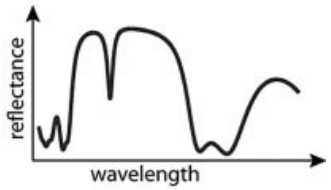
rugate	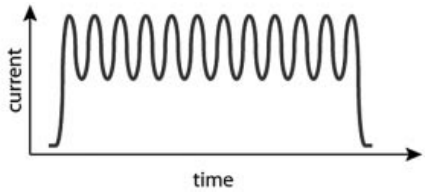	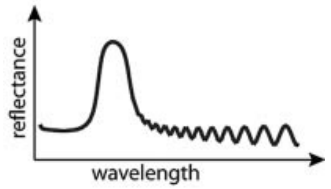
apodized rugate	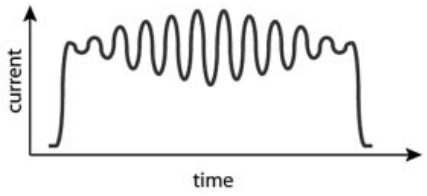	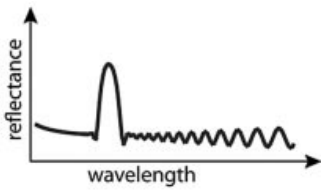

For instance, if we want to prepare a double layer porous silicon, consisting of a layer of larger pores above a layer of smaller pores, we just need to step a current from a higher to a

lower value during the etch. Such structures could be used to separate biomolecules based on size [21].

Besides, Bragg mirror which is a periodic stack of layers with two different porosities and quarter-wavelength optical thickness and microcavity, which is a 1-D photonic bandgap structure contains a symmetry breaking layer between two Bragg mirrors so that there is a resonance position in the reflectance spectrum, are also widely developed as platform for sensing application [22, 23].

2.1.4 Applications of porous silicon

Creation of porous layer in the bulk silicon wafer not only increases the surface to volume ratio, but also induces photoluminescence at room temperature and electroluminescence because of the quantum confinement effect. Considering its photo- and electroluminescent properties, nanostructured PSi was perceived as a good candidate in the field of optoelectronics. Many potential applications were pointed out: light emitting diodes (LED), interference filters, waveguides, photonic crystals, cold cathodes, capacitors, solar cells, etc [3, 24].

Most applications of porous silicon are related to its tunable optical properties, since the refractive index of PSi can be varied continuously between the indices of bulk silicon and air by adjusting the porosity (Table 2.3). Therefore, porous silicon has been used in devices such as filters, dielectric mirrors, waveguides, and optical microcavities [3].

Table 2.3 Different levels of porosity with their respective applications [1].

Void content (%)	Level of porosity	Potential applications of PSi
0-30	Low	Microcapacitors, wafer bonding, tissue boding
30-70	Medium	Micromaching, sensors, silicon on insulator
70-100	High	LED, anti reflection coating, non linear optics

Additionally, some chemical and biological molecules with appropriate size and structure could penetrate into the porous layer and be attracted, especially when the porous layer was modified with acceptors as binding sites, which induce changes in the optical or chemical properties. Thus, porous silicon is widely developed as chemical sensors and biosensors [14, 18].

2.1.5 Challenges of porous silicon

Even though porous silicon provides numerous advantages and conveniences, for instance the ability to fine tune the pore morphology and the special optical and electrochemical properties, allowing for a very promising research in many fields, some challenges still exist

in fabrication. These include [1, 18]:

1) Forming a uniform porous layer on bulk silicon, many factors can affect the electrochemical etching product, thus great changes may be introduced by a slight alteration in any of the parameters;
2) Forming ordered pores: the natural pores are angular and randomly arranged. Other technologies such as photolithography can then be combined with the electrochemical etching;
3) Surface stabilization: freshly etched porous layer is easily oxidized in air and dissolves in alkaline solution;

Another challenge is to address the chemical nature of the formed PSi layer, because the freshly etched PSi is terminated with Si-H_x bonds, as shown in Figure 2.4, which make the surface very unstable [25]. Silicon surface will also commence formation of an oxide layer when exposed to ambient air. So it is necessary to functionalize the PSi surface to render it stable and selective for particular analytes.

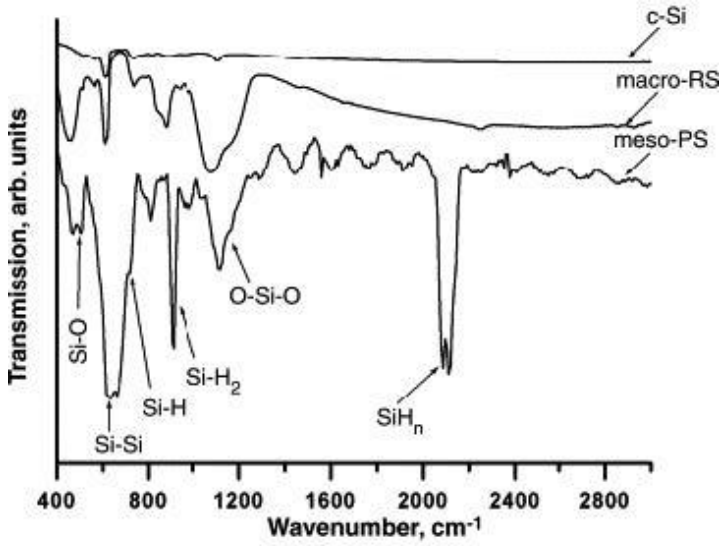

Figure 2.4 Chemistry of PSi. FTIR spectra of crystalline silicon (c-Si), micrometric PSi (macro-PS), and nanostructured PSi (meso-PS) [25].

For instance, Si hydride bonds could be replaced by Si-C bonds by chemical reactions or oxidized as shown in Figure 2.5 [1].

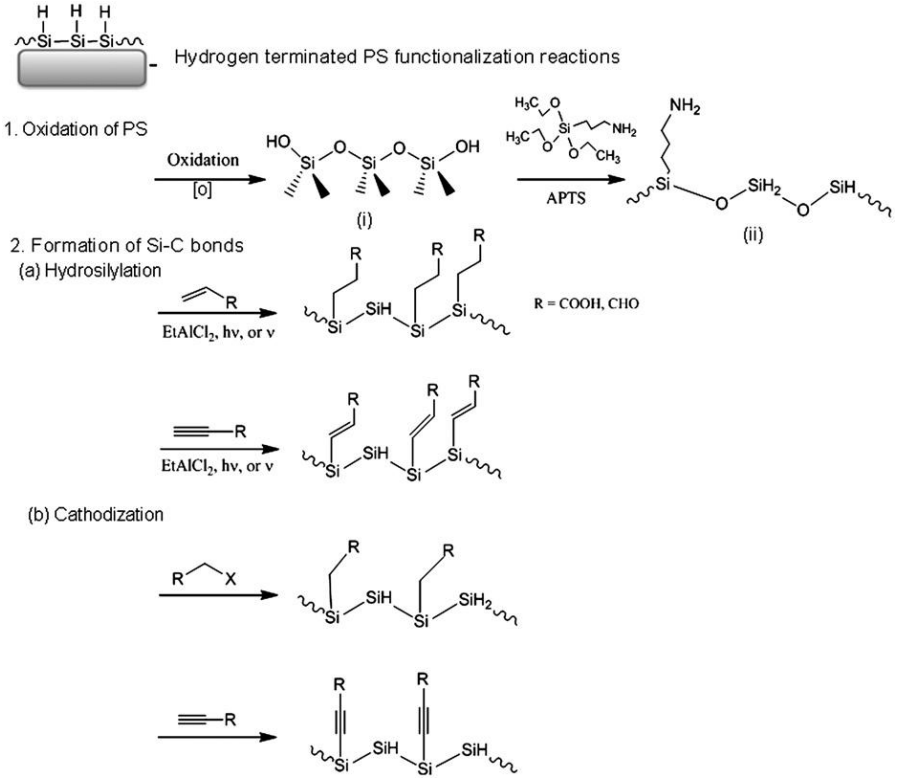

Figure 2.5 Surface chemical reaction of PSi. Si-H_x terminated surface can be (1) oxidized; (2) generation of Si-C bonds on PSi surface by hydrosilylation and cathodization with various precursors like alkene, alkynes, grignard reagens alkyl halides etc [1].

Si-C has been shown to protect flat silicon surfaces from chemical environment. Porous silicon functionalized with hydrophobic groups demonstrates remarkable stability to such adverse conditions as boiling aerated water and boiling aqueous KOH (pH 10) [26]. These surface modifications are also useful in protecting the PSi from ageing effects, this way the surface properties are locked and can't be affected by the environment any more [1].

Another challenge presents itself when working with medical analysis. Indeed, red blood cells in whole blood may cause optical and chemical interference which can trouble the analyte concentration determination. However, this problem is being worked on where porous structure of PSi work as filters [1]. In the future, inexpensive, commercial and hand-held biosensor device based on PSi will be decided upon overcoming these challenges [1].

2.2 Biosensor

2.2.1 Basic concept

“A sensor is a device that as a result of a chemical interaction or process between the analyte and the sensor device, transforms chemical or biochemical information of a quantitative or qualitative type into an analytically useful signal” [27]. Detection can be accomplished only when there is a considerable change of the sensing material properties, for instance, chemical, optical, thermal or electrical properties.

The field of biosensors sprang up in 1962 when Leland C. Clark developed enzyme electrodes that measured dissolved oxygen in the blood of patients undergoing surgery [28]. Figure 2.6 shows the principle of Clark’s glucose sensor. The enzyme Glucose Oxidase (GOD) was placed closed to the platinum (Pt) electrode. When glucose reacts with GOD, gluconic acid is produced, together with two electrons and two protons, while GOD is reduced. The reduced GOD can react with surrounding oxygen, electrons and protons to form hydrogen peroxide and oxidized GOD, thus coming back to its original form and being able to continue glucose catalysis. Thus, more glucose is catalyzed, more oxygen is consumed, while less glucose is catalyzed, more hydrogen peroxide is produced. The concentration of glucose can then be measured by detecting the consumption of oxygen or production of hydrogen peroxide by the electrode [29].

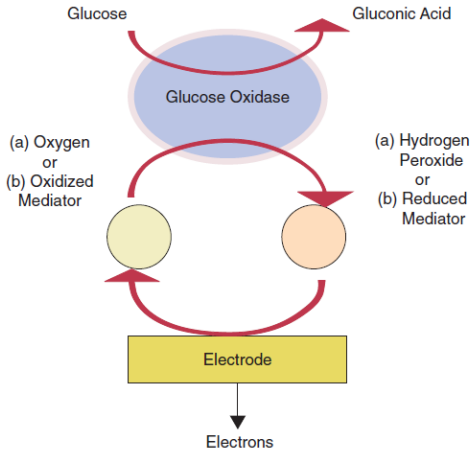

Figure 2.6 Clark’s experiment [29].

A biosensor is one small branch of the sensor family that utilizes biological materials for its sensing application. Two commonly cited definitions by S. P. J. Higson and D. M. Frazer, respectively, are “a biosensor is a chemical sensing device in which a biologically derived recognition entity is coupled to a transducer, to allow the quantitative development of some complex biochemical parameter,” [30] and “a biosensor is an analytical device incorporating a deliberate and intimate combination of a specific biological element (that creates a recognition event) and a physical element (that transduces the recognition event).”

[31]

Current fabrication and device engineering allows biosensors development in the fields of glucose monitoring in diabetes patients, pesticide detection, pathogen detection, remote sensing of airborne bacteria and quantitative measurements of toxicity, determination of drug residues in food, protein engineering, drug delivery, and evaluation of biological activity of new compounds [1].

2.2.2 Elements of a biosensor

A biosensor combines the bioelement (biological receptor) and the transducer (physicochemical detector). The biological recognition element is retained in direct spatial contact with a transduction element. The basic elements of a biosensor are illustrated in Figure 2.7.

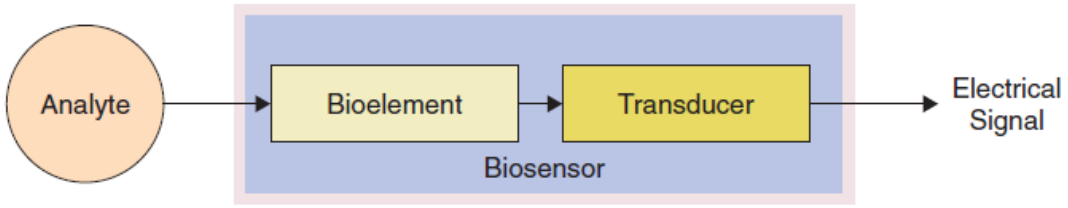

Figure 2.7 Schematic of electrical biosensors [29].

The structure of a biosensor can generally be described as three parts [29]:

(1) Bioelement: biologically sensitive elements, for instance, tissues, microorganisms, immobilized cells, enzymes, antibodies, nucleic acids, etc. which interacts (binds or recognizes) with the targeted analyte.

(2) Transducer or the detector: works in a physicochemical way, pH-electrode, oxygen electrode, ion selective electrode, piezoelectric crystal etc., which transform the signal resulting from the interaction between the receptor and analyte into detectable signal, which can be more easily monitored and quantified.

(3) Electronic system: include a signal amplifier, processor, and display, so we could read the results in a friendly way. Besides, the electronic system is not necessary for all biosensors, but just for those electrochemical biosensors.

Current biosensors normally are self-contained integrated devices, which have shown the ability to provide specific quantitative or semi-quantitative analysis [32-34]. Transducers and electronics can be combined, e.g., in CMOS-based microsensor systems [35]. The bioreceptor uses biomolecule to interact with the analyte of interest. This interaction is measured by the biotransducer which outputs a measurable signal proportional to the presence of the target analyte in the sample. The general objective of a biosensor is to enable quick, convenient testing at the point of concern or care where the sample was obtained [33].

2.2.3 Porous silicon based biosensor

PSi is considered as a promising candidate for biosensors as its large surface-volume ratio and tunable optical and electrochemical properties show great potential for sensing applications.

PSi based biosensor device is a combination of a bioelement and a sensor element. The specific bioelement, bound to the PSi surface, is able to recognize the analyte and then induce a change in optical or electrochemical properties of the sensor. These changes are recorded and conveyed to a transducer which converts the optical or electrochemical information to another form which can be read conveniently by users [1].

PSi-based biosensors are selective and sensitive substrates for detecting biomolecules, owing to the combination effect of sensitive matrix and surface modification. The bioelement can be antibody, enzyme, nucleic acid, tissue, or living cells. The sensing element can be electrical (current, potential, conductance, resistance, capacitance etc), electrochemical (amperometry, potentiometry, conductometry, impedimetry) or optical (reflectance, photoluminescence, etc) [33, 36].

2.2.3.1 Optical biosensor

These are probably the most popular in bioanalysis, due to their selectivity and sensitivity. Optical biosensors have been developed for rapid detection of contaminants [37], toxins or drugs [38], and pathogen bacteria [39].

According to the signals recorded during the measurements, PSi based biosensors are classified into several categories.

1. Photoluminescence detection

PL of PSi has been implied as biosensor ever since room temperature PL has been discovered and adopted for biomolecules recognition. For instance, Starodub et al. showed that light emitting properties of PSi can be used to create a bioaffinic sensor capable of detecting myoglobin in buffer solution and human serum. It was shown that the sensitivity of the sensor created is 10 ng/mL. It is comparable with that of the standard ELISA, but the overall time of the analysis performed by this sensor is much shorter [40].

2. Detection of changes in the refractive index

By varying the current density during the electrochemical etching process, PSi single layer, double layer, multilayer, and microcavitiy could be obtained as mentioned in section 2.1.3.

The simplest kind of PSi based transducer monitors changes in the refractive index that occur in PSi single and double layer upon a specific bio-recognition event, providing a simple yet effective label-free detection mechanism [41].

The first PSi biosensor has been developed based on induced wavelength shifts in the Fabry-Perot fringes in the visible–light reflection spectrum of porous silicon layer. Binding of molecules induced changes in the refractive index of the sensor, including DNA hybridization, antibody cascading and the biotin-streptavidin interaction, were investigated on oxidized and silane-functionalized microporous PSi [42]. These experiments were carried out in a flow cell and used a fiber optics spectrometer, which is shown in Figure 2.8.

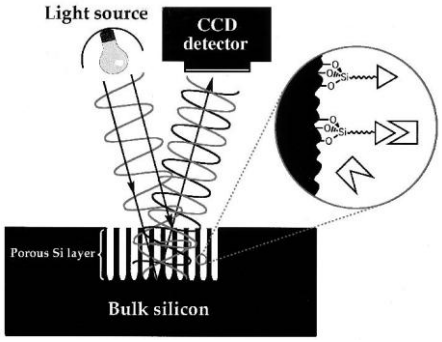

Figure 2.8 Schematic of the PSi-based optical interferometric biosensor. The silicon oxide surface of the porous layer can be modified to express various molecular recognition elements (such as oligonucleotides, biotin, or antibodies). Reflection of white light at the top and bottom of the PSi layer results in an interference pattern (Fabry-Perot fringes) [42].

In this study, reflection of white light at the top and bottom of the PSi layer results in an interference pattern that is related to the effective optical thickness (product of thickness L and average refractive index n) of the film by Eq.2.1

$$m\lambda = 2n\mathrm{L} \qquad (2.1)$$

where m is the spectral order and λ is the wavelength of light. Binding of an analyte to its corresponding recognition partner, immobilized on the PSi substrate, results in a change in the refractive index of the layer and is detected as a corresponding shift in the interference pattern [42].

Fourier transformation of the reflectance spectra returns a peak proportional to the effective optical thickness (EOT) of the film (EOT=2nL) [42, 43]. Thus a change in the refractive index of the porous layer, for instance upon binding of biological macromolecules, reveal a shift of the fringe pattern and a corresponding change in EOT.

However, by periodically changing the current density, 1-D photonic crystals including Bragg reflectors, microcavities and rugate filters can also be generated and applied in biosensor application.

For example, Ouyang et al reported a macroporous silicon microcavities for protein detection. A microcavity based on well defined macropores with sizes from 60-120 nm was fabricated and their sensing performance were investigated using immunoglobulin G (IgG) and the biotin/streptavidin couple. The resonsonance position of microcavity in the

reflective spectrum was pretty sensitive to the optical thickness of each layer in the microcavity so a light penetration of the protein inside the pores causes a red-shift. First rabbit IgG was applied to detect the accessibility of the sensor and then the biotin-modified sensor was exposure to streptavidin solution, red shift was observed in both situation and the total amount of red shift is related to the concentration of protein [22].

Besides, reflectivity could be used in combination with other established methods. For instance, Cho et al. showed that both reflectivity and PL can be measured simultaneously for the detection of human lmmunoglobin G (Ig G) [23, 44].

2.2.3.2 Electrical and electrochemical biosensor

"An electrochemical biosensor is a self-contained integrated device, which is capable of providing specific quantitative or semi-quantitative analytical information using a biological recognition element (biochemical receptor) which is retained in direct spatial contact with an electrochemical transduction element" [33].

An electrochemical biosensor is fabricated with an electrochemical transducer. It is considered a chemically modified electrode (CME) [45, 46] since electronic conducting, semi-conducting or ionic conducting material is coated with a biochemical film. These devices are mainly based on the observation of current or potential changes due to interactions occurring at the sensor-sample matrix interface [36].

Exploitation of the semiconductor properties of PSi has produced biosensors that operate by modulating the space-charge region in the crystalline silicon columns and the dielectric constant of the porous layers upon binding of charged molecules [47]. Traditionally, electrochemical transduction involves the conversion of an electro-active substance in the presence of the target analyte. The incorporation of PSi into such devices offers the advantage of a substantially larger sensing area compared with flat electrodes [41].

An electrical biosensor based on a metal/nano PSi /metal structure was fabricated for the detection of glucose and *Escherichia coli* [48]. The current-voltage characteristics were performed, and a reduction of current for increasing glucose concentration (constant voltage) is observed as shown in Figure 2.9.

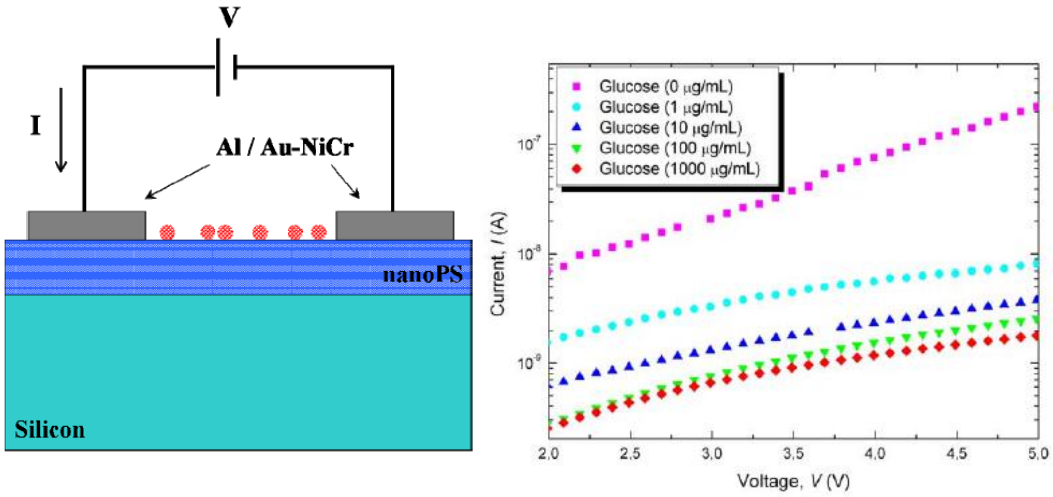

Figure 2.9 Cross section view of a metal/nano PSi/ metal electrical biosensor (left) and current-voltage curve after glucose immobilization at different concentration [48].

According to the observed parameters, electrochemical biosensors may be classified.

(1) Amperometry

As the most common electrochemical method, it works on measuring the current at the working electrode where the potential is set as a constant with respect to the reference electrode. The electrochemical oxidation or reduction of an electroactive species produce a current which is directly correlated with the analyte concentration or its production or consumption rate within the adjacent biocatalytic layer. The linear relationship between the current and the analyte concentration exists because the biocatalytic action rates are often first order dependent on the analyte concentration. Usually a Pt, Au, or C electrode or array of electrodes are used as working electrode in this methods [33].

Song et al fabricated an enzymatic biosensors array for the diagnosis of liver diseases. Cholesterol, bilirubin and aminotransferases were monitored as biomarkers on four different sensors simultaneously since their presence in the serum indicates liver disease. In their work, PSi layer was formed on the Pt working electrode to increase the surface area and the electrodes are placed in wells to minimize the cross interference effect as shown in Figure 2.10. As a result, high sensitivity and selectivity for liver diagnosis are obtained [49].

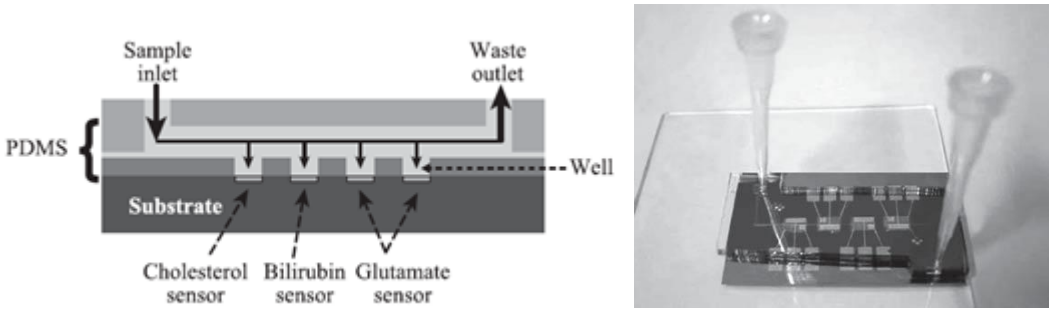

Figure 2.10 Schematic representation of cross section (left) and photo (right) of biosensor array with the microfluidic system made on silicon wafer with PDMS [49].

(2) Potentiometry

Potential difference between an indicator and a reference electrode or two reference electrodes are measured, when there is no significant current flowing between them. A potentionmetric biosensor normally consists of an ion-selective electrode (ISE) as the recognition element, which is based on thin films or selective membranes, and bioactive species such as enzyme. The reaction of bioactive species consumes or generates a substance which is monitored by ISE. Since the potential difference is proportional to the logarithm of the ion activity, this method is able to detect small concentration changes [33, 36].

Setzu et al. fabricated a potentiometric biosensor based on mesoporous Si layer modified by lipases for the detection of triglycerides. Lipases are well known enzymes that catalyze the triglycerides hydrolysis, which results in a decrease of the pH. To maintain the pH at 7, NaOH is added to the system, and then the activity of lipases can be determined as a function of the volume of added NaOH. In this device, PSi act as an electrode and it has been shown to be stable for several months [50].

(3) Conductometry and impedimetry

Many enzyme reactions, such as that of urease, and many biological membrane receptors may be monitored by ion conductometric or impedimetric devices, using interdigitated microelectrodes [51]. Because the sensitivity of the measurement is hindered by the parallel conductance of the sample solution, usually a differential measurement is performed between a sensor with enzyme and an identical one without enzyme.

Marie J. Archer et al. developed a series of PSi-based electrical sensor for real-time detection of DNA hybridization via the conductance measurement of mesoporous silicon layer (pore diameter ~ 20-50nm) and macroporous silicon layer (pore diameter ~1-2 um). The sensors work on space charge region modulation (SCRM) model which is based on the interaction of charged biomolecules, such as DNA, with the surface of PSi layer. The interaction cause changes in the space charge region of the silicon structure, as well as the dielectric constant inside the pores and charge distribution in the silicon structure, resulting in a change of capacitance and conductance.

Thus the impedances of the sensor were obtained by capacitance-conductance characteristics, which are correlated to the presence of DNA. Their study found that a reduction in the impedance followed with the hybridization of DNA with their complementary sequence and the sensitivity of the sensor was related to the PSi thickness and the probe concentration [47, 52].

2.3 Bacteria detection

Rapid detection and identification of bacterial infections and contaminations remains a significant challenge in many fields, especially in monitoring the quality of drinking water [53], detecting spoilage in the food industry, disease diagnosis, etc [54].

2.3.1 Traditional methods for bacteria detection

To date, detection and identification of bacterial contaminations basically rely on traditional microbiology culturing techniques, as well as the polymerase chain reaction (PCR) and enzyme-linked immunosorbent assay (ELISA). They involve counting of bacteria, DNA analysis, and antigen-antibody interactions, respectively [36].

2.3.1.1 Polymerase chain reaction (PCR)

PCR is based on the isolation, amplification and quantification of a short DNA sequence including the targeted bacteria's genetic material [36]. Figure 2.11 illustrates the standard PCR method, consisting in three steps per cycle: (1) denaturation by heat of the extracted and purified DNA, the hydrogen bond between based pairs is broken at 94-95 ℃, resulting in single stranded DNA; (2) annealing, the target specific primers hybridize to the single strand at 25-65 ℃, thus partial double strand is formed; (3) extension, the complementary strand of template is polymerized with the help of Taq enzyme at 70-75 ℃, which are the optimum temperatures for the extension [55].

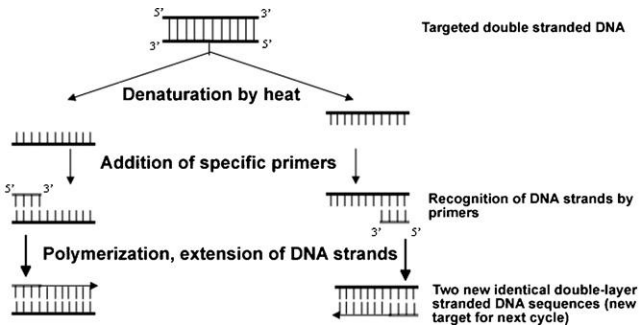

Figure 2.11 Schematic representation for one cycle of PCR taking place in a thermocycler [36].

After the first cycle, we obtained two identical double strands DNA, which are used as targets for the next cycle; after n cycles, we obtain 2^n double strands DNA. The amplified DNA is then detected by gel electrophoresis.

One of the limitations of PCR lies in the fact that the user cannot discriminate between viable and non-viable cells because DNA is always present whether the cell is dead or alive [36].

2.3.1.2 Culture and colony counting methods

The culture and plating method is the oldest bacterial detection technique and remains the standard detection method. Unfortunately, it is excessively time-consuming.

An appropriately diluted sample including bacteria is added to the surface of agar media and spread. After incubation, the presence or absence of bacterial growth can be measured via the development of colonies that may be counted [53]. The whole test requires a minimum of 1 day or more as the formation of colonies need at least 18h in incubator until the presence of bacteria is visible.

Particular bacteria can also be discriminated by various selective media, which add particular inhibitors that stop the growth of non-targeted strains, or substrates that only the targeted bacteria can degrade, into the normal media. For instance, Rambach agar, Rainbow Agar Salmonella, and XLT4 agar were used to detect *Salmonella app.* in naturally-contaminated ground chicken, turkey, and beef, where the presence of *Salmonella app.* were confirmed by particular color of colonies, and then black colonies on Rainbow Agar Salmonella and XLT4 agar, and red colonies on Rambach agar were selected for further test [56].

2.3.1.3 Enzyme linked immunosorbent assay (ELISA)

By applying the antibody-antigen interaction, which provides specificity as well as the assayed enzyme, which provides selectivity (Figure 2.12), ELISA is the most powerful method for bacteria analysis nowadays and also the source of inspiration for many biosensors [36].

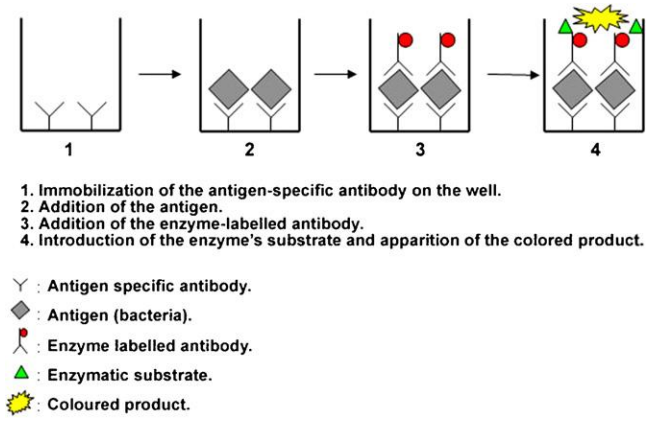

Figure 2.12 Schematic representation of "sandwich ELISA" [36]

Table 2.4 summarizes the main detection technologies of *Escherichia coli (E.coli)* O157:H7 bacteria, and their corresponding detection time and sensitivity values. For instance, culturing techniques, which typically require several days to obtain result, make "real-time" assessment unfeasible. Even advanced "rapid" techniques in microbiology like ELISA and PCR, lack the ability to detect microorganisms in "real time" or outside the laboratory

environment [57].

Table 2.4 Summary of the methods used to detect *E.coli* O 157:H7 [57]

Method	Approximated detection time	Detection limit (CFU/mL)
Plating/culturing	1 day to 1 week	Low CFUs
Biochemical tests	1 day to several days	Low CFUs
ELISA	12 h to 2 days	10-100
PCR	2-24 h (depending on enrichment)	10^2-10^5
Multiples PCR	24h	1-2
SPR biosensor	1 h	10^2-10^6
Fiber optic biosensor	15 min	5×10^2-10^3
Amperometric biosensor	10min	2×10^2-2×10^7
Acoustic wave biosensor	0.5-5h	10-10^6

Because identification of the origin of the infection is time-consuming, it may lead to inappropriate medical treatment [58]. Due to these limitations, there is urgency of finding rapid, accurate, reliable, cost effective, and portable methods for "real time" analysis of biological samples to detect and quantify bacteria in general and pathogenic bacteria.

2.3.2 Porous silicon for bacteria detection

Various biosensors have been reported, of which the most popular are optical biosensors. These biosensors offer a number of advantages, including speed, selectivity, sensitivity, and reproducibility of the measurement [36].

Recently, porous silicon has attracted much attention as a good platform for the design of sensors. One of the favorable properties of PSi is their large surface area (typically 500 m^2/cm^3), which enables large amounts and varieties of biomolecules interactions, including enzymes-substrate [59], DNA hybridization [60], and antibody-antigen, occurring over a small working area, facilitating the miniaturization of the sensor.

The electrical properties of PSi, for instance conductivity, are strongly dependent on environmental conditions, and when the porous layer is exposed to target molecules, large changes in conductivity are observed. Thus, PSi-based electrical biosensors rely on changes in capacity, resistivity or conductivity when molecules adsorb within the porous layer [15].

On the other side, PSi-based optical biosensors monitor changes in the refractive index that occur in PSi layer upon a specific biorecognition event, providing a effective label-free detection method. This kind of biosensor thus received a lot of attention in recent years.

PSi-based biosensors for bacteria detection can be simply classified into two main

categories: “direct” and “indirect” methods. The difference between these two approaches is represented in figure 2.13. For “direct” approach, the detection is accomplished by directly binding the entire bacterium cell to the PSi surface by appropriate capture probes. For “indirect” approach, the detection is accomplished by monitoring only fractions of the bacteria cells or protein/DNA fragments that are secreted by the bacteria (therefore, prior lysis of the bacteria is required) [57].

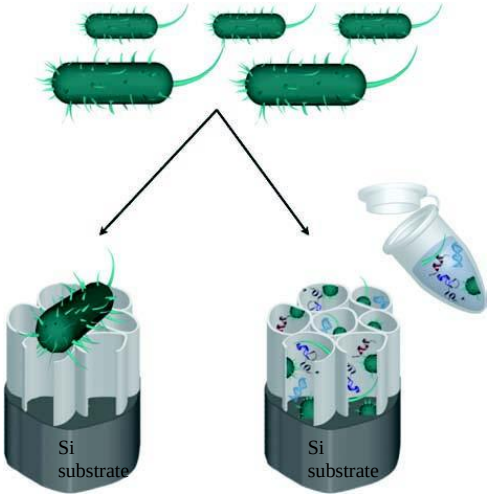

Figure 2.13 A schematic outline of the concepts of “direct” and “indirect” bacteria detection by PSi-based biosensors [57].

2.3.2.1 “Indirect” approach

1. Detection by DNA hybridization

In this approach, detection is achieved by immobilizing a specific DNA probe (ss-DNA) onto the PSi surface. Exposure of this modified PSi to complementary DNA (cDNA) of the target bacteria results in the formation of double-strand DNA (ds-DNA). This recognition results can be monitored in real time.

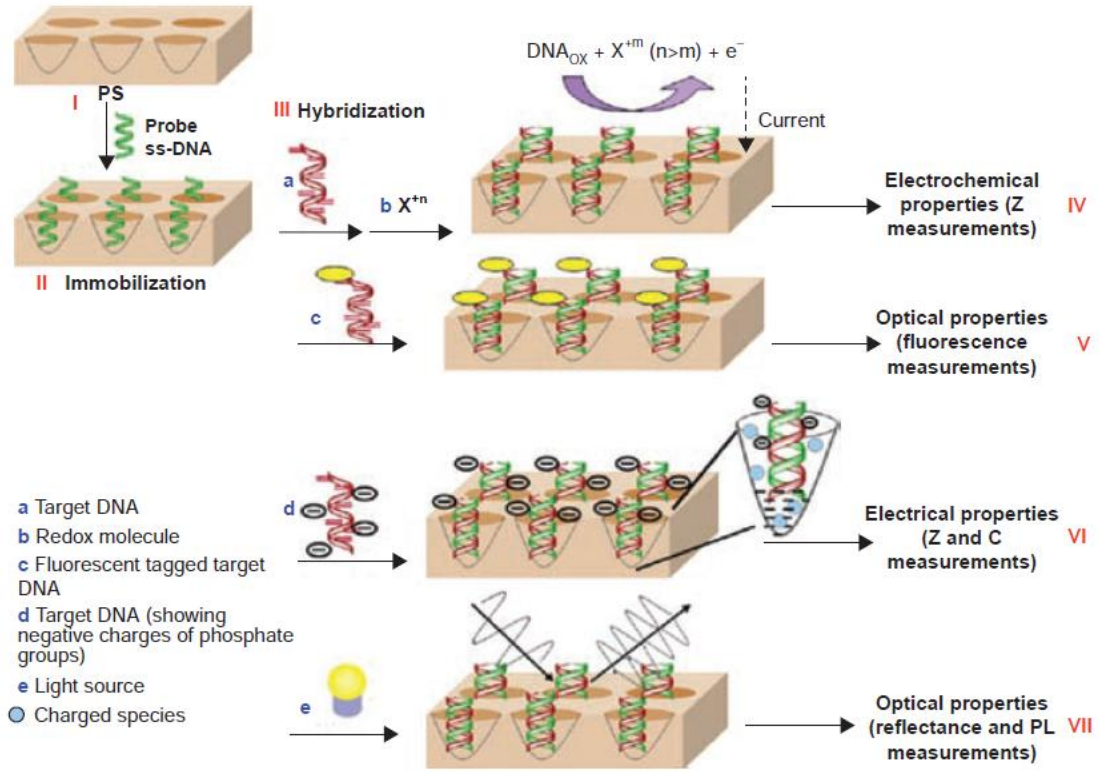

Figure 2.14 Biosensing schemes of bacteria for DNA detection [57].

Common biosensing schemes for DNA detection using PSi transducers are presented in Figure 2.14: (I) and (II) immobilization of DNA probe (ss-DNA); (III)hybridization, resulting in ds-DNA; (IV) change in electrochemical properties (such as impedance); (V) change in optical properties (such as fluorescence); (VI) change in electrical properties; and (VII) change in optical properties (such as reflectance and photoluminescence) [57].

Based on this approach, Zhang and Alocilja have fabricated a label-free DNA electrochemical biosensor based on nano-scale PSi chips for the detection of *Salmonella enteritidis* as model bacteria for food-borne pathogens [60].

2. Detection of cell-secreted molecules

Bacteria can also be quantified using the interaction between their secreted molecules and selective substrate. Mathew and Alocilja designed a porous silicon-based biosensor for rapid "indirect" detection of *Escherichia coli*. In this work, dioxetane-polymyxin B (cell wall permeabilizer) was selected as the substrate to modify the surface of sensor for a selective interaction with β -galactosidase, which is an enzyme produced by *E.coli* as part of its metabolic process. The chemiluminescent reaction between the selective substrates on PSi surface and the enzyme from the *E.coli* culture generated light at 530 nm. Following the functional porous silicon sensor placed in the luminometer, diluted bacteria culture with different concentration was added to the sensor surface, and then the emitted light intensity

was measured. Results showed that light emission for the PSi biosensor was greater than that of the planar Si chip. This biosensor has a limit of detection limit of 10 and 10^2 CFU/mL for *E.coli* at 30 and 40 min, respectively [61].

3. Detection of cell wall lysate

This approach uses capture probe molecules that are specific for certain sites/ molecules present in the target bacteria cell walls. The detection is achieved by monitoring only fractions of the bacteria cell.

In 2011, Li et al. designed a porous silicon microcavity (PSM) based optical biosensor for bacteria detection, which is shown in Figure 2.15. The reflectance spectrum of the PSM structure show a resonance peak whose position is determined by the refractive index of the layers composing the microcavity. Thus molecules penetrating into the nanopores of the PSM cause a change in the reflective spectrum. In this work, the nanopores of PSM were modified by undecylenic acid (UA) and vancomycin, an antibiotic which specifically recognize D-alanyl-D-alanine of bacteria by hydrogen bonding and form stable complexes. So when the vancomycin functionalized PSi sensor was exposed to a bacteria lysate solution, the wall fragments were immobilized in the pores and on top of the PSM. These interactions caused changes in the refractive index and resulted in a red shift of the Fabry-Pérot fringes. This red-shift demonstrates linear relationship with bacteria concentration with a high sensitivity and low detection limit of 20 bacteria mL^{-1} [62].

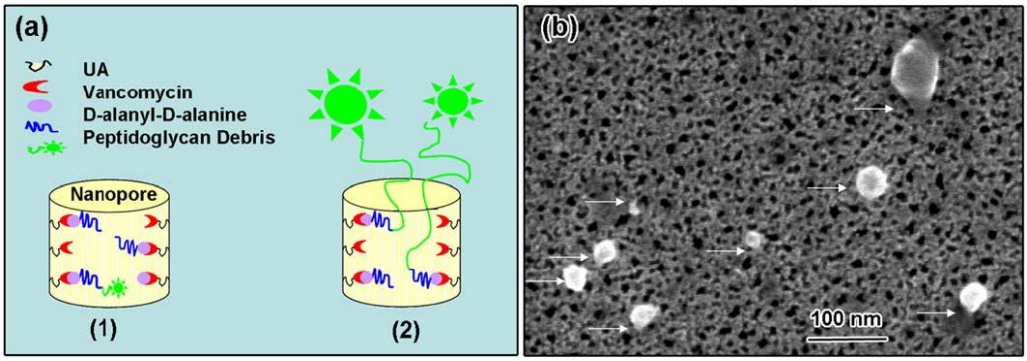

Figure 2.15 (a) two possible ways of bacteria cell wall debris capture on the PSM: the small sized targets filled in and captured on the inside wall of the nanopores, and the large sized targets drifted on the top of the PSM with their heads captured in the nanopores. (b) SEM images of the vancomycin-modified PSi surface after exposure to the bacteria cell lysate (the captured cell debris are marked by white arrows) [62].

Chan et al. fabricated a PSM based biosensor capable of differentiating between Gram-negative and Gram-positive bacteria by detecting the presence of lipid A. The detection is based on the fact that lipopolysaccharide (LPS) , which contain lipid A, is a primary constituent of the outer cellular membrane of Gram-negative bacteria (such as

E.coli) but not in Gram-positive (such as *Bacillus subtilis*). Therefore, tetratryptophan *ter*-cyclo pentane (TWTCP), which bind lipid A specifically, was selected as the receptor for their sensor. Thus exposure of the TWTCP modified PSi sensors to the lysed Gram-negative cells solution results in a photoluminescence red-shift while exposure of this sensor to a lysed Gram-positive cells results in no shift [63].

The traditional and "indirect" detection approach normally require pre-treatment of the bacteria samples, such as enzymatic treatment or sonication, which is time consuming and requires a lab set-up. That means, the biosensors are exposed to suspensions of bacteria fragments with different concentrations [57].

2.3.2.2 Whole cell detection of bacteria on PSi

In this approach, detection is accomplished by directly immobilizing the intact bacteria cells to the PSi surface by appropriate capture probes or nonspecific interactions.

1. "Nonspecific" cell detection

In this approach, no recognition elements were used to modify the surface of the sensor to target the bacteria. Therefore, proper design of the transducer architecture and appropriate surface chemistry are necessary for the spontaneous capture of the bacteria cells.

Michael J. Sailor's group fabricated a series of 1D porous silicon photonic crystal as biosensors for bacteria detection. In 2007, Alvarez prepared a photonic structure with a sharp reflectively peak in the visible region of the spectrum and demonstrated a non-invasive method to monitor the growth and $\Phi 6$ virus infection of *Pseudomonas syringae* bacteria. When bacteria grow on sensor surface, the scattering of light increases, thus a change in intensity of the reflective spectrum from the sensor can be monitored. A linear relationship between bacteria concentration and intensity of light is shown in Figure 2.16. Most significant is that these were "real-time" measurements and the experiment could be performed in incubator to keep the bacteria in their ideal condition [64].

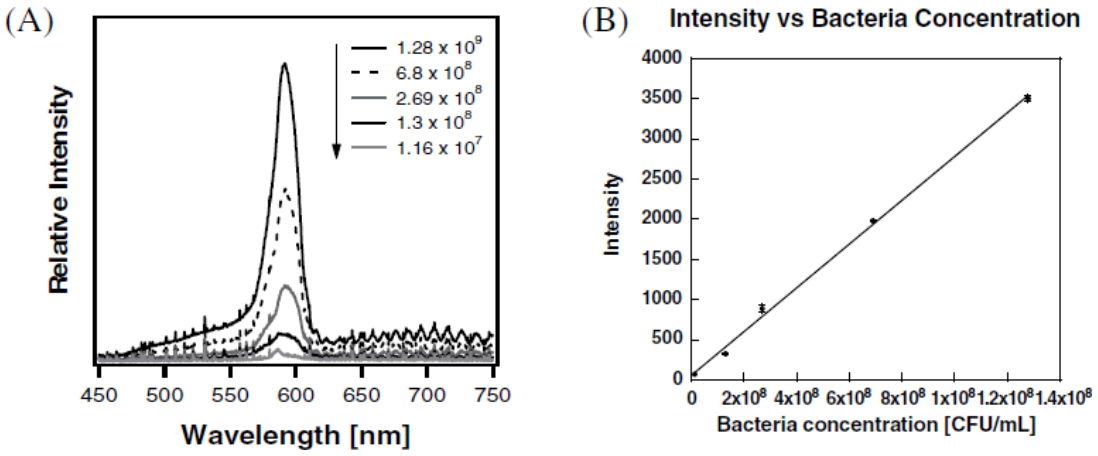

Figure 2. 16 Scattered light intensity of 1D PSi photonic crystal as a function of cell concentration. (A) The reflected scattering spectra from various concentration of *Pseudomonas syringae* applied to the sensor. (b) intensity of scattered light (wavelength =591 nm) vs cell concentration [65].

In 2014, a label-free optical sensors based on a 2D periodic structure of PSi photonic crystals was introduced by Massad-Ivanir et al, in which the pore size and the surface are designed to capture bacteria cells. The 2D ordered arrays of macro-PSi structure with hexagonal or orthogonal lattice patterns, was prepared as shown in Figure 2.17. First, a 2D pattern was defined on top of the Si wafer by photolithography. Second, macro PSi is formed by wet chemical etching and electrochemical etching and then followed by oxidation. At last, the surface of sensor was modified by 3-aminopropyltriethoxysilane (APTES) to bind positively charged amine group, to improve the adhesion of *E.coli* which includes negative charge on surface. When the APTES-modified sensor was exposed to *E.coli* suspension, the bacteria cells were trapped inside the pores and the reflectivity was recorded during the whole measurement. Fast Fourier transform (FFT) of the reflectivity spectrum yielded the effective optical thickness (EOT) of the optical sensor. As a result, the increase of EOT was observed as the entrapment of bacteria led to a increase of the refractive index, while the decrease of intensity was observed as the light scattering induced by the bacteria cells. What's more, this device was able to distinguish between live and dead bacteria cells and to monitor bacterial growth after appropriate surface functionalization [66].

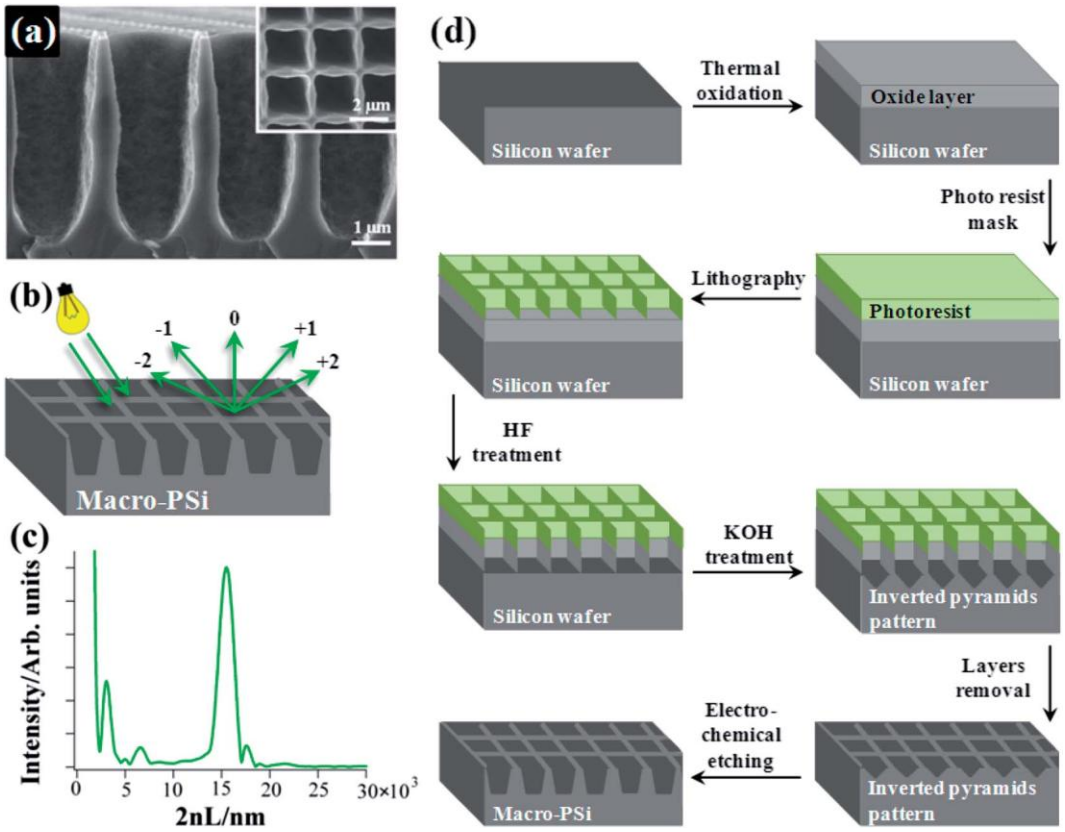

Figure 2.17 (a) SEM images on cross-section view and top view (inset) of a typical macro-PSi array structures. The periodicity is about 2.5 microns while the thickness of the silicon walls is about 0.5 microns. (b) Schematics of the RIFTS lamellar grating sensor and the diffraction orders. (c) FFT of the resulting reflectivity spectrum leading to a single peak, whose position and magnitude are monitored upon introduction of an analyte solution. The presence of the bacteria in the pores affects the spectral interference pattern. (d) Preparation scheme of macro-PSi array structure [66].

2. "Specific" cell detection

In this approach, the surfaces of PSi are modified with selective capture probes, such as antibodies and biotins. The specific interaction between antibodies/antigens, or biotins/ avidins offer "specific" bacteria detection via selective recognition between biosensor and bacteria [67].

Another work of Massad-Ivanir in 2011 demonstrated an optical label-free biosensor for the detection of *E.coli* K12 via "direct-cell-capture" approach. This oxidized PSi based biosensor is functionalized with monoclonal antibodies on the surface as the capture probes. When the IgG-modified biosensor was exposed to the *E.coli* K12 suspensions, reflectance spectrum were monitored throughout the whole experiment. Fabry-Pérot fringes were recorded and "cell capture" events were detected by monitoring the intensity shift, resulting in a measurement of the bacteria attachment in "real time". As shown in Figure 2.18, Ig-G

modified sensor shows a decrease of intensity because the bacteria cells captured on the surface scatter the light, while the neat sensor show no change in intensity as there is no bacteria captured [68].

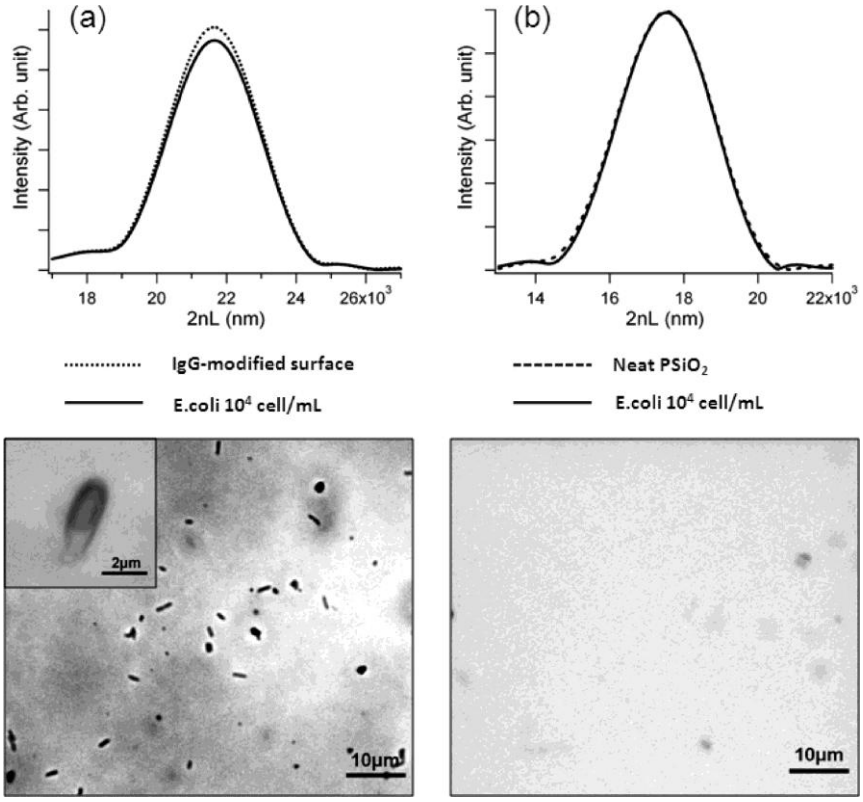

Figure 2. 18 *E.coli* K12 biosensing experiments and corresponding optical microscope images of $PSiO_2$-based biosensors immediately after sensing experiments. (a) $PSiO_2$ conjugated with monoclonal antibodies and (b) unmodified $PSiO_2$ [68].

Finally, various PSi-based biosensor structures for the detection of a wide range of biomolecules as well as bacteria are summarized in Table 2.5 and 2.6, respectively.

Table 2.5 Summary of sensing parameters of various biomolecules using porous silicon architectures.

Porous layer	Analyte	Key property	Detection range	Response time	Ref.
single layer (10-100nm)	myoglobin	Optical: PL	0.1-1ug/mL	10-30min	[40]
single layer (~200 nm)	DNA, Proteins	Optical: reflectance	protein: 10^{-14}-10^{-6}M; DNA:10^{-16}-10^{6}M;	30min	[42]
double layer	BSA and sucrose	Optical: reflectance	1mg/mL BSA in 0-100mg/mL sucrose	~20 min	[21]
Bragg	Human IgG	Optical: reflectance	20uM	~30min	[23]
Single layer	Human IgG	Optical: reflectance and PL	10^{-12}-10^{-4}M	~30min	[44]
single layer-mesopores	DNA	Electrical: impedance	0-5$\times10^{-6}$M	real time	[47]
Single layer-mesopores	Triglycerides	Electrical: potential	0-0.12mol/dm^3	17h	[50]
Single layer-12-20nm	DNA	Electrical: conductance	50uM	240min	[52]
Microcavities (60-120nm)	Protein: biotin/streptavidin, rabbit IgG	Optical: reflectance	1-2uM, (1-2% of a protein monolayer)	NG	[22]

Table 2.6 Summary of biosensors for bacteria detection based on PSi architectures.

Porous layer	analyte	Key property	Sample preparation	Detection range	Response time	Ref.
1-D photonic crystal	ϕ6 infection of *Pseudomonal syringae*	Optical: Scattered light	no	10^7 -10^9CFU/mL	5.2h	[64]
1-D photonic crystal	*E.coli*	Optical: Scattered light	no	0-1500 cell/mm^2	~5h	[65]
Single layer	Protein produced by *E.coli*	Optical: reflectance	no	0-200mg/L	~3h	[54]
single layer	*E.coli*	Optical:reflectance	no	10^3-10^5cells/mL	~1h	[68]
Al/PSi/Al and Au-NiCr/PSi/ Au-NiCr	Glucose and *E.coli*	Electrical: conductivity	no	Glucose: 1-10^3ug/L; *E.coli*: 0-100ug/L	~30min	[48]
Single layer (10-30nm)	*Salmonella* Enteritidis	Electrical: cyclic voltammetry	PCR	10^{-1}-10^{-4}ug/mL	~1.5h	[60]
microcavity	bacteria	Optical: reflectance	lysis	10^2-10^3cells/mL	~30min	[62]
2-D photonic crystal	*E.coli*	Optical: reflectance	no	10^5-10^7cells/mL	Real time	[66]
PSi microcavity	Gram-positive and Gram-negative bacteria	Optical: photoluminescence	no	Gram-positive and Gram-negative bacteria	Real time	[63]

3 Materials and Methods

The mesoporous silicon in this master thesis is fabricated by electrochemical etching. The porosity, pore size and thickness of series PSi samples are characterized by spectroscopic liquid infiltration method (SLIM) and scanning electron microscopy (SEM). The PSi samples with appropriate pore size are chosen as sensors to detect *Staphylococcus epidermidis* by optical method. The sensors are placed in a flow cell and then *S.epidermidis* is flowed on the surface of the porous layer. Following this, lysostaphin is injected in order to selectively lyse *S.epidermidis.* This way, bacteria lysates are allowed to penetrate into the pores. During the whole process, the reflectance spectrum is continuously recorded. FFT is then used to treat the data so intensity and effective optical thickness (EOT) changes are obtained over time.

3.1 Fabrication of porous silicon

PSi thin films are prepared by electrochemical etching using a series of parameters. Then the PSi samples are thermally oxidized at two temperatures, 400 and 800 ℃, for 1 h, resulting in porous silicon oxide ($PSiO_2$) layers.

3.1.1 Electrochemical etching

An electrochemical etching cell normally consists of one power supply, one cathode which supplies electrons to the solution, one anode which removes electrons from the solution and the electrolyte solution which help to complete the electrical circuit, as shown in Figure 3.1. So there are two reactions occurring simultaneously in an electrochemical cell, the oxidation taking place at the anode reaction and the reduction reaction at the cathode.

Here the silicon wafer acts as the anode, and is then being oxidized. A platinum wire used for the cathode, and it is separated from the silicon electrode by a few mm to several cm of electrolyte solution. The electrochemical reaction occurring at the platinum electrode is primarily the reduction of protons to hydrogen gas. So the silicon electrode is referred as "working electrode" and the platinum as "counter electrode".

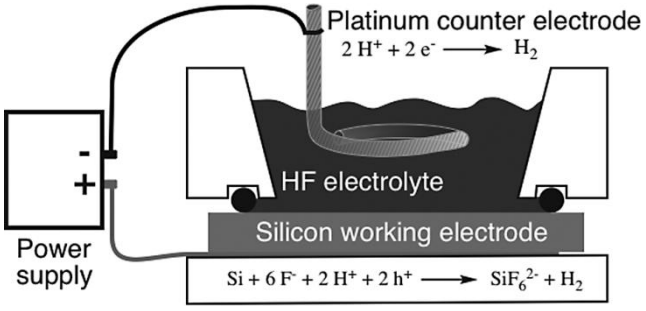

Figure 3.1 Scheme of the electrochemical etching cell [15].

When mesoporous silicon is prepared from highly-doped P^{++} type silicon, a top "crust" layer with smaller pores than the rest of the PSi film is generated because of the segregation of dopants at the Si surface [15]. A convenient way to circumvent this problem was used. A sacrificial porous silicon layer is etched and then removed by KOH aqueous solution [15]. The chemical principle is that in basic solution hydroxide ions attack and dissolves the oxide following the reaction [15]:

$$SiO_2 + 2\ OH^- \rightarrow [SiO_2(OH)_2]^{2-}$$

The net dissolution reaction for silicon in basic media then becomes:

$$Si + 2\ OH^- + 2H_2O \rightarrow [SiO_2(OH)_2]^{2-} + 2H_2$$

The products are water soluble, so they can be removed by rinsing in DI water.

In this work, to form a structure with distinct PSi layer, a series of PSi samples are prepared at different current density and etching time, as shown in Table 3.1. The etching rate increased when the current density increases, smaller etching time were used for higher current density in order to obtain PSi films of approximately the same thickness. The dependence of pore sizes and current density is investigated.

Table 3.1 Si wafer and etching parameters for porous silicon fabrication

Sample No.	Current density (mA/cm^2)	Etching time (s)
1	5	600
2	25	300
3	50	300
4	75	300
5	100	300
6	150	300
7	200	100

All samples were fabricated using P-doped Si wafer with a resistivity of 0.8-1.2 mΩ·cm and an electrolyte composed of 3 parts of 49% HF and 1 part ethanol.

Since the pore diameter of PSi samples and then the size of bacteria lysate are measured by SEM, No.7 which has the appropriate size for lysate penetration is selected for the next biosensing application. That is, all the PSi samples for biosensing experiment were prepared using a constant current density of 200 mA/cm^2 applied for 50s.

After the electrochemical etching, the PSi samples are rinsed adequately using isopropanol (IPA) and then blown dry with nitrogen flow.

3.1.2 Thermal oxidation

One significant challenge of PSi-based biosensors is their instability in biologically relevant environments. As PSi can be oxidized and / or dissolved in aqueous solution such as PBS buffer, their optical properties will vary over time, thus cause baseline shift [69].

Si scaffold is thermodynamically unstable in air or water, and it reacts with oxygen spontaneously to form oxide layer. The native thin oxide layer can protect the underlying silicon from further oxidation. However, the optical property of the material is strongly modified after oxidation as the refractive index of SiO_2 is 1.4 while the refractive index of Si is only 3.5, thus the performance of optical biosensor vary as the degree of oxidation [70].

Another dissolution problem not only cause change in refractive index but also collapse of the porous matrix [70]. What's more, the high surface area of PSi may speed up the reaction. Thus the optical properties change with the time-dependent dissolution of the porous layer.

The stability of PSi can be greatly improved through several routes to create a hydrophilic $PSiO_2$ matrix, such as thermal oxidation [70, 71], surface alkylation [72], hydrosilysation [73], electrochemically treatment [44], chemically oxidation [66]. The Si-H bonds on the surface of PSi convert into Si-O bonds, resulting a optical stable material.

Thermal oxidation is chosen for its convenience of use. The freshly etched PSi samples are placed in a tubular furnace, heated at the required temperature, 400℃ or 800℃, for 1 hour with a constant O_2 flow of 1.8 L/min. They are then slowly removed to avoid thermal shock while cooling down.

3.2 Characterization of porous silicon

After the PSi samples are fabricated, their pore diameters and thickness are measured by means of scanning electron microscopy (SEM). The porosity and the thickness values are determined by optical characterization methods. The real-time detections of bacteria on the PSi-based biosensors are also accomplished by optical methods.

3.2.1 Scanning electron microscopy (SEM)

The pore morphology of PSi and the size of bacteria and lysate are characterized by high resolution SEM.

3.2.1.1 Principle

Scanning electron microscopy (SEM) is an electron-based powerful technology which utilizes the interactions of electrons with specimen to reveal the composition as well as the topographical information. Typically, it consists of several main components and each part has its specific function in the SEM system, ranging from the electron source (gun), a series of electromagnetic lens to condense and direct a beam, detectors to the displaying screen, shown in Figure 3.2 [74].

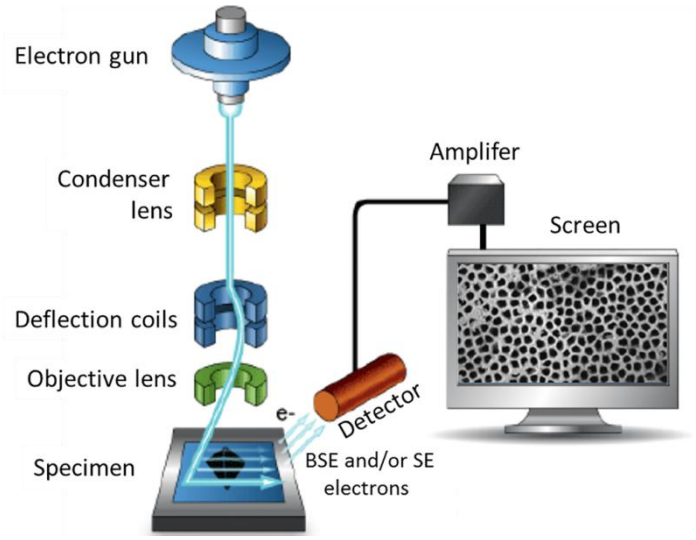

Figure 3.2 Schematic representation of a SEM [74].

In addition, high vacuum environment is required to avoid the contamination. The use of a focused beam of electrons distinguishes SEM from optical microscopy, producing images with high resolution at high magnification and providing other crucial information, for example, elemental information, and crystallography.

Typically, the electron beam is produced thermally from a filament and then accelerated by anode. When the electron beam strikes the sample under vacuum, the electrons penetrate inside it to nano/micro scale depths, depending on the energy of incident electrons and the atomic density of the specimen. They interact both elastically and inelastically with the solid, forming a limiting interaction volume from which four main signals will be generated: secondary electrons (SE), backscattered electrons (BSE), characteristic X-rays and visible light [75]. These signals can be collected by different types of detectors, among which secondary electrons and/or backscattered electrons are typically recorded to create an image, enabling topographical analysis of samples. This is the main purpose we used SEM in our work.

Due to the high vacuum working environment, materials containing water has to be dried prior to SEM investigation. The samples are also required to be conductive to avoid charge accumulation. For non-conductive materials, a thin conductive metal coating (several nanometers) has to be deposited by either sputtering or evaporation to improve image quality. Typical coating materials include Au, Pt, Pd and their alloys, as well as carbon.

In this work, the pore sizes of PSi are measured from the top view images and the thickness of PSi are measured from the cross-sectional SEM images.

3.2.2 Optical characterization

The reflectance spectrum of PSi films will display an optical interference pattern which refers to Fabry- Pérot fringes.

3.2.2.1 Optical setup description

The instrumentation used to collect the reflectance spectrum of a sample is composed of a spectrometer, a light source, a bifurcated optical fiber, a collimator, and a computer. A principle scheme of the optical characterization system is shown in Figure 3.3.

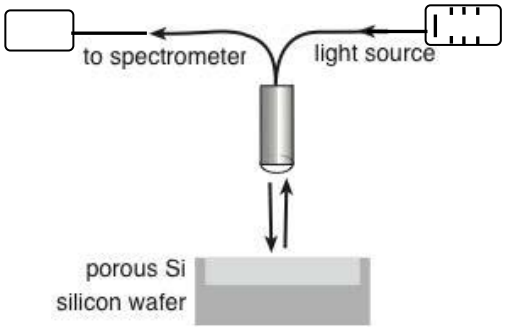

Figure 3.3 Schematic diagram of the optical set-up [15].

In this work, the Tungsten-Halogen light source providing a constant-intensity white light between 300 and 2600 nm is supplied by Thorlabs (US). The bifurcated optical fiber with 400 μm diameter fiber is purchased from Ocean Optics.

The computer program Oceanview 2.0 (Ocean Optics, US) is used to record the data. White light arrive at the surface of the sample through the optical fiber, then illumination of one spot on the surface and collection of reflected light are performed along the normal axis. As a result, the reflectance spectra collected by the spectrometer is recorded by the computer as a wavelength versus intensity plot.

3.2.2.2 Signal recording and FFT application

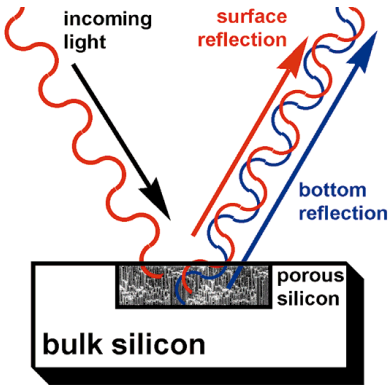

Figure 3.4 Scheme of the reflection in a PSi sample [14].

As shown in Figure 3.4, light is shone upon the PSi sample resulting in a multiple reflection from the PSi-medium (surface reflection) and PSi-bulk Si interfaces (bottom reflection), producing an interference pattern, which is called Fabry-Perot fringes and obeys the following equation :

$$m\lambda = 2n\mathrm{L}$$

A Fast Fourier transform (FFT) is then applied to the interference spectrum, thus providing intensity vs frequency information, and yields a peak whose position corresponds to the effective optical thickness 2nL (EOT) while the amplitude indicate the index contrast [21], as shown in Figure 3.5. The optical thickness of the film, the product of refractive index and film thickness are determined from the reflectance spectrum.

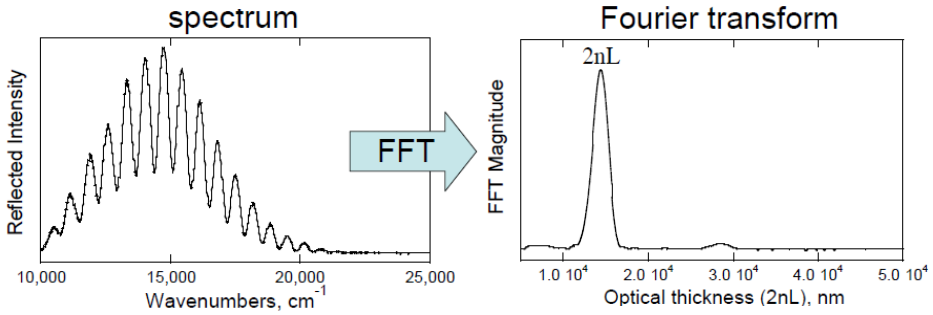

Figure 3.5 FFT of a reflectance spectrum [15].

The PSi-based biosensor monitor change in the refractive index induced by the penetration or binding of biomolecules such as DNA and proteins, as well as the changes in the intensity resulting from the light scattering by biological cells such as bacteria, manifesting itself in a shift of EOT or change in intensity, respectively.

3.2.2.3 SLIM method

Spectroscopic liquid infiltration method is a non-destructive method to determine the thickness and porosity of a PSi sample. SLIM is based on two reflectance spectra at the same spot, one of which is measured from the sample in air and the other in a liquid of known refractive index, as shown in Figure 3.6. The effective optical thicknesses (2nL) of both spectra are obtained, then fit to a two-components Bruggeman model, performing a least-squares fit of the two sets of data to determine both porosity and thickness [15].

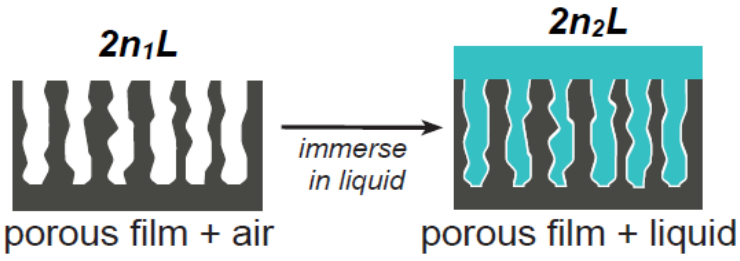

Figure 3.6 Scheme of SLIM [15].

In our experiment, pure ethanol with the reflective index of 1.3611 was used to determine the porosity of the PSi samples. After both the reflectance spectra were collected by the optical system, a program "Fringe_24_5" courtesy of Michael Sailor was used to compute the values, including the spectra load, FFT, fit of the data to the model. FFT of the spectra gives both the values of 2nL in air and in ethanol simultaneously, showing a peak shift caused from the change of refractive index by penetration of ethanol. Since the average refractive index of porous layer (n_{layer}) can be calculated and the reflective index of Si and ethanol are already known, the Bruggman effective medium approximation was applied to give the porosity and thickness.

In addition, the value of thickness obtained by SEM can be used to determine the best index for porous silicon.

3.2.2.4 Characterization over time

In this work, we need to monitor the change of EOT and intensity when the bacteria suspension and lysostaphin solution flow on the sensor surface, so the optical signal need to be record continuously. The sensor was placed in a custom-made flow cell, and then the flow cell was fixed to make sure they don't move during the whole process. For the bacteria detection, the PBS buffer, bacteria suspension and lysostaphin solution were injected into the flow cell system successively, while the reflect spectra of the same spot on the sensor surface were recorded every 10 s.

After one experiment finished, all the reflective data for this detection were analyzed by the program simultaneously to obtain the EOT and intensity change over time.

3.3 Bacteria preparation

The bacteria strains *Staphylococcus epidermidis* ATCC 35984 and *Escherichia coli* HTOO6 were used in this master thesis. The protocols of media preparation, bacteria strains inoculation, culture incubation, suspension preparation and detection were performed in ELI Institute Applied Microbiology (ELIM).

3.3.1 Bacteria culture media

To obtain the stationary phase of *S.e* ATCC 35984, Tryptic Soy Broth (TSB) and Tryptic Soy Agar (TSA) media were prepared and autoclaved at 121℃ for 15 min as soon as they were prepared, which has been proved as the best choice for the growth of *S.e.* ATCC 35984 in previous research.

Table 3.2 Composition of the TSB mixture used for the preparation of 1L of TSB liquid medium.

Tryptic	17.0 g	total weight: 30.0 g
Soy	3.0 g	
Glucose	2.5g	
NaCl	5.0 g	
K_2HPO_4	2.5 g	
pH	7.1-7.5	

The composition of the commercial TSB mixture is given in Table 3.2. The liquid medium was prepared by dissolving 30 g of the mixture in 1L of distilled water, then vortexing it to ensure a good homogeneity. 50 mL of medium were then transferred into 250 mL Erlenmeyers that were then used for bacteria incubation.

In addition, TSA plates were prepared by adding 1.5% agar to liquid TSB, that is 3.8g for each bottle containing 250 mL of TSB. As soon as the media were sterilized by autoclave, the warm solution was poured into clean Petri dish with appropriate volume and left on bench at room temperature for solidification. Normally 250 mL of medium are sufficient to prepare 12 Petri dishes. After one day, the TSA plates are stored at 4 ℃ in inverted position.

3.3.2 Buffer

Commercialized tablets were used for the preparation of Phosphate Buffered Saline (PBS) solution; their composition is given in Table 3.3. 0.01M PBS is obtained simply by diluting 1 tablet in 200 mL of distilled water. PBS is also sterilized by autoclave at 121℃ for 15 min as soon as it is prepared.

Table 3.3 Composition of the PBS mixture used for the preparation of 1L of PBS buffer.

NaCl	8.0 g
KCl	0.2 g
Na_2HPO_4	1.44g
K_2HPO_4	0.24 g
pH	7.2-7.4

3.3.3 Bacteria strains

The bacteria strains are placed in storage tubes filled with a sterilized mixture of 30% glycerol and 70% culture media, and stored at -80℃ in a refrigerator.

To proceed to a bacteria culture, the strain from the storage tube is spread onto a Petri dish filled with solid media and then incubated at 37 ℃ for 24h, leading to a formation of bacteria colonies are. This Petri dish is stored in a 4 ℃ refrigerator and refreshed every 2 weeks to keep the strain active and stationary.

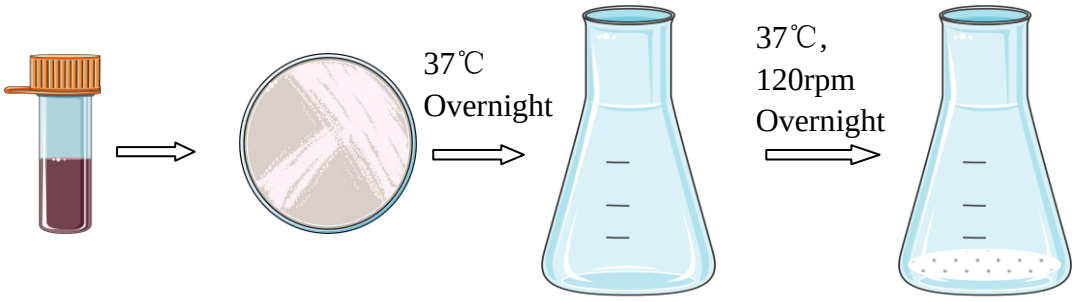

Figure 3.7 Scheme of bacteria culture.

Each day before the biosensing experiments, a bacteria culture prepared in a 250 mL Erlenmeyer flask containing 50 mL of TSB. A single colony from the TSA Petri dish inoculated into TSB media using an inoculating loop. The Erlenmeyer is then fixed in a shaking incubator at 120 rpm and 37 ℃, for 16~18h. The general protocol of bacteria culture is shown in Figure 3.7.

3.3.4 Preparation of bacteria suspension

Bacteria suspensions in PBS buffer are prepared for the flow cell experiment. The bacteria culture is rinsed by PBS to remove all the nutriment by repeating centrifugation, supernatant removal and resuspension process twice as shown in Figure 3.8:

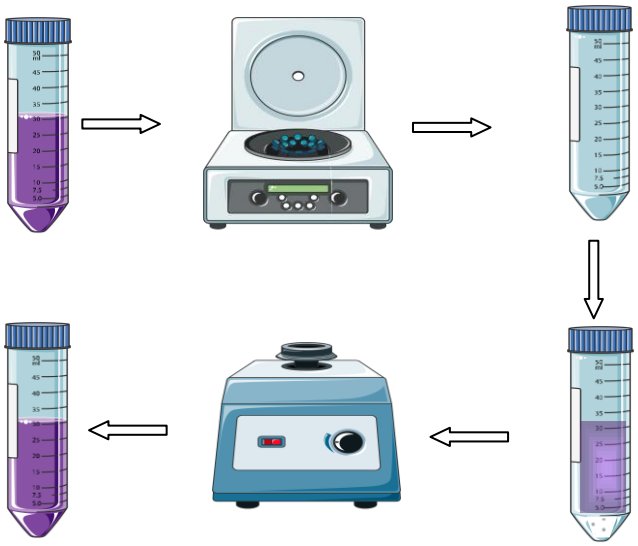

Figure 3.8 Preparation of bacteria suspension.

1) Stationary phase culture of *S.epidermidis* ATCC 35984 is prepared.
2) One falcon (50 mL standard centrifuge tube) containing 40 mL of bacteria solution, as well as one falcon containing 40 mL water with precisely the same weight, are centrifuged for 20 min at 10000 rpm, 4℃.
3) The supernatant of bacterial culture is discarded and the bacteria pellet is kept (all the bacteria are concentrated at the bottom).
4) 40 mL of PBS is added and the total weights of 2 falcons are modified to keep them in balance.
5) The falcon is then vortexed to resuspend the bacteria in solution and obtain an homogeneous distribution.
6) Centrifuge again as step 2.
7) The supernatant is discarded and the bacteria are resuspended in PBS.

In order to obtain different concentration of bacteria solutions for the biosensing application, the original suspensions are diluted by a factor of 10, 10^2, or 10^3. Bacteria suspension at 10^6 CFU/mL is prepared by adding 0.4mL of the original bacteria solution in 39.6 mL of PBS, while 10^7 CFU/mL bacteria suspension is prepared by diluting 4 mL of the original bacteria solution in 36 mL of PBS. Then real number of bacteria suspension used in each experiment is assessed by counting the CFU (Colony Forming Unit) per mL.

3.3.5 Bacteria counting

The number of bacteria in a suspension is estimated by visible colonies formed on TSA after appropriate incubation. First the suspension is ten-fold diluted in PBS and then 100 μL of series dilutions are spread on the surface of media. After incubation at 37 ℃ for 24h, the number of colonies is counted only on Petri dish whose number is larger than 15 and smaller than 200. The final number of bacteria is calculated by following equation, where n is the number of Petri dish taken into account:

$$\mathrm{CFU}/_{\mathrm{mL}} = \sum_{i=1}^{n} \left(\frac{\mathrm{number\ of\ colonies}/_{\mathrm{plate}} \times \mathrm{factor\ of\ dilution}}{0.1\ \ \mathrm{mL}/_{\mathrm{plate}}} \right) \times \frac{1}{n}$$

3.3.6 Bacteria lysis

Top-agar experiment is used to detect the bacteria lysis with lysostaphin of different concentration. Some liquid LB media containing 0.8% agar mixed with a solution of bacteria culture is poured onto the surface of LB plate to form a thin layer. It is left at room temperature for about 20 min in order to solidify. Then 10 μL of lysostaphin solution of decreasing concentration 20 μM, 10 μM, 5 μM, 2 μM, 1 μM, 0.5 μM, 0.25 μM, 0.1 μM, 0 μM (only PBS) is added to the surface of media and marked (Figure 3.9).

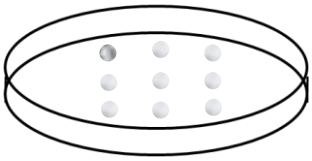

Figure 3.9 Scheme of Top agar experiment.

The plate is incubated at 37℃ overnight. Formations of negative colony, which indicate the lysis of bacteria, are observed.

3.4 Bacteria and lysate measurements

SEM was also used to measure the size of bacteria and their lysate. However, the samples could not be directly observed in their natural state as the water in the bacteria rapidly evaporate in the condition of high vacuum and bring distortion to the result. So the bacteria should be fixed, dehydrated, dried and coated with gold before SEM observation.

A 2.5% glutaraldehyde solution is used to fix the bacteria cells and their lysate on the substrates. They are prepared by diluting 2.5 mL glutaraldehyde solution (50%) in 47.5 mL PBS buffer.

Since the original bacterial suspension is highly concentrated, a 100-fold dilution in PBS is performed for the experiments.

Both dynamic and static conditions were used, with the only difference being that the dynamic experiments are performed in flow cell and the static experiments are performed in triplicate in 12-wells plate.

The dynamic experiments were performed in 3 flow cells based on the following protocol:

1) The flow cell systems were assembled, autoclaved and dried.
2) Three clean Si wafer of 1×1 cm were placed in flow cells as substrates. The flow cells were placed in a chamber at 37 ℃.
3) The whole system was filled with PBS.
4) The adequate solution was injected in the flow cell during 20 minutes with a flow of 0.615 mL/min at 1.85 rpm. PBS was injected in the first flow cell as the negative control, the bacteria suspension in the second and third flow cells with the second flow cells acting as the positive control, while the bacteria in the third flow cell will be lysed.
5) The system was then rinsed with PBS for 1 h at 0.615 mL/min at 1.85 rpm.
6) A 1 μM solution of lysostaphin was then injected and left to react with the bacteria for 30 min in the third flow cell.
7) The third flow cell was rinsed at a flow rate of 0.615 mL/min with PBS for 20 min.
8) The glutaraldehyde solution was then injected in all the flow cells, the solution was renewed once after 30 min but otherwise no flow was applied.
9) After 30 min, the system was rinsed at 0.615 mL/min with PBS for 20 min and the

samples were removed from the flow cell.

10) The samples were then transferred in a 12-wells plate and dehydrated in ethanol solutions with an increasing concentration: 25%, 50%, 75% and absolute 99.99%. The samples were immersed in each solution for 15 min.
11) The samples were dried in an incubator at 58℃ overnight then stored in an dessicator.
12) The samples were coated with a 10 nm gold layer before SEM observation.

For the static conditions, the protocol is the following:

1) Clean Si wafer were used as substrates and placed in a well.
2) 3 mL of bacterial suspension was added to the first well as positive control, 3 mL of PBS was added to the second well as negative control, and a lysate solution, previously incubated for 1 hour at 37 ℃ under constant agitation ,containing 1 mL of bacteria solution and 50 µL of 20 µM lysostaphin was added to the third well.
3) The 12-wells plate was incubated at 37 ℃ during 1 h.
4) The samples were rinsed with PBS 5 times.
5) A 2.5% glutaraldehyde solution was injected in each well and left to react for 1 h.
6) The glutaraldehyde was removed and the samples were rinsed with PBS three times.
7) The samples were then dehydrated by immersing them in solution with increasing ethanol concentration: 25% in DI water, 50%, 75%, and 99.99 % for 15 min each.
8) The samples were dried in an incubator at 58℃ overnight then stored in a desiccator.
9) The samples were then coated with a 10 nm gold layer before SEM characterization.

3.5 Bacteria detection experiments

The oxidized PSi samples are placed in a custom-made flow cell. The whole flow cell system consists of glass bottles, plastic caps, filters, long pipes, pump, flow cell and temperature conditioner. According to the requirement of our experiments, the number of bottles and pipes, the volume of solutions, the size of filters as well as the connection can be adjusted (Figure 3.10).

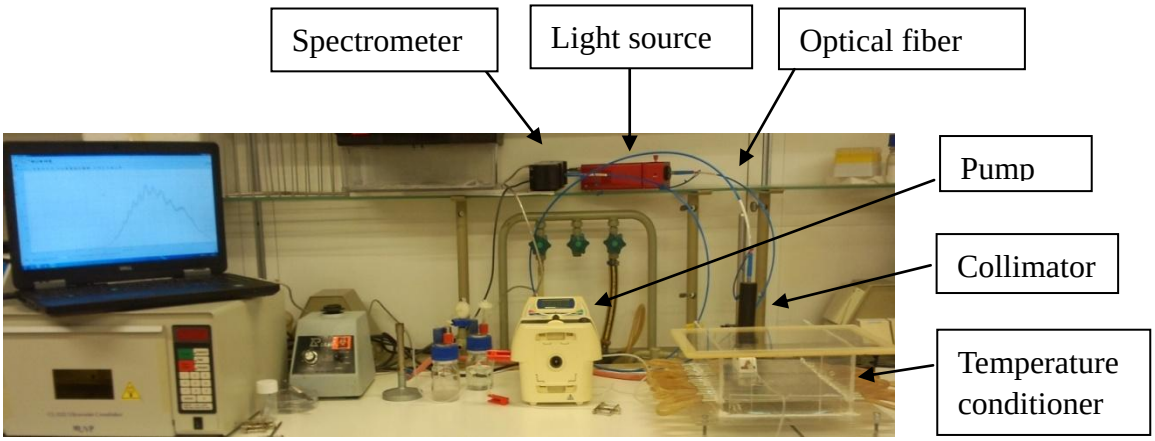

Figure 3.3 Photo of the optical characterization system.

PBS solution is first delivered in the system prior the measurement to remove the air from the pipes, and then the flow cell is fixed with tape in the temperature conditioner system to ensure that the sample reflectance spectrums are measured at the same spot during the whole measurement at 37℃. The PBS and bacterial suspension is flown at 1.85 rpm (0.615 mL/min) under optical measurements.

Usually one day before the flow cell experiment, the bottles, caps and filters are assembled and sterilized in autoclave and then the dried at 58 ℃ in an incubator. Also after the experiment, the system should be decontaminated in autoclave and then disassembled. In addition, the plastic pipes need to be rinsed with DI water, then ultrasonicated and finally rinsed with Milli-Q water. Besides, the pipes should be renewed every 2 weeks to avoid contamination.

3.5.1 Negative control

As the bacteria cells and lysostaphin used in this work are all suspended in PBS buffer, so the optical readout stability of PSi samples freshly etched and oxidized at 400℃and 800℃ is measured under flow conditions by long buffer flow experiments of several hours. The samples are placed in a flow cell, in which the PBS solution is delivered at 1.85 rpm for 5 h and the reflectance spectra are recorded every 10 s.

3.5.2 Positive control

It is generally believed that the bacteria cells secret some kinds of proteins during the overnight incubation, so there are some proteins left in the supernatant when we do the culture centrifugation. As the size of most proteins is considered to be in the range of a few nm, they would be capable of penetrating into the pores of our PSi substrate. It would be interesting to use the supernatant as the positive control to detect the infiltration properties of the sensor.

The experiment was performed by collecting 40 mL of supernatant, which contains some proteins in the media solution, after centrifugation. The positive control experiment is accomplished by flowing the PBS for 30 min and then the supernatant for 30 min into the flow cell, finally the flow cell is rinsed with PBS for 30 min. The flow rate used is 1.85 rpm during the whole 90 min and the reflectance spectra are recorded every 10 s.

3.5.3 Bacteria detection

Fresh bacteria suspensions are prepared just before the flow cell experiment.

The bacteria detection is accomplished by flowing the PBS for 30 min first and then the bacteria suspension for 60 min into the flow cell at 37 ℃, finally the system is rinsed with

PBS for 30 min. The flow rate sued is 1.85 rpm during 2h and the reflectance spectra are recorded every 10 s.

To ensure the accuracy of the results, every experiment is repeated in the same condition and the number of bacteria is counted.

3.5.4 Lysate detection

For this experiment, the lysostaphin with a constant concentration of 1 μM is applied to lyse the bacteria on the surface of sensors. Normally, the stocks stored in -20℃ are took out at the beginning of the experiment, so they would melt at room temperature, after that they are suspended in PBS buffer to reach the desired concentration.

After flowing the bacterial suspension as described in 3.4.3, 3 mL lysostaphin solution is flown at 1.85 rpm for 4.5 min to reach the flow cell and then the flow rate is decreased to 0.18 rpm for 40 min to allow the bacteria lysis.
Since the lysostaphin itself is a small protein, it can also penetrate into the pores with the lysate. A control experiment is then carried out by injecting the lysostaphin solution at 1.85 rpm for 4.5 min and then 0.18 rpm for 40 min after flowing PBS solution for 90 min. Finally the system is rinsed with PBS for 30 min at 1.85 rpm. The reflectance spectra are recorded every 10 s during 165 min.

3.5.5 Selectivity of the detection

In order to study the selectivity of the sensor, a 10^7 CFU/mL *E.coli* suspension in PBS is used in this work.

For convenience, the strain *E.coli* HT006 is incubated using the same medium as *S.epidermidis* and the bacterial suspension is prepared using the same procedure. Since the concentration of the original *E.coli* suspension is about 10^9 CFU/mL, 0.4 mL of the original *E.coli* suspension is added to 39.6 mL of PBS to reach a desired concentration of 10^7 CFU/mL.

For the first detection experiment, 40 mL of 10^7 CFU/mL *E.coli* suspension is used instead of *S.epidermidis,* and the process is the same as described in section 3.4.4. The precise number of *E.coli* is counted by spreading the bacteria on TSA plates.

In the second detection experiment, a mixture of 20 mL of 10^7 CFU/mL *E.coli* and 20 mL of 10^7 CFU/mL *S.epidermidis* suspension is applied. The number of *E.coli and S.epidermidis* are counted, seperately.

The reflectance spectra of both experiments are recorded every 10 s during 165 min.

Table 3.4 Summary of bacteria detection experiments

No.	solution	Bacteria concentration (CFU/mL)	lysostaphin
1	PBS	—	—
2	supernatant	—	—
3	*S.e*	10^8	—
4	*S.e*	10^7	—
5	*S.e*	10^6	—
6	*S.e*	10^8	+
7	*S.e*	10^7	+
8	*S.e*	10^6	+
9	*S.e and E.coli*	10^7 10^7	+
10	*E.coli*	~10^7	+

All the bacteria detection experiments are summarized in Table 3.4, including the control detection, bacteria detection, lysate detection and the selective detection of *E.coli*. The Fabry-Pérot fringe patterns in these experiments are monitored by Oceanview program and the data are saved as txt files. After that FFT of the reflective spectra is performed by program “Fringe_24_5”, at last the figures are draw by Origin.

Appendix 1: Materials

Highly doped P^{++} type Si wafers (0.0008-0.0012 Ω·cm resistivity, <100>-oriented, Boron-doped) were purchased from Sil'tronix Silicon Technologies (France). Aqueous HF (49%) and isopropanol were purchased from Chem-Lab (Belgium) and ethanol absolute was supplied by VWR Chemicals (Belgium), Potassium hydroxide (KOH) and Glutaraldehyde solution (50%) was obtained from Sigma-Aldrich Chemicals (Belgium). All reagents are of analytical grade and used as received.

The TSB (Tryptic Soy Broth) powder was purchased from Biorad (UK), the PBS (Phosphate Buffered Saline) tablets were supplied by Sigma-Aldrich Chemicals (Belgium). Glycerol was purchased from Merck (Germany). The media are prepared by dissolving TSB powder in distilled water and the buffer are prepared by dissolving PBS tablet in ultrapure water (18.2 $M\Omega\ cm^{-1}$) which is purified by a Milli-Q system from Millipore Co.

The lysostaphin from staphylococcus staphylolyticus was purchased from Sigma- Aldrich. Commercialized lysostaphin was diluted in 1 mL of PBS supplemented with 30 % of glycerol (700 µL PBS + 300 µL glycerol), and transferred into 50 µL aliquots stored at -20 ℃. Working solutions were prepared by adding 950 µL of PBS to 50 µL of stock solution (20 µM) yielding a 1µM lysostaphin solution.

The bacteria strains *Staphylococcus epidermidis* ATCC 35984 and *Escherichia coli* HTOO6 were supplied by Prof. Mahillon in bio-engineering faculty.

The custom-made flow cell system is supplied by Catherine Nannan in the bio-engineering faculty.

4 Results and discussions

4.1 PSi fabrication

In order to fabricate a distinct PSi film, it is important to find out the dependence of the pore morphology on the etching current density. PSi samples etched with different current density from 5 mA/cm^2 to 200 mA/cm^2 have been prepared and their morphology was measured by SEM and optical method. According to the results, PSi etched with a current density 200mA/cm^2 is selected for the next biosening applications. After that the pore diameter and porosity of samples with and without a sacrificial layer are compared.

4.1.1 Different current density

The cross section of PSi layer is characterized by SEM and the thickness is measured simultaneously as shown in Figure 4.1. All PSi samples with different current density from 5 mA/cm^2 to 200 mA/cm^2 create straight and smooth mesopores.

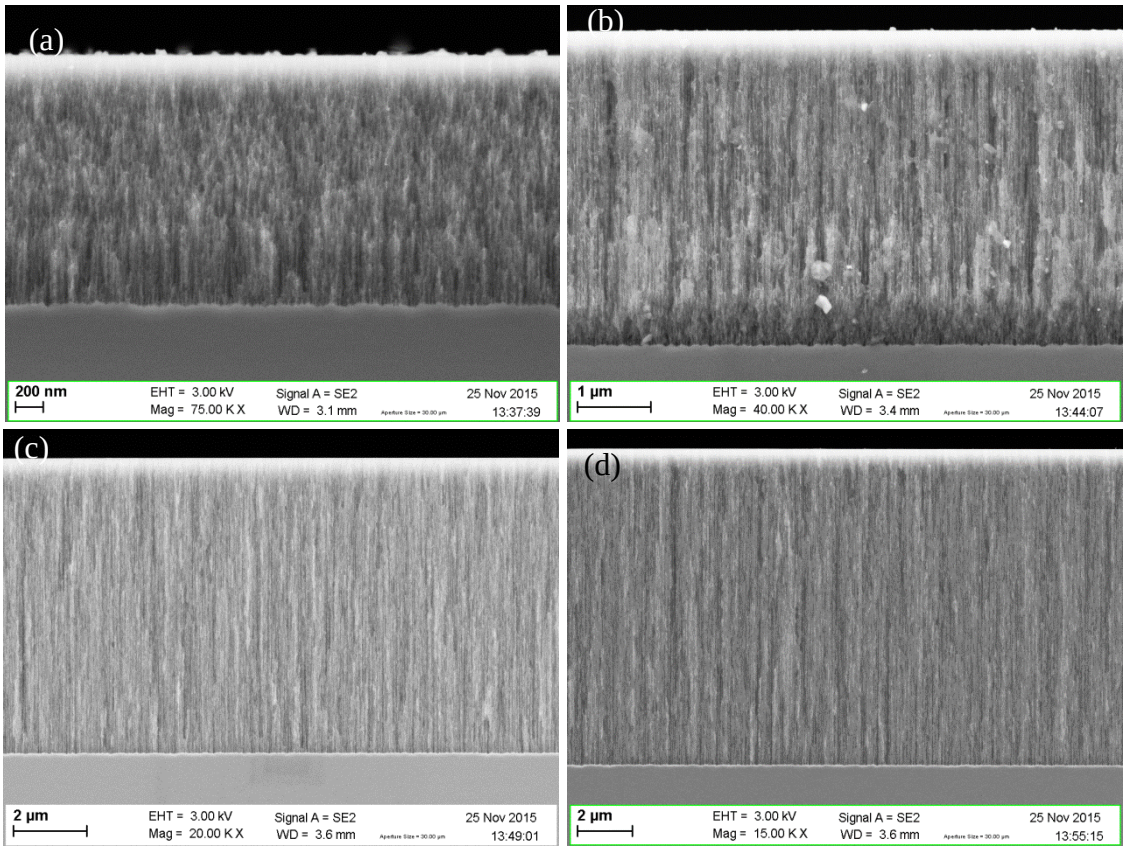

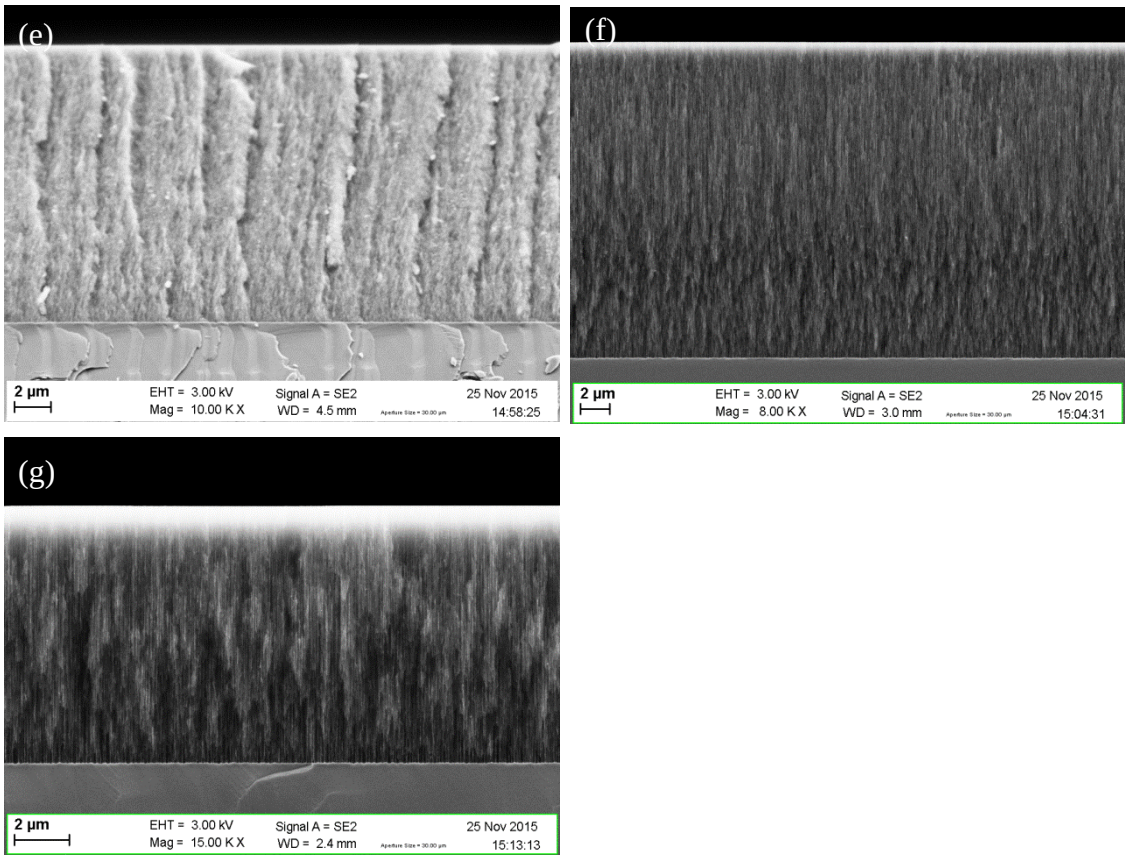

Figure 4.1 Cross-sectional SEM images of freshly etched PSi layers at different current densities: (a) 5 mA/cm^2 for 600 s; (b) 25 mA/cm^2 for 300 s; (c) 50 mA/cm^2 for 300 s; (d) 75 mA/cm^2 for 300 s; (e) 100 mA/cm^2 for 300 s; (f) 150 mA/cm^2 for 300 s; (g) 200 mA/cm^2 for 100 s.

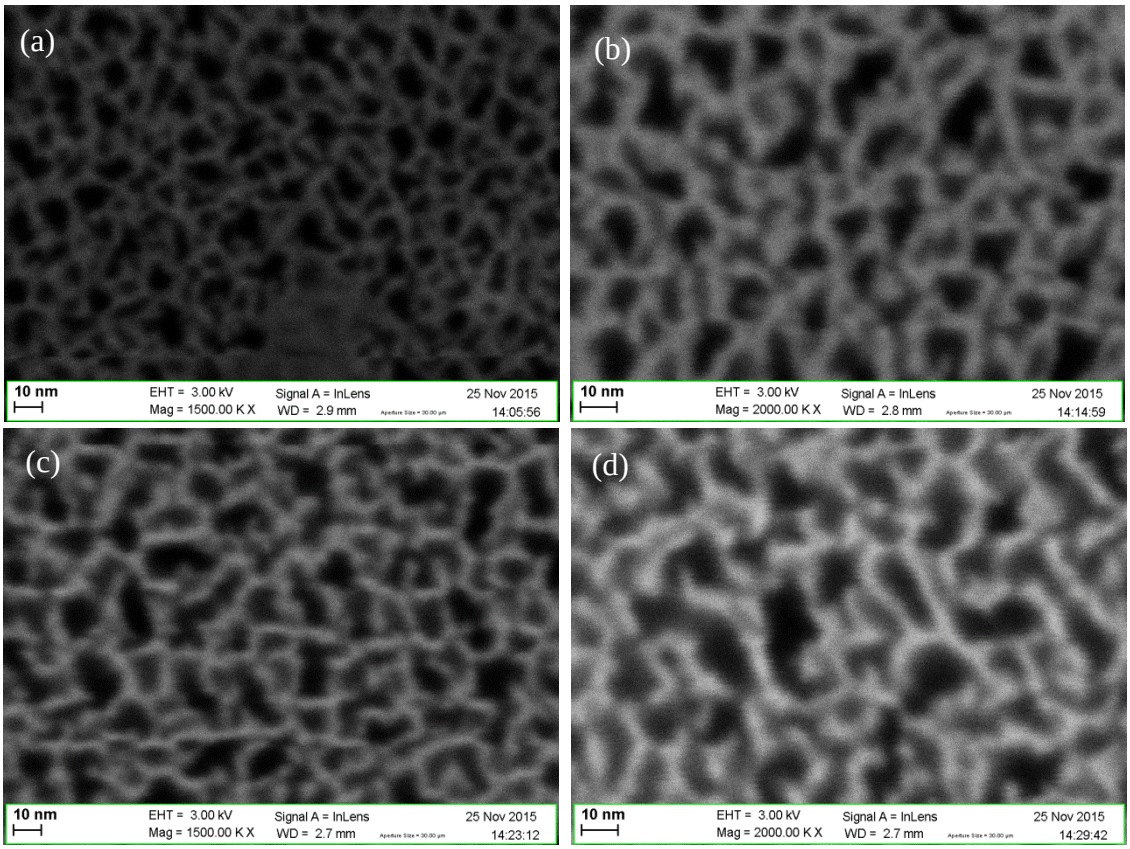

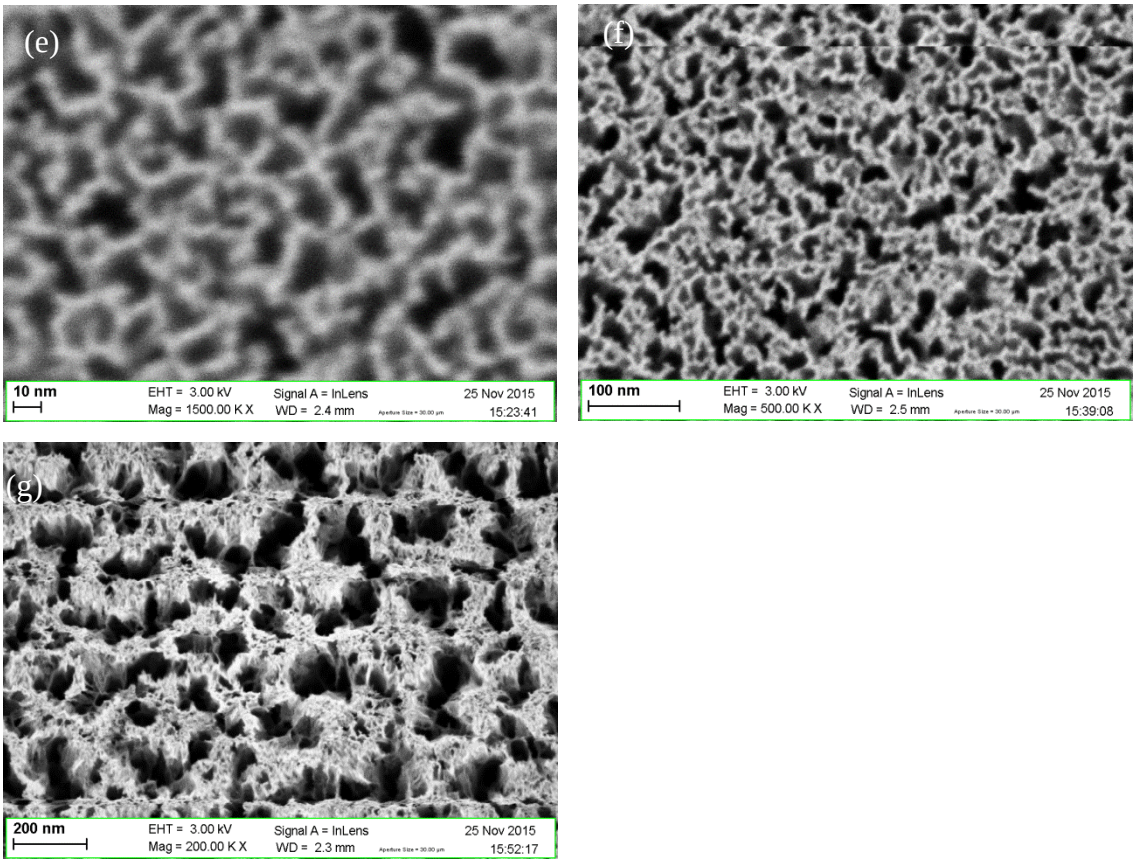

Figure 4.2 SEM images of the surface of freshly etched PSi layers at different current densities: (a) 5 mA/cm^2 for 600 s; (b) 25 mA/cm^2 for 300 s; (c) 50 mA/cm^2 for 300 s; (d) 75 mA/cm^2 for 300 s; (e) 100 mA/cm^2 for 300 s; (f) 150 mA/cm^2 for 300 s; (g) 200 mA/cm^2 for 100 s.

Front sides of PSi films are shown in Figure 4.2. By increasing the current density, the pore diameter increased from a maximum pore size of 10 nm to 90 nm range. With low current density from 5-50 mA/cm^2, approximately round pores are formed as shown in Figure 4.2a-d. As the current density increases, elliptical pores are formed and it is seems like they are formed by a few adjacent pores connected to each other as shown in Figure 4.2 d-g.

Table 4.1 Thickness and pore size of PSi measured by SEM.

No.	Current density (mA/cm^2)	Etching time (s)	Thickness (μm)	Etching rate (μm/s)	Pore size (nm) (sample)
1	5	600	1.9	0.0032	10.7
2	25	300	4.3	0.014	12.0.
3	50	300	8.1	0.027	11.8.
4	75	300	11.6	0.0387	12.5 [26.6, 14.3]
5	100	300	15.2	0.0507	15.3 [26.1, 10.4]
6	150	300	21.7	0.0723	43.6 [55.1, 46.3]
7	200	100	9.4	0.094	91.4 [80.9, 34.3]

The thickness and pore diameter data are summarized in Table 4.1. For the pore size measurement, a few representative pores in the images are selected and the average value of their diameter is calculated. The length and width of the elliptical pores are also present between brackets.

Table 4.2 Thickness and porosities of PSi measured by SLIM

No.	Current density (mA/cm^2)	Etching time (s)	Thickness (μm)	Porosities (%)
1	5	600	1.821	52.9
2	25	300	4.310	56.7
3	50	300	8.09	66.0
4	75	300	11.54	71.8
5	100	300	15.17	76.2
6	150	300	21.68	81.5
7	200	100	9.367	84.0

The thickness and porosities of PSi samples are also investigated by SLIM as shown in Table 4.2. The thickness of PSi obtained by optical method is pretty close to the data obtained by SEM in Table 4.1. Besides, by increasing the current density, the porosities increased from 52.9 % to 84 %.

When the thickness data of the seven samples are investigated, it is found that the etching rate is propotional to the current density. By increasing the current density from 5 to 200 mA/cm^2, the etching rate which is equal to how thick pore layer is etched per second increased from 3.2 nm/s to 94 nm/s, and the linear relationship is present in Figure 4.3.

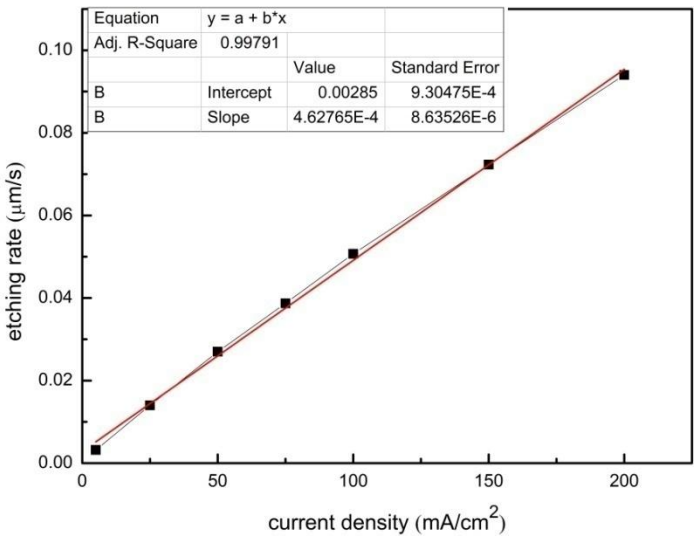

Figure 4.3 Dependence of etching rate on the current density.

At last, PSi film with a current density 200 mA/cm^2 is selected for bacterial detection experiments. Indeed, the pore size of about 90 nm is large enough to allow the lysate of bacteria to penetrate as shown in section 4.2.2.

4.1.2 PSi with sacrificial layer

During the characterization of PSi surfaces by SEM, some unexpected images, as shown in Figure 4.4, drew our attention. For sample No.6, which is etched with a current density of 150 mA/cm^2, the top layer is peeled off partially from the sample surface so the underneath mesopores are exposed. As shown in Figure 4.4 b, most pore sizes are in the range of 35-55 nm with a minimum size of approximately 15 nm in diameter.

The morphology of the underneath layer is different from the top layer, as the pore-walls become thinner and the pores have larger openings. These openings would be more advantageous for biomolecules penetration into the mesoporous layer. It would thus be interesting to be able to remove the whole "crust" layer. A convenient way to pattern the wafer surface prior to its porosification is then introduced into the fabrication of PSi. A sacrificial layer is first etched under the desired current density (200mA/cm^2, 30s) then is dissolved by KOH solution completely.

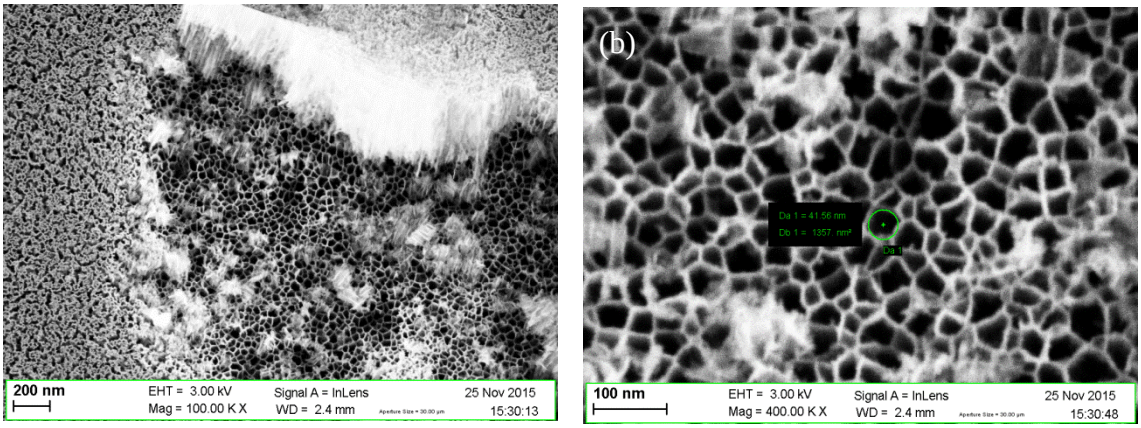

Figure 4.4 Top views of PSi film etched with a current density 150mA/cm^2: (a) A "crust" layer is partly removed so the pores underneath are exposed; (b) the mesopores under the crust layer are measured.

PSi samples with and without the sacrificial layer are prepared at the same time, using the same Si wafer, the same electrolyte composition, the same current density and etching time. Their morphologies are compared below. In Figure 4.5 (a) and (b), even though there are elliptical pores as large as 100 nm in length, there are still many irregular pores as small as a few nm. Conversely, most pores in Figure 4.5 (c) and (d) are round, in the range of 100 nm to 200 nm in diameter, with a few pores as small as 20-30 nm.

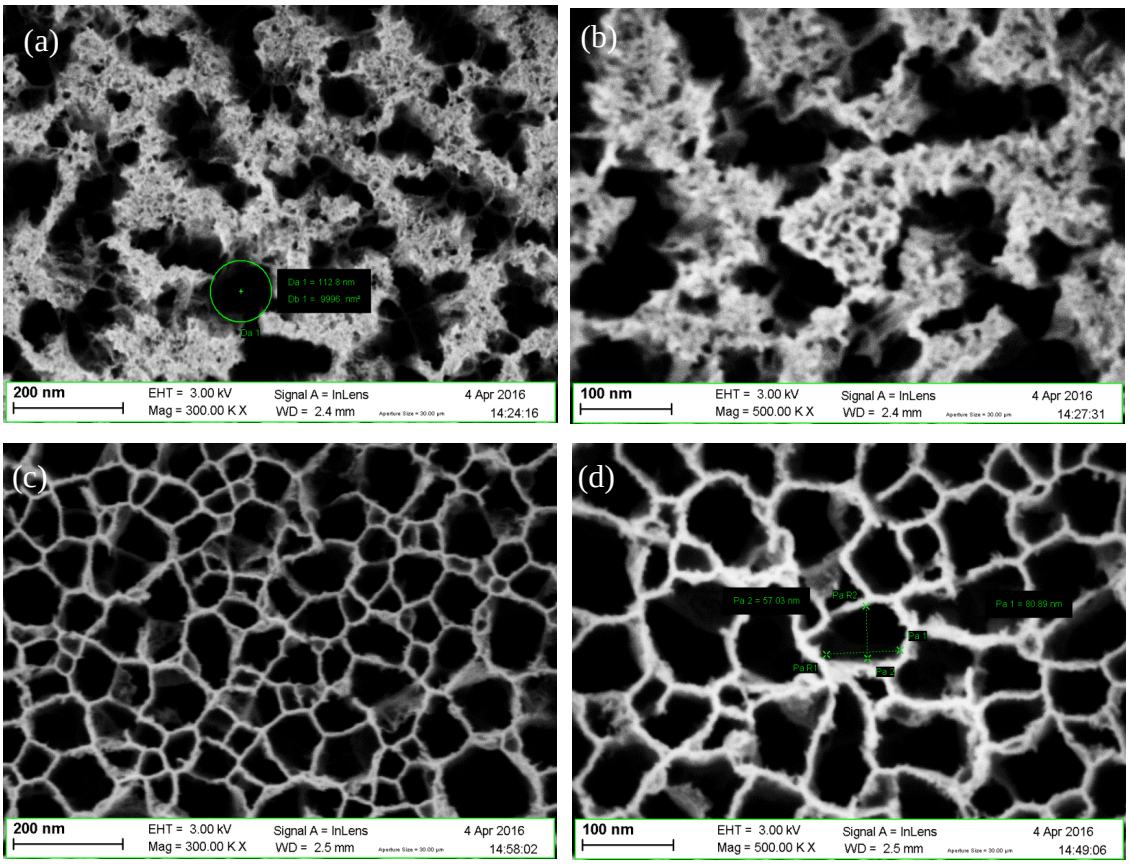

Figure 4.5 Top view SEM images of PSi sample etched at: (a) (b) 200 mA/cm^2 for 50 s without a sacrificial layer; (c)(d) 200 mA/cm^2 for 50 s with a sacrificial layer which is removed by KOH prior the etch.

Table 4.3 Comparison of PSi with and without a sacrificial layer.

Properties	200mA/cm^2, 50s	Sacrificial layer _ 200 mA/cm^2, 50s
Average thickness (L)	2913 nm	2893 nm
Average porosity	83.15%	87.15%
Average index of layer in air (n)	1.2348	1.1705
Average Pore size	30~50 nm	80~100 nm

As two parallel samples are prepared at each condition, both of their thickness, porosity, index of layer in air, pore size are measured by combination of SEM and optical method, shown in Table 4.2. After introduction of sacrificial layer, the porosity increased. What's more important, the pore diameter of PSi with a sacrificial layer increased by approximately 50 nm, and this is because pores are completely open. These pores are round instead of elliptical so they should allow a more effective biomolecule penetration.

4.2 Bacteria experiment

For the bacteria detection, two bacteria strains were cultured and counted first to make sure stationary-state *S.epidermidis* and *E.coli* were obtained. A top agar experiment was also performed to ensure the activity of the lysostaphin against *S.epidermidis*. *S.epidermidis* and the products of its lysis were characterized by SEM to assess the possibility of penetration of the lysate into the porous layer.

4.2.1 Bacteria culture and lysis

After overnight incubation, *S.epidermidis* ATCC 35984 and *E.coli* HTOO6 were inoculated to Petri dishes with TSA medium as shown in Figure 4.6. Bacterial colonies of *S.epidermidis* look white and round, while colonies of *E.coli* are light yellow, and are a few times bigger than *S.epidermidis* when prepared in the same condition.

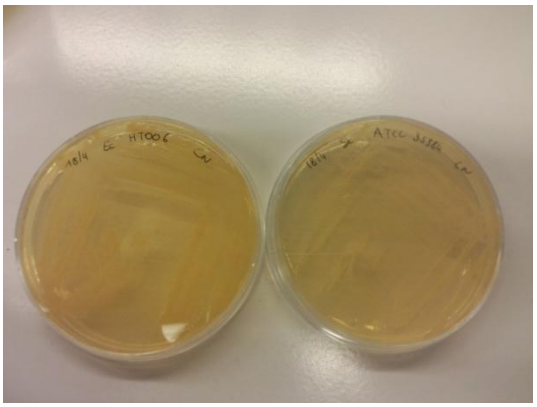

Figure 4.6 *S.epidermidis* and *E.coli* colonies on Petri dish with TSA medium.

The suspensions of both bacteria in PBS were prepared and their numbers counted on plates. The stationary phase culture of *S.epidermidis* results in a concentration of 9.8×10^8 CFU/mL, while for *E.coli* a concentration 5.2×10^9 CFU/mL was obtained. These values only give an approximate concentration for the original bacterial suspensions and help to determine the dilution factor needed for the preparation of bacterial solutions used in the bacteria detection experiments. This is explained by the fact that the growth is strongly dependent on the environment thus resulting in varying final concentration. It is then necessary to count the bacteria when we prepare bacterial suspension for each single experiment.

Lysis of *S.epidermidis* is controlled by performing top agar experiment, as the result show in Figure 4.7.

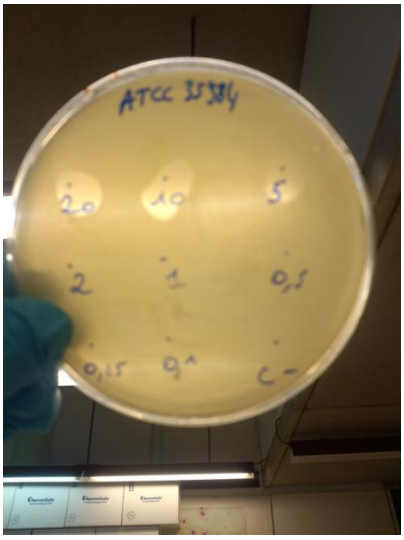

Figure 4.7 Top agar experiment.

Lysostaphin solutions with a concentration ranging from 0.1 µM to 20 µM was added to a TSA plate with an agar-*S.epidermidis* film previously spread. After incubation, the bacteria are totally lysed by lysostaphin for the concentrations of 20 µM, 10 µM and 5 µM, and just partly lysed by lysostaphin with the concentrations of 2 µM and 1 µM, but can not be lysed by lysostaphin with lower concentration.

In this experiment, the original bacterial suspension of 10^8 CFU/mL was used. The number of bacteria to be lysed is then higher than the number of bacteria that would adhere on the surface of a sample in a flow cell. We then make the hypothesis that a concentration in lysostahin of 1 µM is enough for biosensing applications. This application is supposed to be correct as N. Couniot [75] used the same concentration for the lysis of *S.epidermidis*.

4.2.2 Size of bacteria cells and lysate

Based on SEM images, the size of bacterial cells and lysate were measured. The experiments were performed in static condition (Figure 4.8 and 4.9) and dynamic condition (Figure 4.10).

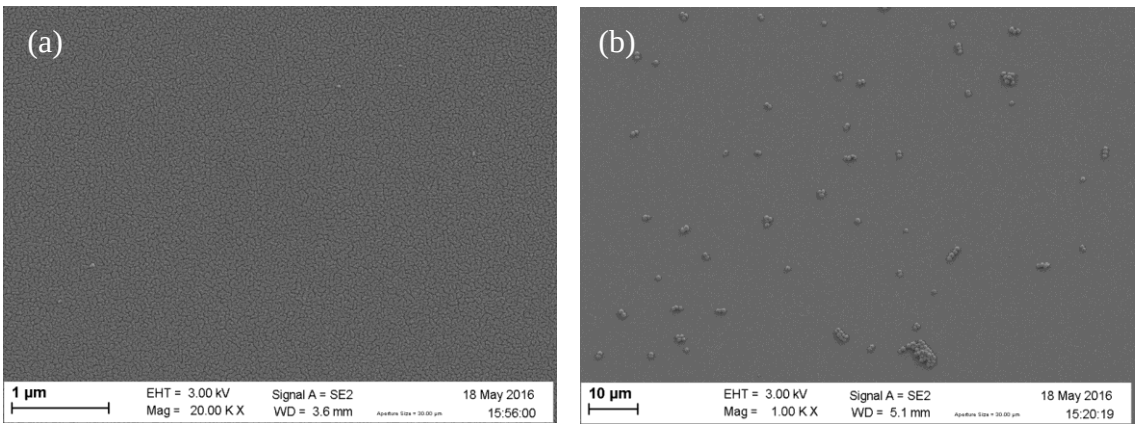

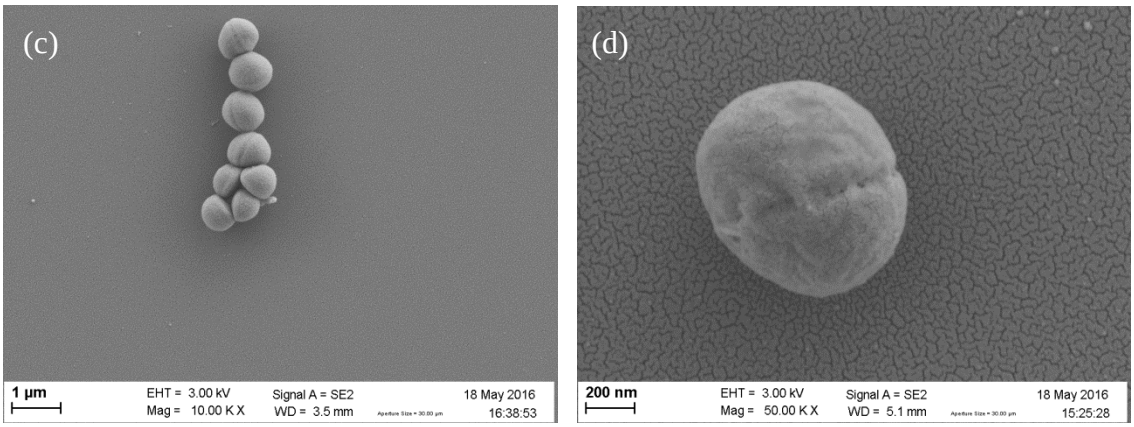

Figure 4.8 SEM images of (a) substrate and (b)(c)(d) *S.epidermidis* in static condition.

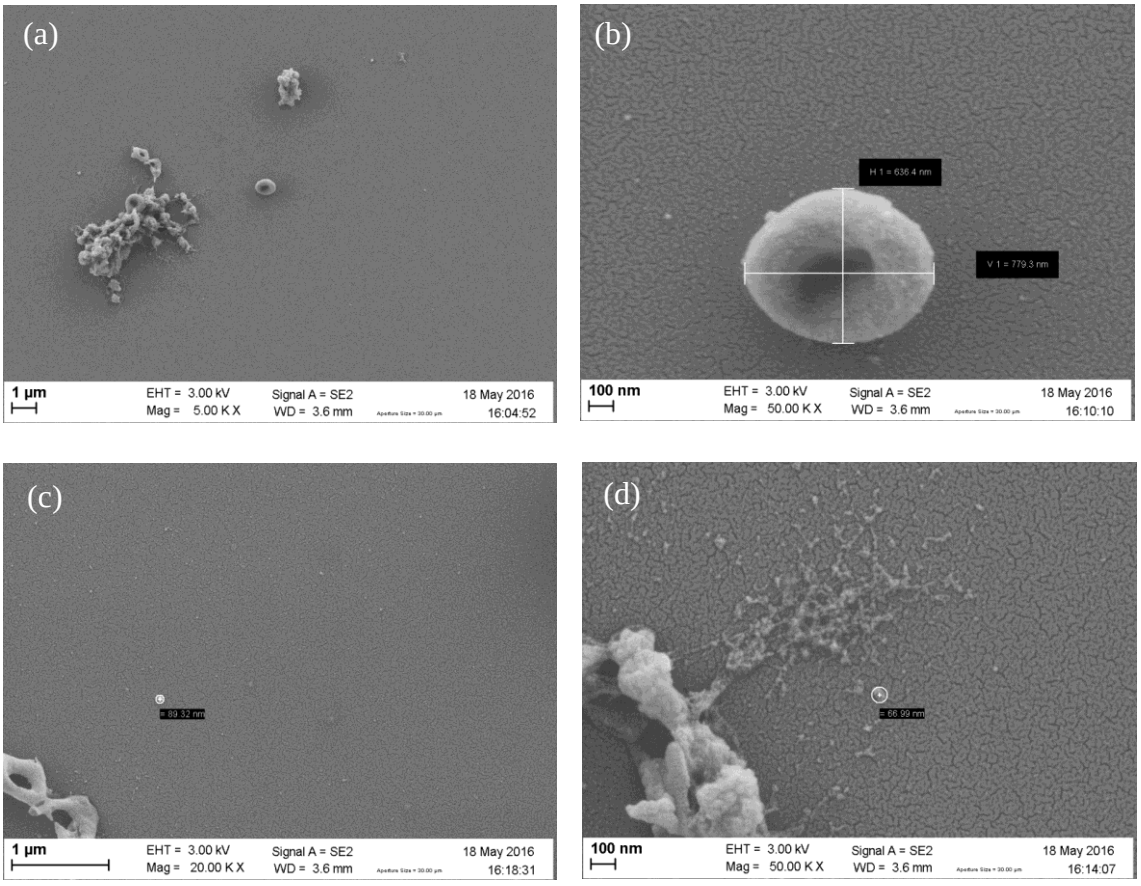

Figure 4.9 SEM images of lysed bacteria in static condition.

The morphology of *S.epidermidis* in static condition is observed (Figure 4.8). The bacterial cells are sphere and look like cluster of grapes, equally distributed. What's more, there is a dent in the central of the bacteria cells for most bacteria, which is considered as the results of mitosis process when the cell divides into two daughter cells. The average size of bacteria is about 1 µm. For example, the bacterium cell in Figure 4.8 (d) is 920 nm in diameter.

The lysed bacteria are shown in Figure 4.9. The cluster of bacteria does not burst completely but just collapse (Figure 4.9 a). For instance, the cupped bacteria cell in Figure 4.9 b is about 700 nm in diameter. However, the lysate from the broken cells are much smaller than 100 nm, for example the particles shown in Figure 4.9 (c) and (d) are 89 nm and 67 nm, respectively. Additionally, some particles smaller than 30 nm have been observed.

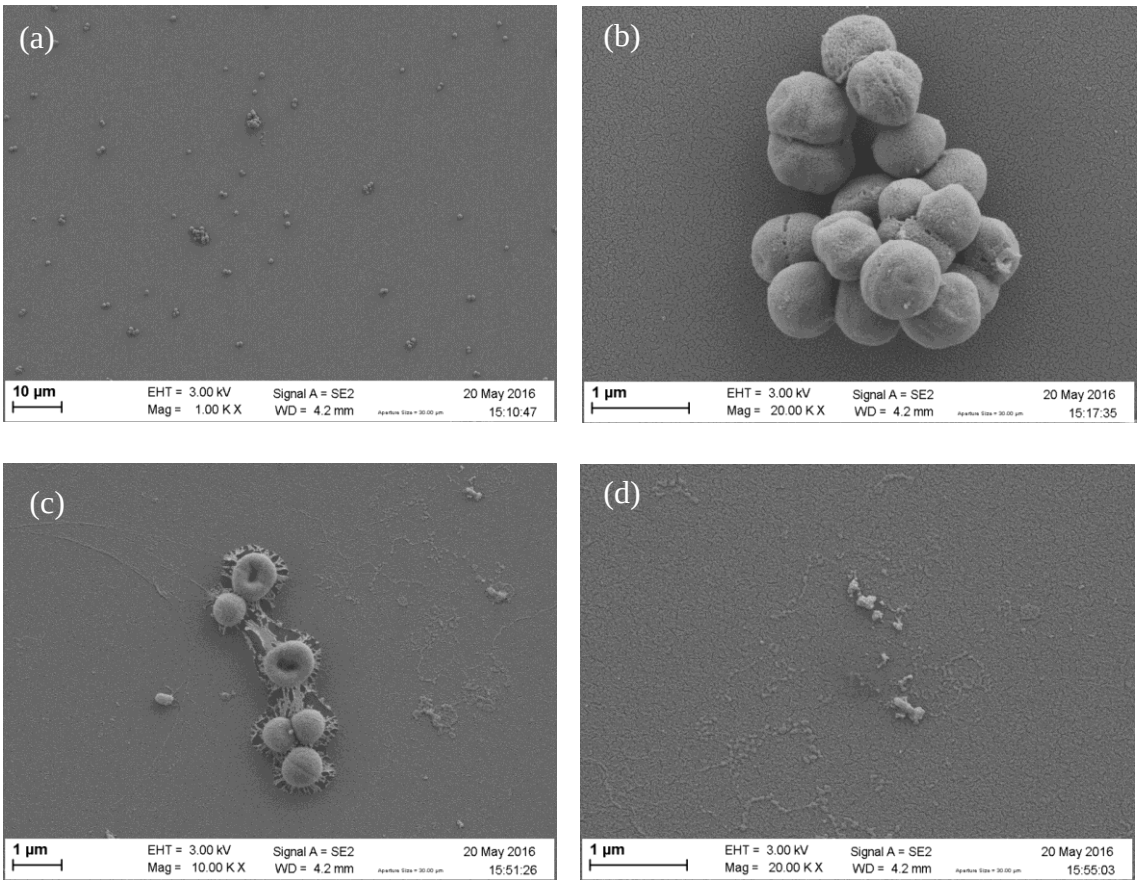

Figure 4.10 SEM images of (a)(b) bacteria and (c)(d) lysed bacteria in dynamic condition.

The size of bacteria and lysate obtained in dynamic condition are similar to the results obtained in static condition, which means they are credible. As shown in Figure 4.10 (b), the bacteria is about 1 µm while the lysate is a few tens of nm as shown in Figure 4.10 (d).

4.3 Bacteria detection

The well-resolved Fabry-Pérot fringes were collected for all experiments. FFT of the reflective spectra were performed with "Fringe_24_5" program as well as the obtention of the EOT and the intensity shift. All the figures in this section are draw with Origin.

4.3.1 Control

The optical readout stability of the PSi-based sensor and $PSiO_2$-based sensor under flow conditions was characterized by long time PBS buffer flow experiments. The samples were placed in flow cell, in which a sterilized PBS solution was delivered at a constant flow of 0.615 mL/min and the reflectivity spectra was collected every 10 s.

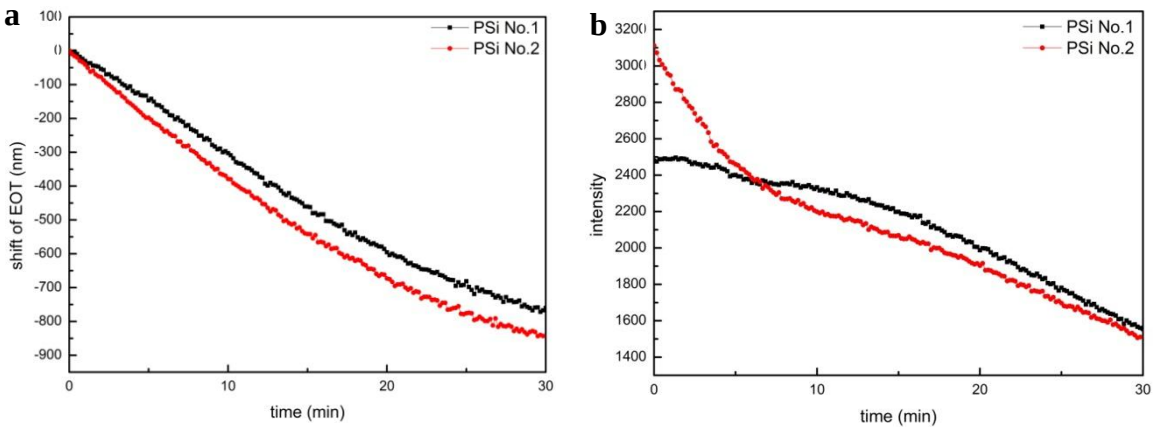

Figure 4.11 Buffer flow experiments onto PSi-based sensors. (a) EOT changes over time and (b) intensity changes over time.

The buffer flow experiments were performed twice with 2 freshly etched PSi samples. The shift of EOT and the reflected light intensity as a function of time are shown in Figure 4.11. The EOT values of the two PSi samples decrease by 760 nm and 840 nm within half an hour, respectively. The intensity drops by approximately 1500 (from 3100 to 1550) for the first sample, and approximately 1000 (from 2500 to 1510) for the second sample. These results indicate the freshly etched PSi samples dissolves quickly in the buffer solution so they are not stable for following biosensing application.

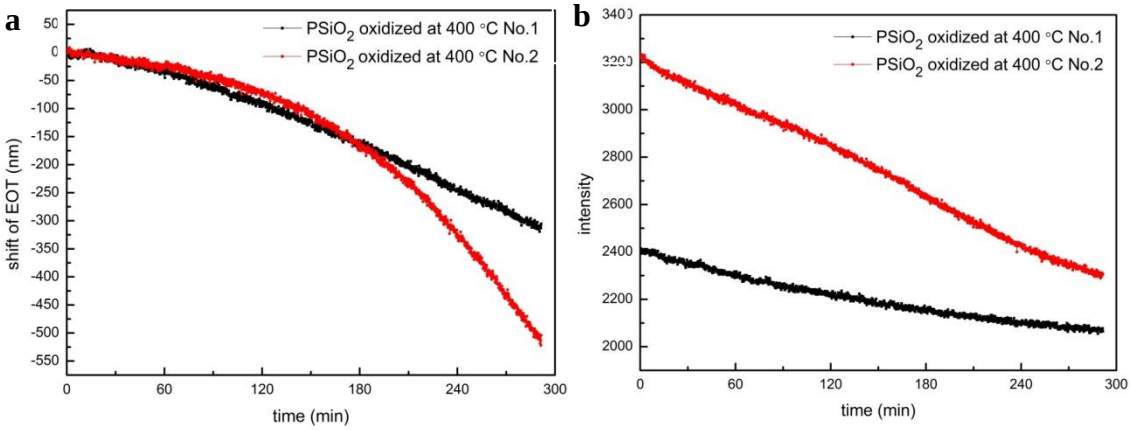

Figure 4.12 Buffer flow experiments onto $PSiO_2$-based sensors oxidized at 400 ℃. (a) EOT changes over time and (b) intensity changes over time.

The same experiment was also conducted on samples oxidized at 400 ℃ for 1 h (Figure 4.12) and 800 ℃ for 1 h (Figure 4.13). For samples oxidized at 400 ℃ we observed that within 5 h, the EOT values decreases by approximately 320 nm for the first sample and 500 nm for the second. The intensity decreases by 900 for the first sample (from 3200 to 2300), while shifts by 350 for the second sample (from 2400 to 2050). In this case the PSi was passivated by an oxidation layer so the degradation of sample in buffer solution decreases significantly compared to a fresh sample, resulting in a slow decrease of EOT and intensity.

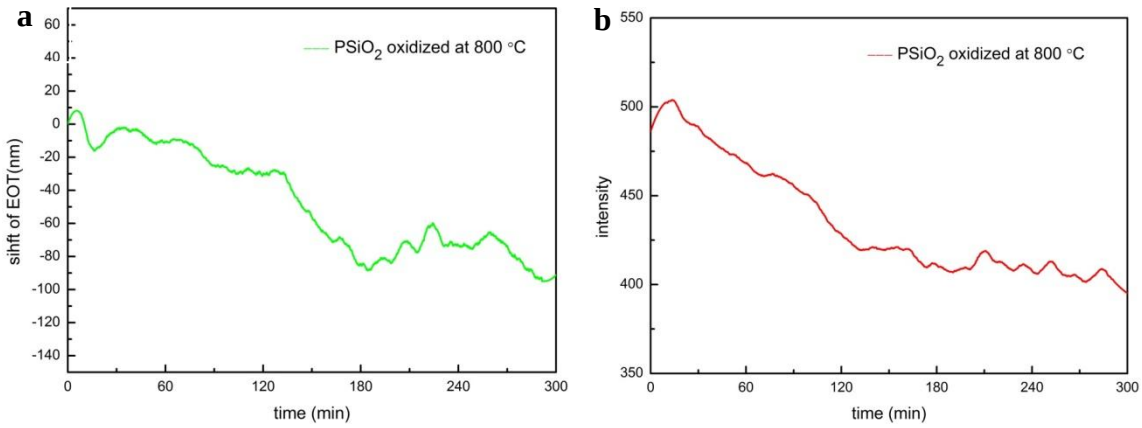

Figure 4.13 Buffer flow experiments onto $PSiO_2$-based sensors oxidized at 800 ℃. (a) EOT changes over time and (b) Intensity changes over time.

In the case of samples oxidized at 800 ℃ we observe a decrease in EOT of approximately 90 nm, and the intensity drops by 100 (from 500 to 400). This is because at such a high process temperature, the freshly etched PSi is considered to be entirely converted into $PSiO_2$, which acts as a protection layer against the dissolution in buffer solution.

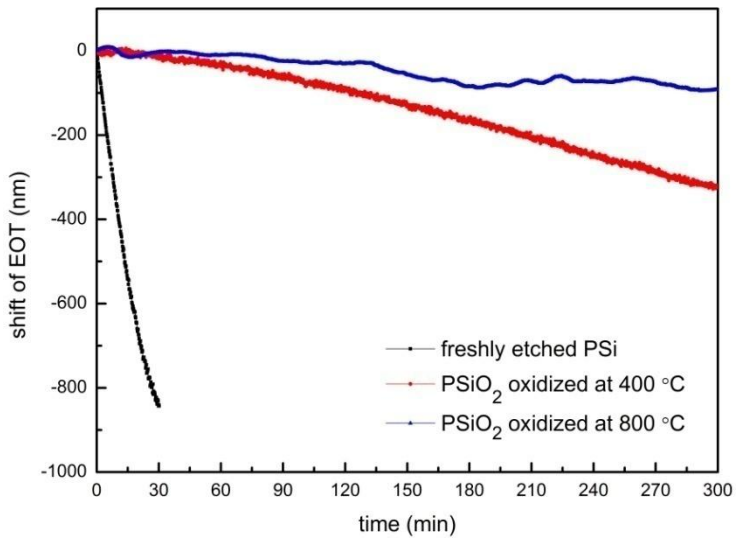

Figure 4.14 Comparison of EOT shift in buffer for freshly etched PSi, $PSiO_2$ oxidized at 400 ℃ and 800 ℃.

The comparison in Figure 4.14 demonstrates that the optical stability of sensor is highly increased by oxidation. For the freshly etched PSi-based sensor, both the EOT value and intensity exhibits significant shift, which is generally caused by the degradation of the porous scaffold. However, the sensor based on $PSiO_2$ shows high stability with a smaller baseline drift after the PSi is oxidized, especially for the PSi oxidized at 800 ℃. As a result, changes of 100 nm in EOT and 100 in intensity for the sensor based on $PSiO_2$ are obtained for a total experiment time of 5 h.

It is worth mentioning that during the buffer flowing on the $PSiO_2$ sample oxidized at 800 ℃ the EOT shift is equal to 70 nm while the intensity changes is equal to 85 within 165 min. Since 165 min is the time for the following bacteria detection experiment thus these values can be used as the baseline shift.

As the positive control, the EOT value and intensity shift of supernatant were compared with PBS in Figure 4.15. We observe that the EOT value increased after the introduction of supernatant and decreased after PBS rinsing, resulting in a 40 nm higher than EOT in PBS after 30 min. The increase of EOT was caused by the penetration of proteins in the supernatant that secreted by bacteria cells during the incubation. The intensity also increased 40 during 30 min, probably because the refractive index of porous layer increased by the penetration, so the contrast of solution /porous layer interface increased.

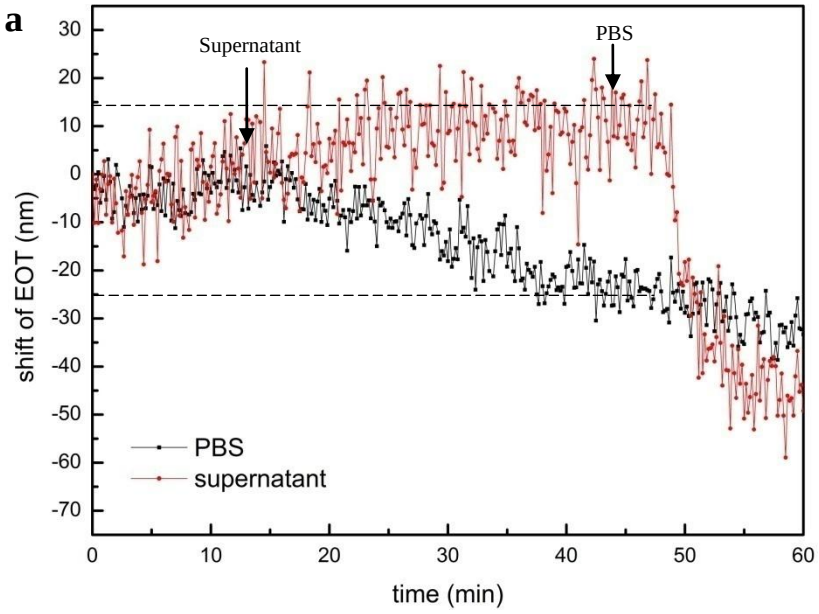

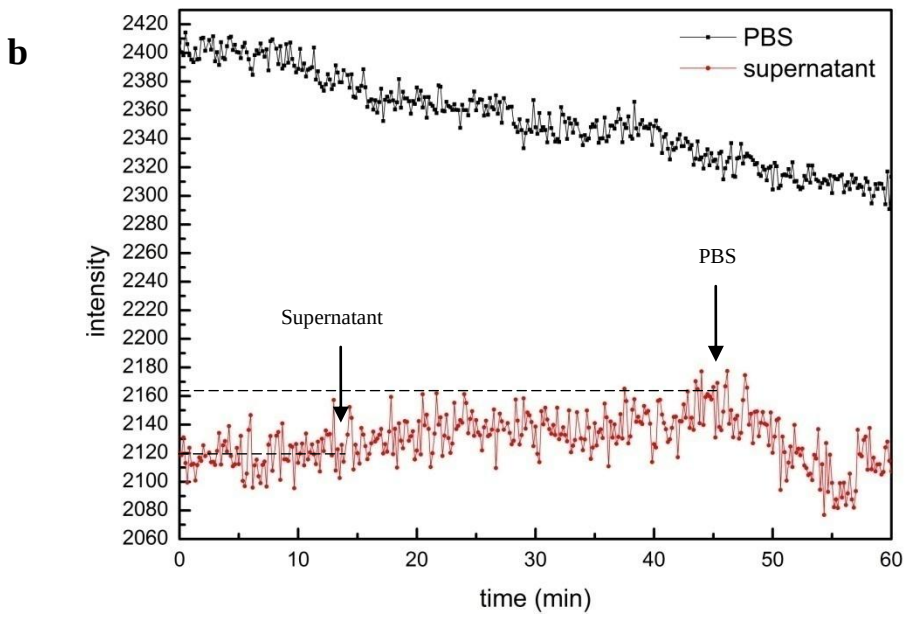

Figure 4.15 Comparison of supernatant and PBS flow onto $PSiO_2$-based sensors oxidized at 400 ℃ (a) EOT shift and (b) intensity change over time. Arrow indicates the introduction of supernatant and PBS rinsing.

4.3.2 Bacteria experiments

Experiments were conducted with bacteria solution of varying concentration (10^6, 10^7, and 10^8 CFU/mL) to study their impact on the EOT and reflected light intensity following the protocol described in Section 3.5.3.

Since *S.epidermidis* is about 1 μm in diameter and the pore size of our sensor is only 80-100 nm, binding of bacteria may only occur on the surface of sensor and not inside the porous layer. As a result, the bacteria cells present on the surface can scatter the light resulting in a decrease of intensity.

When working with a bacteria concentration of 10^8 CFU/mL on sample oxidized at 800 ℃ (Figure 4.16), we observe a decrease in EOT of 30 nm during bacteria flowing within 1 h, while the intensity reduces quickly from 1.2 to 0.6 as soon as the bacteria is introduced. However, the intensity increases fast as soon as the PBS rinsing start. This sudden drop in intensity is due to the turbidity of the highly concentrated solution which diffracts most of the light in the bulk of the solution. When we start rinsing, the opaque solution was replaced by PBS which is transparent, hence the jump observed. The real number of bacteria obtained from colonies plate counting is 7.6×10^8 CFU/mL.

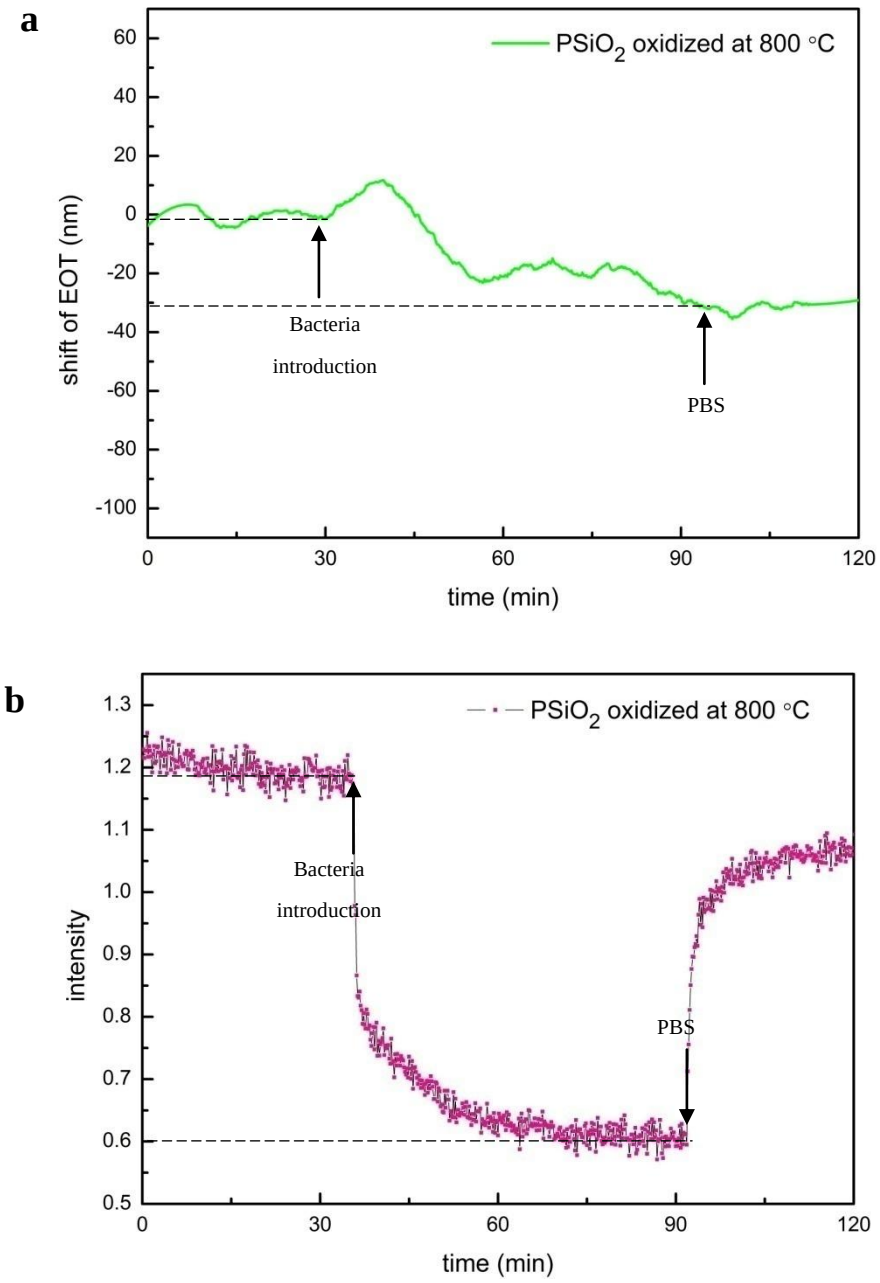

Figure 4.16 Real-time monitoring of *S.epidermidis* (10^8 CFU/mL) flow onto $PSiO_2$-based sensors oxidized at 800 ℃. (a) EOT changes over time and (b) intensity changes over time. Arrow indicates the introduction of *S.epidermidis* suspension and PBS rinsing.

We also observe that the values of EOT shift in bacteria flow are approximately equal to the EOT shift in buffer, which indicate no biomolecules penetration. However, the intensity reduces dramatically, this is due to the opaque solution more than bacteria adhering to the surface as explained above. In this way, the real density shift caused by the bacteria adhesion is only 0.2.

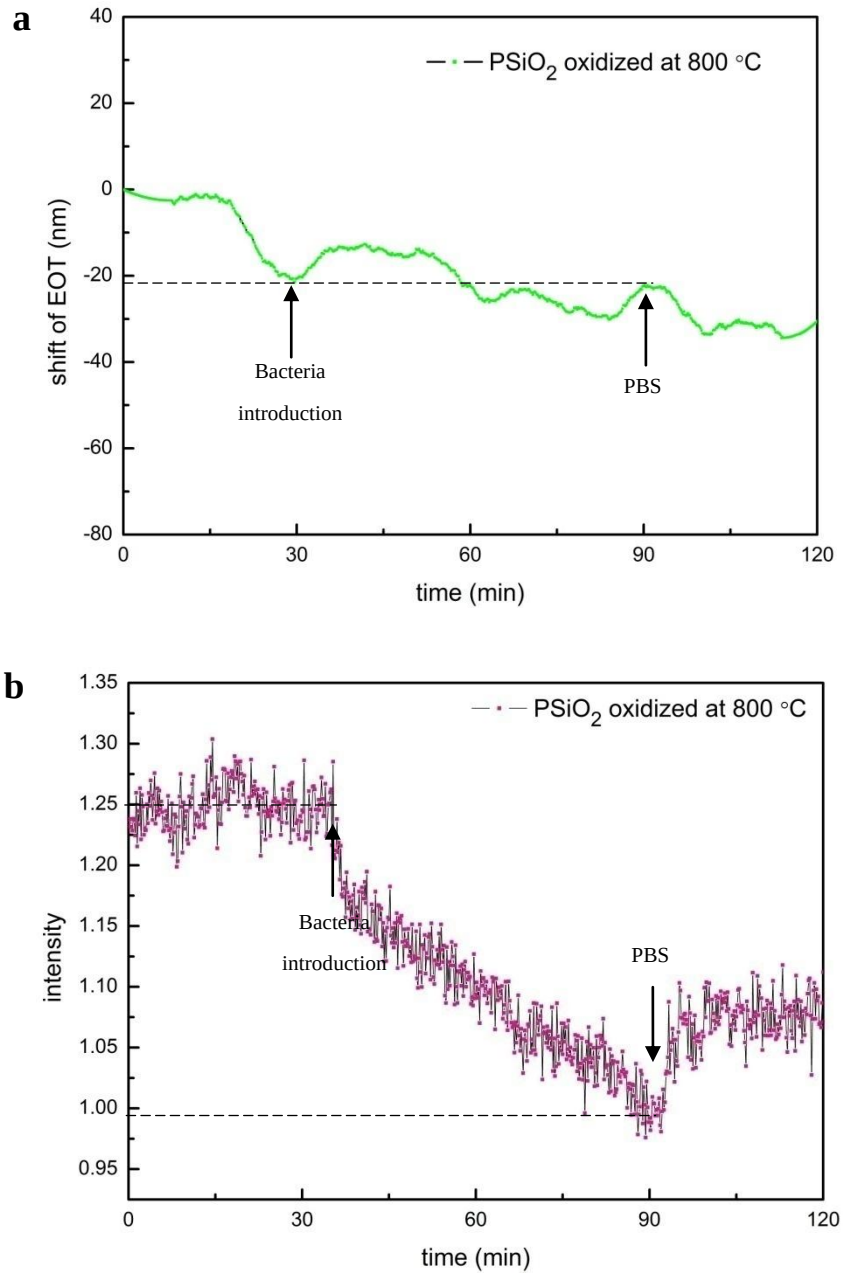

Figure 4.17 Real-time monitoring of *S.epidermidis* (10^7 CFU/mL) flow onto $PSiO_2$-based sensors oxidized at 800 ℃. (a) EOT changes over time and (b) intensity changes over time. Arrow indicates the introduction of *S.epidermidis* suspension and PBS rinsing.

When working with a bacteria concentration of 10^7 CFU/mL, we observe almost no shift in EOT while the intensity decreases from 1.22 to 1.0. The drop and jump in intensity is less important than for a concentration of 10^8 CFU/mL as the solution does not diffract light as much. The gradual decrease following the drop is due to the adhesion of bacteria on the surface. The real number of bacteria obtained from colonies counting is 1.07×10^8 CFU/mL.

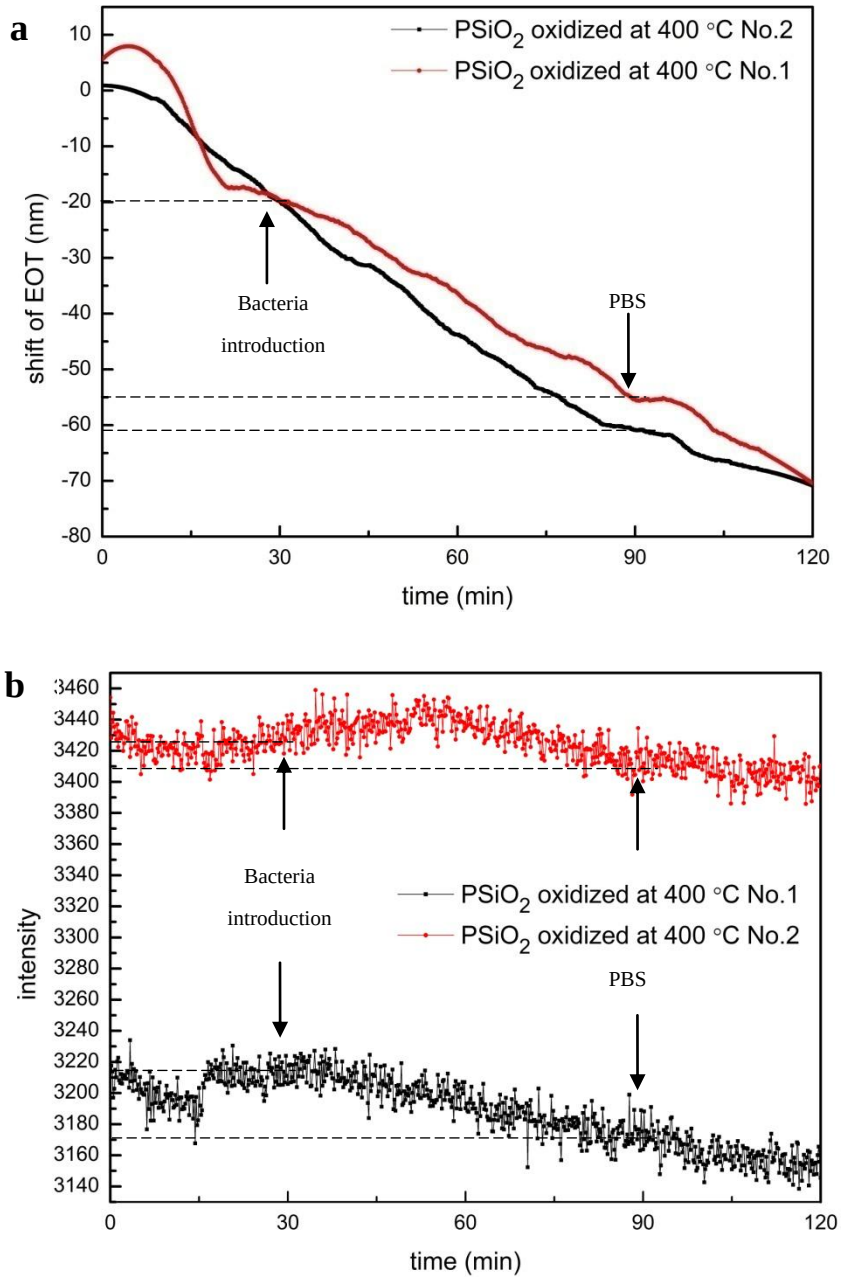

Figure 4.18 Real-time monitoring of *S.epidermidis* (10^6 CFU/mL) flow onto $PSiO_2$-based sensors oxidized at 400 ℃. (a) EOT changes over time and (b) intensity changes over time. Arrow indicates the introduction of *S.epidermidis* suspension and PBS rinsing.

The experiment with a bacteria concentration of 10^6 CFU/mL was only conducted on samples oxidized at 400 ℃. In this case we observe a decrease in EOT of 35 nm and 40 nm while a decrease in intensity of 17 and 40. The number of bacteria obtained from colonies counting is 6.4×10^6 CFU/mL for the first experiment and 7.1×10^6 CFU/mL for the second.

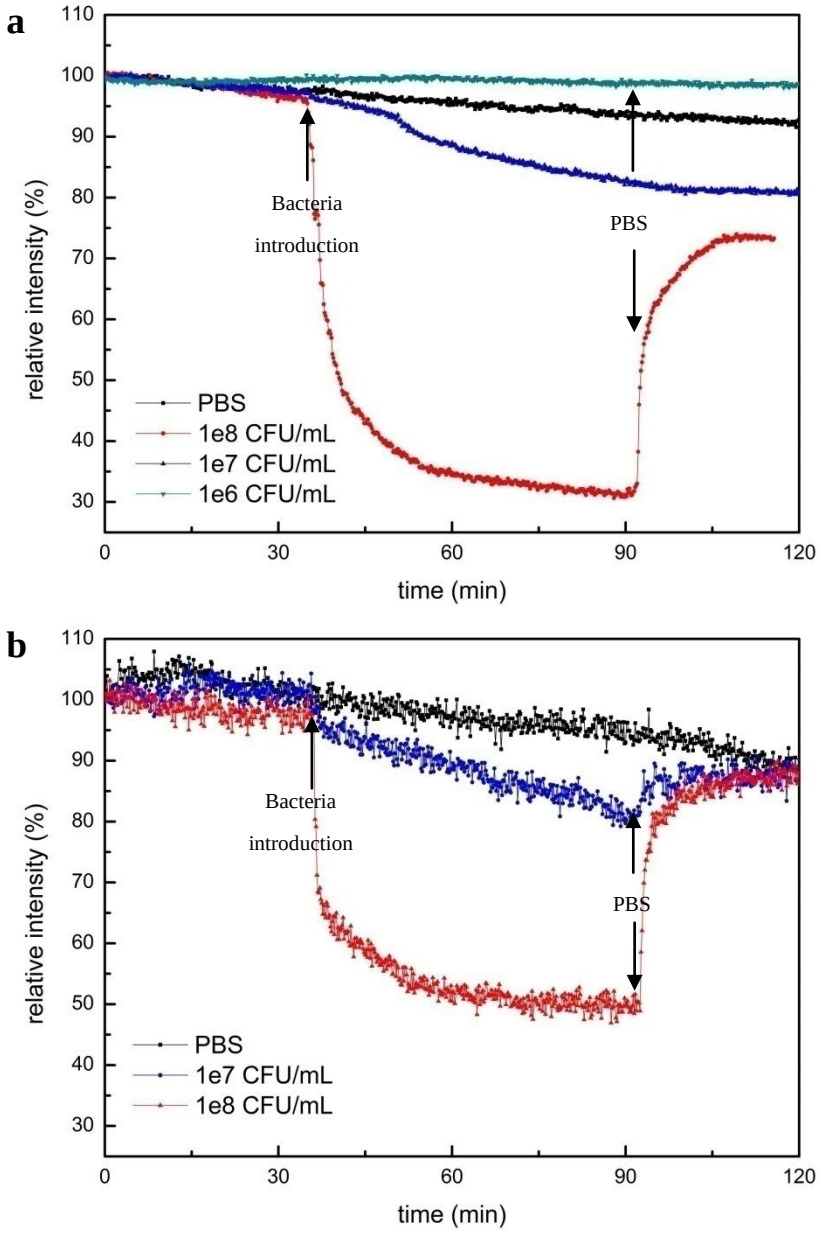

Figure 4.19 Comparison of relative intensity shift on $PSiO_2$-based sensors oxidized at (a) 400 ℃ (b) 800 ℃ with different concentration of bacteria suspension.

The intensity data for a porous silicon layer oxidized at 400 ℃ are summarized in Figure 4.19 a, to compare the decrease of intensity with bacteria concentration. When the highly concentrated bacteria suspension of 10^8 CFU/mL flows onto the sensor surface, the intensity decreases by 50% as soon as the bacteria solution is introduced and this value increases to 70% as the bacteria flow continue with the bacteria cells adhering to the surface. For a concentration of 10^7 CFU/mL, the intensity only decreases by approximately 15 % at last and the intensity decreases gradually. However, for the lower bacterial suspension 10^6 CFU/mL, the intensity decreases is even smaller than the PBS which is probably because of the different stability of samples. These preliminary experiments show detection limit of 10^6 CFU/mL, so we will not ab able to detect concentration lower than that.

The dependence of intensity decrease with bacteria concentration for a porous silicon oxidized at 800 ℃ are shown in Figure 4.17 (b). For a concentration of 10^8 CFU/mL, the intensity decrease by 30% and then 50% after introducing the bacteria solution for 60 min, so the intensity decrease caused by bacteria adhesion is about 20%. For a concentration of 10^7 CFU/mL, the intensity only decreases by 15%. After rinsing PBS for 30 min, the intensity reach the same level at the end for PBS and both the bacteria concentration, which means most of the bacteria cells were removed by buffer flowing.

4.3.3 Lysate test

Based on the bacteria test, lysostaphin is introduced to lyse bacteria cells and allow the penetration of lysate into the pores which should result in an increase of EOT.

The selective bacteria detection using lysostaphin for a bacteria concentration of 10^8 CFU/mL is performed using the EOT shift and intensity changes over time as shown in Figure 4.18. As the lysostaphin is introduced, the bacteria cells adhering to the surface are lysed and the lysate is expected to penetrate into the pores resulting in an EOT increase. This increase is comprised between 85 and 100 nm depending on the experiment. The intensity increases by 0.75 and 0.8 caused by the penetration of lysate and lysostaphin.

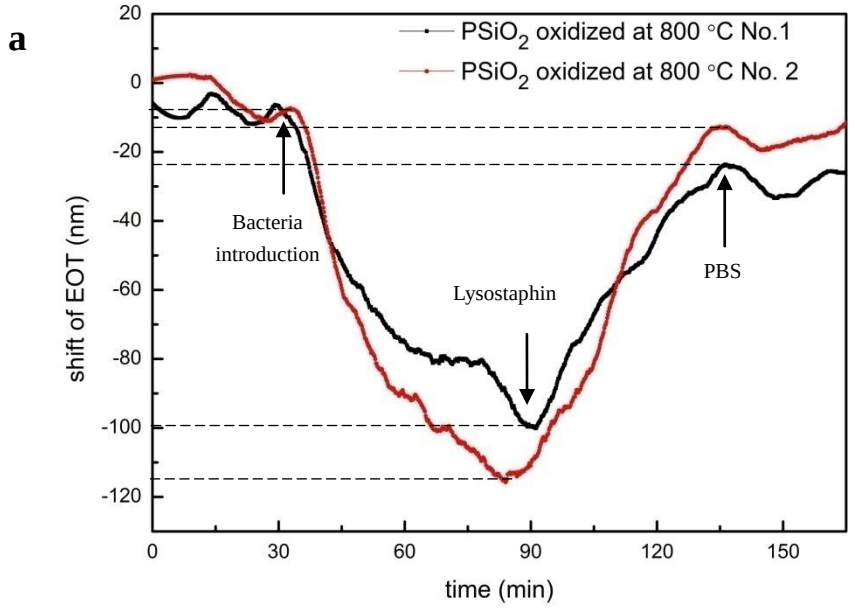

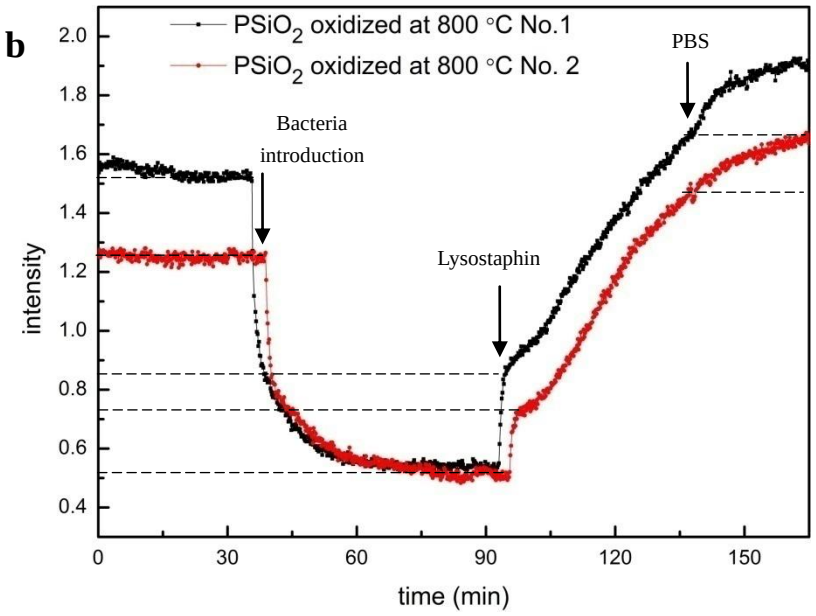

Figure 4.20 Real-time monitoring of *S.epidermidis* (10^8 CFU/mL) injection followed by lysostaphin flow onto $PSiO_2$-based sensors oxidized at 800 ℃. (a) EOT changes over time and (b) intensity changes over time. Arrow indicates the introduction of *S.epidermidis* suspension, lysostaphin solution and PBS rinsing.

Beside, the quick shift in intensity after the lysostaphin introduction, caused by the replacement of the opaque bacteria solution by the clear lysostaphin solution, we observe a gradual increase of the intensity caused by the lysis of the bacteria cells.

The number of bacteria obtained from colonies counting is 4.5×10^8 CFU/mL for the first experiment and 9.3×10^8 CFU/mL for the second one. This can also explain that both the EOT shift and intensity change of the second experiment is larger than the first one.

The bacteria detection using lysostaphin for a bacteria concentration of 10^7 CFU/mL is also performed using the EOT shift and intensity changes over time shown in Figure 4.21. After the lysostaphin injection, the EOT increases by 77 nm and 45 nm. This is probably because the different stability of the sample as the EOT of first sample decreases about 20 nm in PBS flowing at the beginning of the experiment. Even though we prepare all the sensors under the same conditions, they can be impacted by many factors thus their behavior during the sensing experiments could be affected. The intensity increases by 0.55 for both experiments, which is approximately 35% for the first experiment and 40 % for the second one.

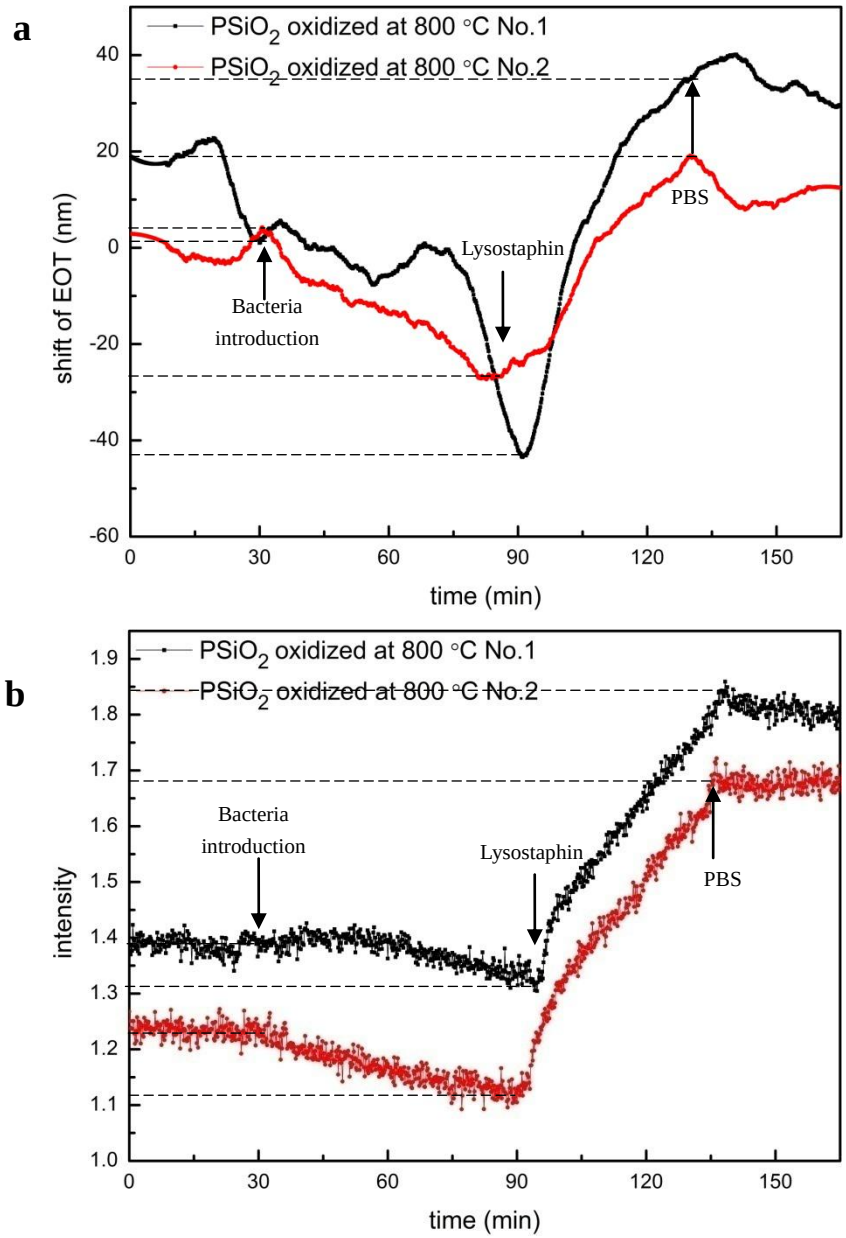

Figure 4.21 Real-time monitoring of lysostaphin injection followed by *S.epidermidis* (10^7 CFU/mL) flow onto $PSiO_2$-based sensors oxidized at 800 ℃. (a) EOT changes over time and (b) intensity changes over time. Arrow indicates the introduction of *S.epidermidis* suspension, lysostaphin solution and PBS rinsing.

The number of bacteria obtained from colonies counting is 7.4×10^7 CFU/mL for the first experiment and 6.1×10^7 CFU/mL for the second.

The selective bacteria detection using lysostaphin for a bacteria concentration of 10^6 CFU/mL is performed using the EOT shift and intensity changes over time shown in Figure 4.22.

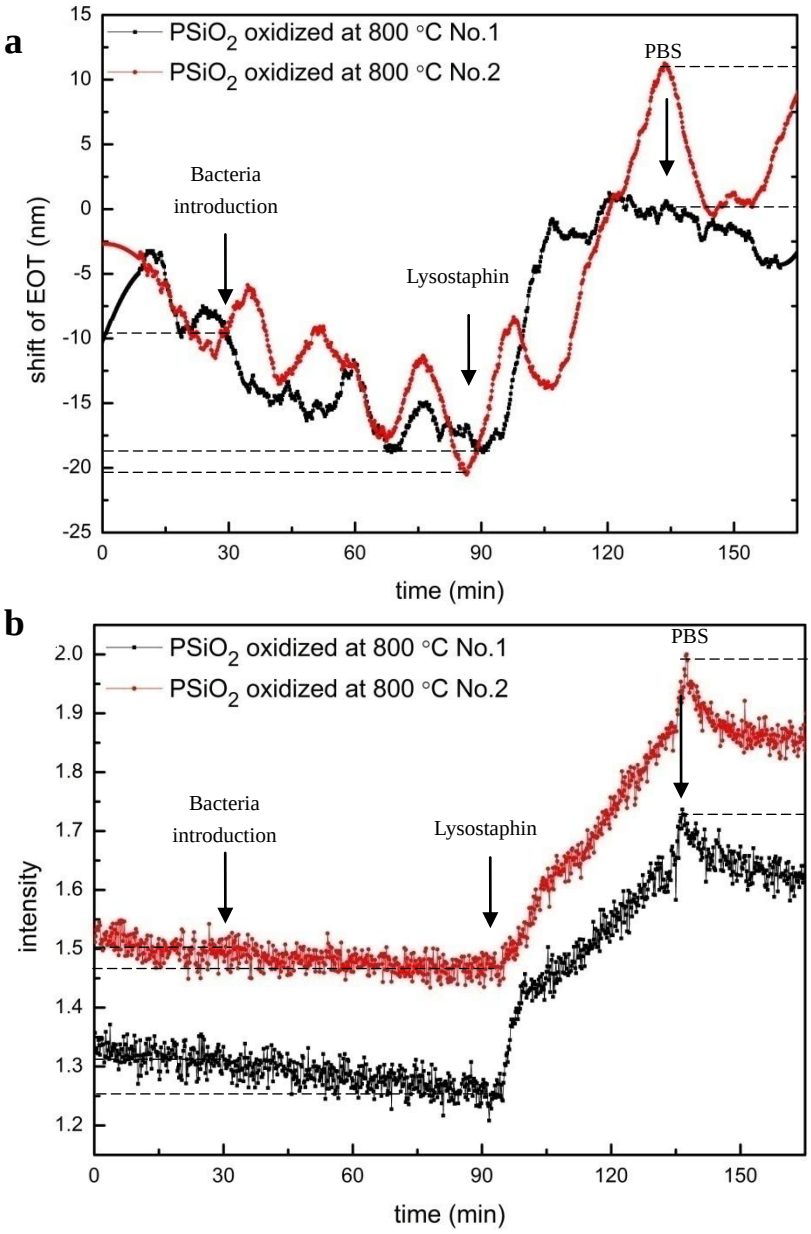

Figure 4.22 Real-time monitoring of lysostaphin injection followed by *S.epidermidis* (10^6 CFU/mL) flow onto $PSiO_2$-based sensors oxidized at 800 ℃. (a) EOT changes over time and (b) intensity changes over time. Arrow indicates the introduction of *S.epidermidis* suspension, lysostaphin solution and PBS rinsing.

In this experiment, the EOT increases by 19 nm and 31nm after the lysostaphin injection. The intensity increases by 0.46 and 0.49, which is approximately 30%. In this case the bacteria solution is prepared by dilution of 100 times of original suspension, so there are less bacteria cells flowing on the sensor surface. Since the number of bacteria is smaller than the prior experiments with high concentration, the EOT shift and intensity changes were more impacted by the lysostaphin themselves. The EOT shift includes the penetration of lysate as well as the lysostaphin.

The number of bacteria obtained from colonies counting is 1.07×10^7 CFU/mL and 1.11×10^7 CFU/mL, respectively, probably because the room temperature is so high when these bacteria are cultured and during the following experiments so the growth of bacteria is improved.

In Figure 4.20-22 b, the intensity increases after injection of lysostaphin, but at last the intensity is higher than the reference lever, which draw our attention. To investigate the behavior of lysostaphin molecules in the biosensing experiments, the EOT and intensity shift during only lysostaphin flowing onto the sensor is shown in Figure 4.23. The results indicate that the lysostaphin penetration cause both EOT increase and intensity increase.

In Figure 4.23, the EOT increase by 20 nm and 9 nm, respectively. The increase is considered as the contribution of lysostaphin molecules penetration. The intensity increases by 0.4 (from 1.3 to 1.7) during the flowing of lysostaphin. Considering that the refractive index of pure PBS buffer (n=1.33) is close to the refractive index of $PSiO_2$ (n=1.4), the contract of the PBS/($PSiO_2$+PBS) interface is small so the intensity of FFT peak is small. When PBS buffer in the porous layer is replaced by lysostaphin flowing, the average refractive index of porous layer ($PSiO_2$ + lysostaphin) increase by the penetration, thus the contract is more pronounced and intensity increases. This experiment gives an explanation of the strong intensity increase in Figure 4.20b, 4.21b and 4.22b after the flowing of lysostaphin.

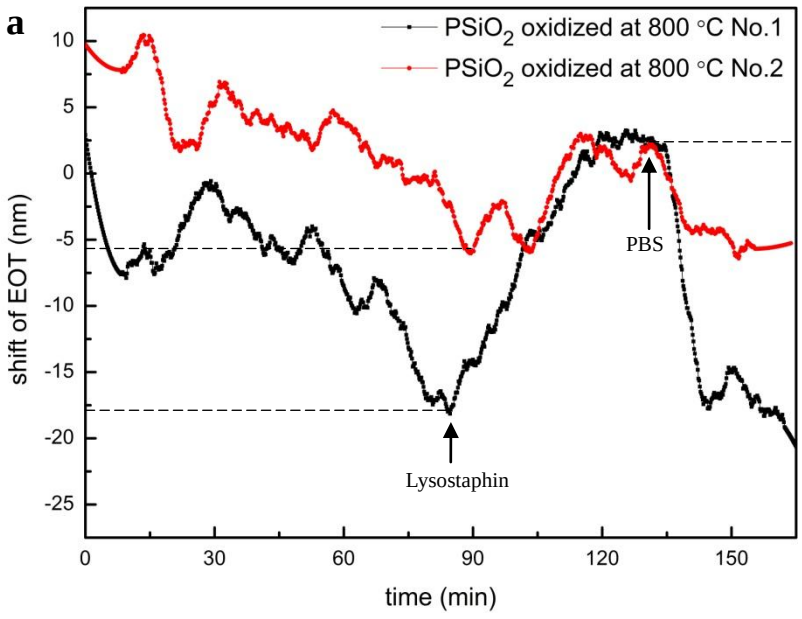

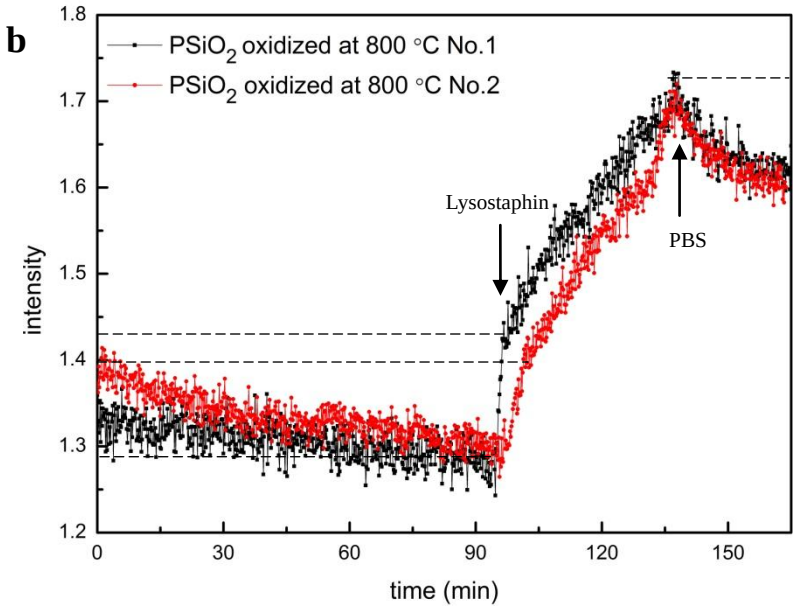

Figure 4.23 Real-time monitoring of lysostaphin flow onto $PSiO_2$-based sensors oxidized at 800 ℃. (a) EOT changes over time and (b) intensity changes over time. Arrow indicates the introduction of lysostaphin and PBS rinsing.

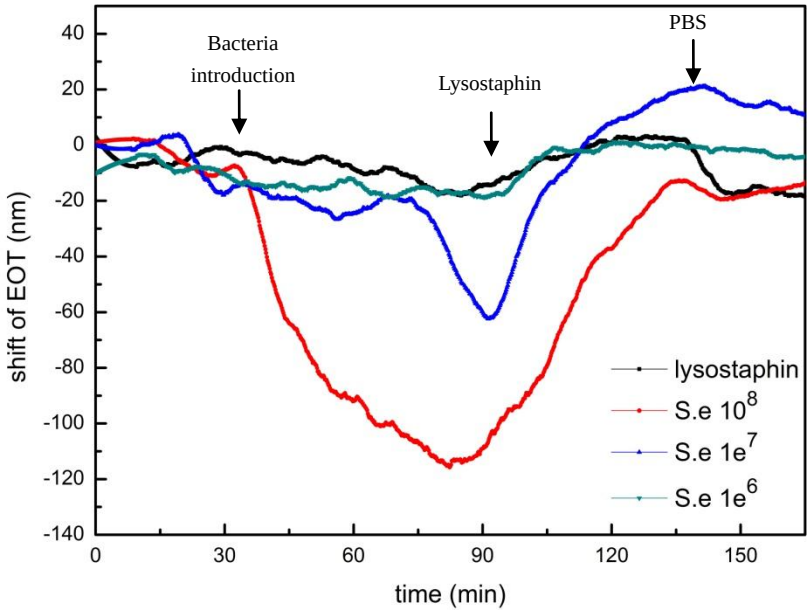

Figure 4.24 Summary of EOT shift over time when bacteria solution with different concentration flow onto $PSiO_2$-based biosensors oxidized at 800 ℃. Arrow indicates the introduction of bacteria suspension, lysostaphin solution and PBS rinsing.

Dependence of EOT shift with time is shown in Figure 4.24. As bacteria concentration increase from 10^6 to 10^7, 10^8, there are more bacteria cells presence on the surface of sensor which produce more lysate when the lysostaphin is delivered, resulting in a higher EOT increase.

4.3.4 Selectivity of the detection

To assess the selectivity of our sensor, the suspension of *E.coli* is introduced as a comparison of *S.epidermidis*. The detection using lysostaphin for a *E.coli* concentration of 10^7 CFU/mL is performed using the EOT shift and intensity changes over time as shown in Figure 4.25.

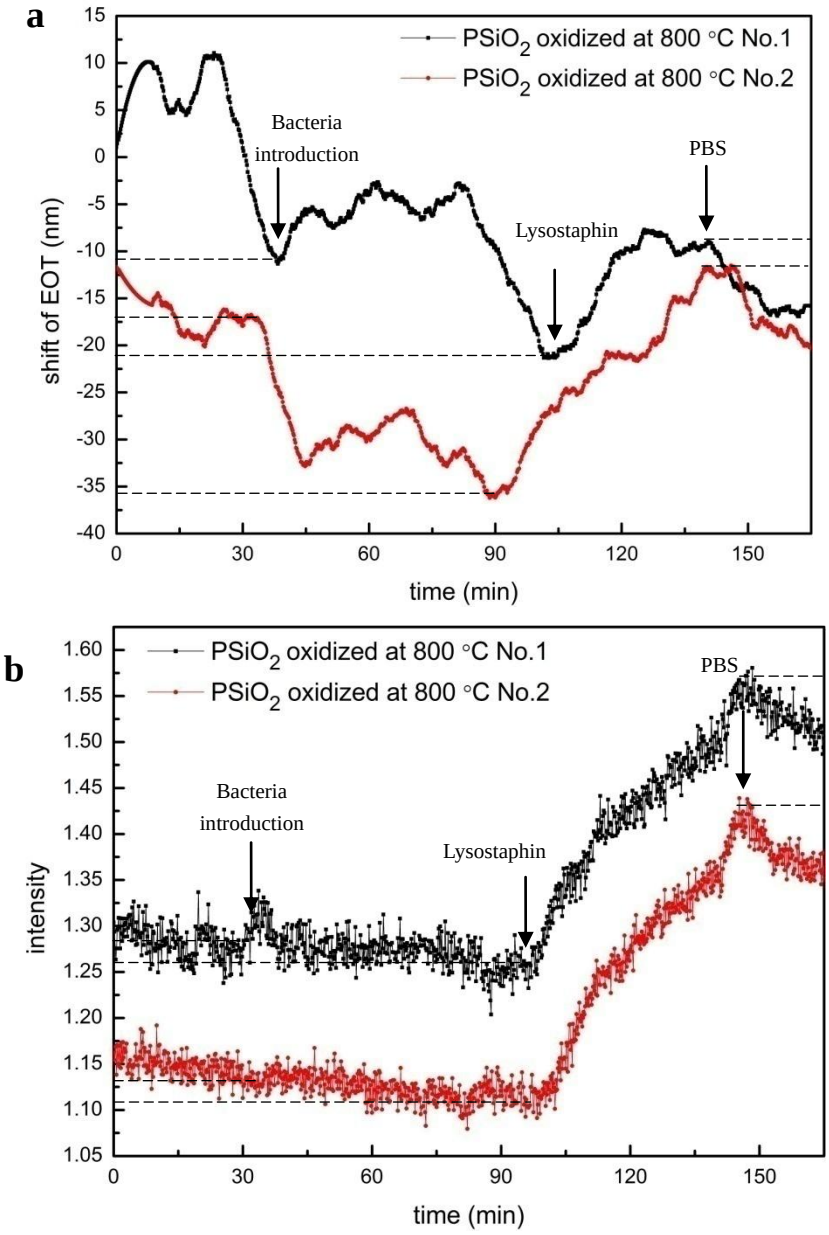

Figure 4.25 Real-time monitoring of lysostaphin injection followed by *E.coli* (10^7 CFU/mL) flow onto $PSiO_2$-based sensors oxidized at 800 ℃. (a) EOT changes over time and (b) intensity changes over time. Arrow indicates the introduction of *E.coli* suspension, lysostaphin solution and then PBS rinsing.

In this experiment, the EOT increases by 14 nm and 24 nm, respectively. The intensity both increases by 0.32 (from 1.25 to 1.57 for the first experiment and from 1.11 to 1.43 for the second one). The EOT shift and intensity change are approximately equal to the EOT shift and intensity change in Figure 4.21 for detection only flowing lysostaphin, and much smaller than the change in Figure 4.19 for detection using lysostaphin for *S.epidermidis* of 10^7 CFU/mL. The results indicate that *E.coli* cannot be lysed by lysostaphin so there is no lysate penetration during the delivery of lysostaphin. Besides, the rod-shaped *E.coli* bacteria cells which are approximately 0.5 μm in width and 2 μm in length adhering on the sensor surface also diffract light, so the intensity decreases during the injection of bacteria. After that, the intensity increases because of the injection of lysostaphin as observed before. In this experiment, it is proved that *E.coli* cannot be detected using the lysostaphin.

The number of *E.coli* obtained from colony counting is 3.1×10^7 CFU/mL and 5.0×10^7 CFU/mL, respectively. The number of *E.coli* used in these two experiments are a little smaller than the number of *S.epidermidis* used in the experiment shown in Figure 4.19, and the dimension and shape of *E.coli* are much different from the *S.epidermidis*, probably these reasons are why the intensity change in this experiment is slightly lower than in Figure 4.19.

In order to study the performance of our sensor when the bacteria solution is flowing onto the sensor, the detection using lysostaphin for a bacteria solutision including *E.coli* suspension and *S.epidermidis* is performed using the EOT shift and intensity change over time as shown in Figure 4.26.

In this case, the EOT increases by 54 nm and 58 nm while the intensity increases by 0.65 for the first experiment and 0.55 for the second experiment after the lysostaphin injection. The EOT and intensity results show approximately equivalent shift with Figure 4.21, in which only 10^7 CFU/mL *S.epidermidis* was flown onto $PSiO_2$-based sensors.

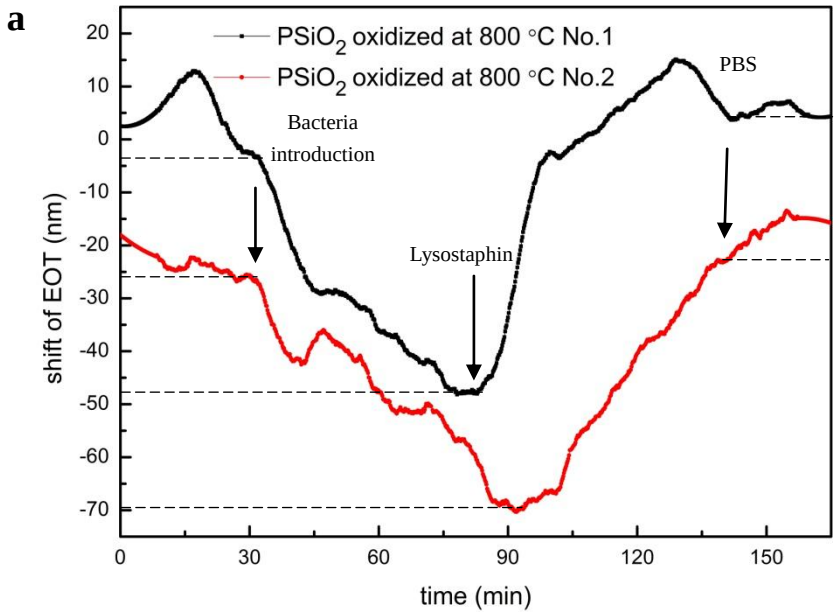

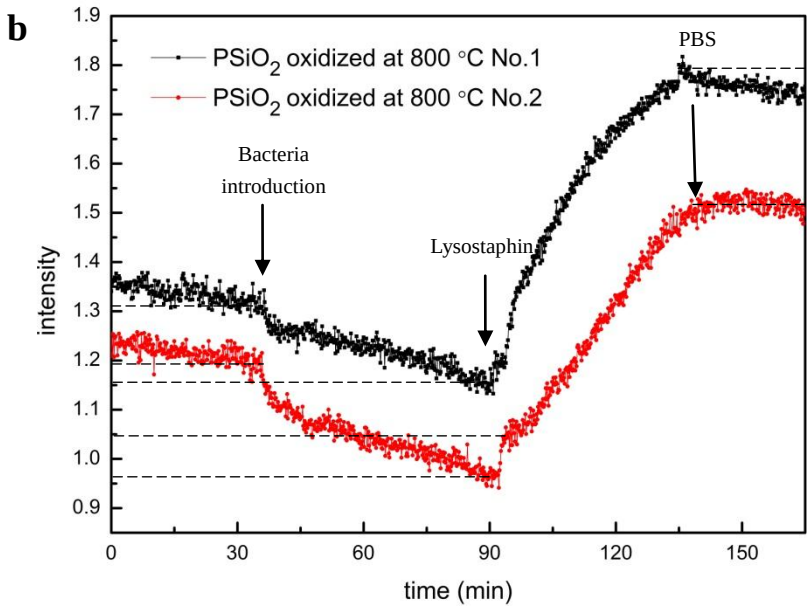

Figure 4.26 Real-time monitoring of lysostaphin injection followed by *E.coli* (10^7 CFU/mL) and *S.epidermidis* (10^7 CFU/mL) flow onto $PSiO_2$-based sensors oxidized at 800 ℃ (a) EOT changes over time and (b) intensity changes over time. Arrow indicates the introduction of bacteria suspension, lysostaphin solution and PBS rinsing.

The number of *E.coli* used in these experiments are obtained from colonies counting, which is 2.6×10^7 CFU/mL and 4.0×10^7 CFU/mL, while the number of *S.epidermidis* is 4.7×10^7 CFU/mL and 7.9×10^7 CFU/mL, respectively.

The results of these experiments indicate there are no *E.coli* lysate penetrating into the pores but just the *S.epidermidis* lysate and the lysostaphin themselves, so our sensor using lysostaphin for the bacteria detection is selective for *S.epidermidis.*

The dependence of EOT shift of these lysate tests as well as the EOT shift of just lysate penetration (extract the EOT shift of lysostaphin itself) are summarized in Figure 4.27.

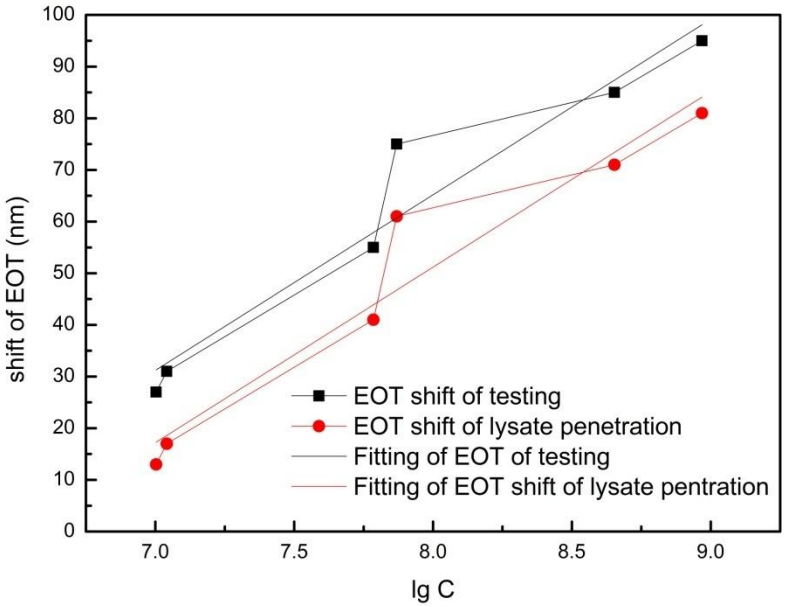

Figure 4. 27 Dependence of EOT shift and concentration.

5 conclusion

Throughout this project, an oxidized porous silicon-based biosensor was fabricated, followed by selective detection of *S.epidermidis* with different concentration. The reflect spectra of sample, which display Fabry-Pérot fringes, were recorded when bacteria solution flowed on the sensor surface followed by the injection of lysostaphin. FFT was applied on the spectra to obtain the EOT shift and intensity change. This work was conducted towards the fabrication of a label-free biosensor for bacteria detection.

5.1 Results

In the first step, porous silicon was prepared by electrochemical etching and characterized by SEM and optical method (SLIM). The experiment results indicated that by increasing current density form 5 mA/cm^2 to 200 mA/cm^2, pore size increased from about 10 nm to 90 nm and porosity increased from 52.9% to 84%. However, the pores formed at higher current density above 75 mA/cm^2 were elliptical. To have larger openings, a sacrificial layer was first etched then dissolved by KOH solution completely. As a result, the porosity and pore diameter were increased after introduction of sacrificial layer. PSi films etched at a current density 200 mA/cm^2 have an average pore size of 80-100 nm and were then selected for bacteria detection. After that, the PSi samples were oxidized at 400 ℃ and 800 ℃ to increase the stability.

Secondly, the bacteria were cultured and lysed. To obtain stationary phase of bacteria, both *S.epidermidis* and *E.coli* were inoculated to TSB media and incubated. Later the suspensions of both bacteria were prepared by centrifugation, removal of supernatant, resuspension in PBS buffer and their number of were counted by colony plate counting. Lysis of *S.epidermidis* is controlled by performing top agar experiment, indicating the bacteria were lysed by lysostaphin. What's more, the size of *S.epidermidis* and lysate were measured by SEM. The bacteria cells are sphere and look like cluster of grapes with a diameter about 1 μm while most of the lysate are much smaller than 100 nm and some particles even smaller than 30 nm.

Finally, the bacteria detection is performed with a custom-made flow cell. The optical readout stability of the freshly etched PSi sample, $PSiO_2$ oxidized at 400 ℃ and 800 ℃ under flow conditions were first compared. The freshly etched PSi dissolved quickly in the PBS solution while the oxidized PSi dissolved slowly, especially the PSi oxidized at 800 ℃. This is because the PSi was passivated by the oxidation layer so the dissolution decreases in the buffer solution. The bacteria suspension experiment with different concentration (10^6, 10^7, 10^8 CFU/mL) showed that by decreasing the bacteria concentration, the intensity shift caused by bacteria adhesion decreased. Since the bacteria cannot penetrate into the pores,

the shift of EOT almost equal to that in buffer solution. The lysate detection showed that by decreasing the bacteria concentration, the shift of EOT caused by lysate penetration decreased. As bacteria concentration change from 10^8 to 10^6 CFU/mL, the bacteria on the sensor surface decrease so the lysate produced by lysostaphin is less, resulting in a smaller EOT shift. Finally, the selectivity of the detection was assessed by *E.coli* suspension instead of *S.epidermidis*. The experiments showed that *E.coli* cannot be lysed by lysostaphin so there is no EOT shift caused by *E.coli* adhesion, and *S.epidermidis* could also be detected when there was *E.coli* in the solution.

5.2 Areas for improvements

There are still some issues in this study that can improve the performance of the sensor but there was not enough time to explore.

First of all, the stability of sensor. The PSi were oxidized at 400 ℃ and 800℃ to passivate, and it has been proved that the PSi oxidized at 800 ℃ was more stable. However, there were still some experiments performed on samples oxidized at 400 ℃ and morphology of samples after oxidation was not observed. During the detection, we also found baseline drift for some $PSiO_2$ oxidized at 800 ℃, and the amount of drift depended on the experiment.

Secondly, polydopamine molecule can be used to improve the interaction of bacteria and the PSi surface. The polydopamine was used by Couniot in his sensor so maybe they can also be used in PSi based sensor. On one hand, bacteria solution with lower concentration maybe detected with the help of polydopamine as there would be more bacteria adhering on the sensor surface at the same condition compared to this work; on other hand, the polymerization should occur at dark condition so this will increase the time and difficulty of experiment.

Thirdly, other PSi nanostructure instead of singer layer used in this structure can be fabricated and applied to bacteria detection. And PSi samples with higher current density above 200 mA/cm^2 can be studied.

In the present work, studies directed towards the fabrication of biosensor for bacteria detection was carried out on single layer of PSi and oxidation, which do not exhibit a very high stability. Therefore, similar nanostructure should be implemented on PSi film to enhance the stability. Surface modification such as polydopamine can also be used to expand the detection range of bacteria concentration.

References

[1] S. Dhanekar and S. Jain, "Porous silicon biosensor: current status," *Biosensors and Bioelectronics,* vol. 41, pp. 54-64, 2013.

[2] K. Fukami, F. A. Harraz, T. Yamauchi, T. Sakka, and Y. H. Ogata, "Fine-tuning in size and surface morphology of rod-shaped polypyrrole using porous silicon as template," *Electrochemistry Communications,* vol. 10, pp. 56-60, 2008.

[3] L. T. Canham, P. D. Calcott, A.G.Cullis, "The structural and luminescence properties of porous silicon," *Applied Physics Reviews,* vol. 82, pp. 909-965, 1997.

[4] A. Uhlir, "Electrolytic Shaping of Germanium and Silicon," *Bell System Technical Journal,* vol. 35, pp. 333-347, 1956.

[5] C. S. Fuller and J. A. Ditzenberger, "Diffusion of donor and acceptor elements in silicon," *Journal of Applied Physics,* vol. 27, pp. 544-553, 1956.

[6] Y. Watanabe, T. Sakai, "Application of a thick anode film to semiconductor devices," *Reviews of the Electrical Communications Laboratories,* vol. 19, pp. 899-903, 1971.

[7] Y. Watanabe, Y. Arita, T. Yokoyama, and Y. Igarashi, "Formation and properties of porous silicon and its application," *Journal of The Electrochemical Society,* vol. 122, pp. 1351-1355, 1975.

[8] L. T. Canham, "Silicon quantum wire array fabrication by electrochemical and chemical dissolution of wafers," *Applied Physics Letters,* vol. 57, pp. 1046-1048, 1990.

[9] V. Lehmann and U . Gösele, "Porous silicon formation: A quantum wire effect," *Applied Physics Letters,* vol. 58, pp. 856-858, 1991.

[10] L. Canham, "Silicon optoelectronics at the end of the rainbow?," *Physics World,* vol. 5, pp. 41-45, 1992.

[11] A. Halimaoui, C. Oules, G. Bomchil, A. Bsiesy, F. Gaspard, R. Herino*, et al.*, "Electroluminescence in the visible range during anodic oxidation of porous silicon films," *Applied Physics Letters,* vol. 59, p. 304, 1991.

[12] A. Richter, P. Steiner, F. Kozlowski, and W. Lang, "Current-induced light emission from a porous silicon device," *IEEE Electron Device Letters,* vol. 12, pp. 691-692, 1991.

[13] N. Koshida and H. Koyama, "Visible electroluminescence from porous silicon," *Applied Physics Letters,* vol. 60, p. 347, 1992.

[14] M. P. Stewart and J. M. Buriak, "Chemical and Biological Applications of Porous Silicon Technology," *Advanced Materials,* vol. 12, pp. 859-869, 2000.

[15] M. J. Sailor, *Porous Silicon in Practice: Preparation, Characterization and Applications*, Wiley-VCH Verlag GmbH& Co. KGaA, 2012.

[16] S. Dhanekar, S. S. Islam, T. Islam, and Harsh, "Photoluminescence Quenching Technique: A Sensitive Probe for Detecting Organic Vapors at Low Ppm," *International Journal of Nanoscience,* vol. 10, pp. 777-781, 2011.

[17] A. Janshoff, K.-P. S. Dancil, C. Steinem, D. P. Greiner, V. S. Y. Lin, C. Gurtner, K. Motesharei, M. J. Sailor and M. R. Ghadiri, "Macroporous p-Type silicon Fabry−Perot layers. Fabrication, characterization, and aplications in biosensing," *Journal of the American Chemical Society,* vol. 120, pp. 12108-12116, 1998.

[18] F. A. Harraz, "Porous silicon chemical sensors and biosensors: A review," *Sensors and Actuators B: Chemical,* vol. 202, pp. 897-912, 2014.

[19] F. A. Harraz, S. M. El-Sheikh, T. Sakka, and Y. H. Ogata, "Cylindrical pore arrays in silicon with intermediate nano-sizes: A template for nanofabrication and multilayer applications," *Electrochimica Acta,* vol. 53, pp. 6444-6451, 2008.

[20] M. S. Salem, M. J. Sailor, F. A. Harraz, T. Sakka, and Y. H. Ogata, "Electrochemical stabilization of porous silicon multilayers for sensing various chemical compounds," *Journal of Applied Physics,* vol. 100, p. 083520, 2006.

[21] C. Pacholski, M. Sartor, M. J. Sailor, F. Cunin, and G. M. Miskelly, "Biosensing using porous silicon double-layer interferometers: reflective interferometric Fourier transform spectroscopy," *J ournal of the American Chemical Society,* vol. 127, pp. 11636-11645, 2005.

[22] H. Ouyang, M. Christophersen, R. Viard, B. L. Miller, and P. M. Fauchet, "Macroporous Silicon Microcavities for Macromolecule Detection," *Advanced Functional Materials,* vol. 15, pp. 1851-1859, 2005.

[23] B. Cho, B.-Y. Lee, H.-C. Kim, H.-G. Woo, and H. Sohn, "Fabrication of human IgG sensors based on porous silicon interferometer containing bragg structures," *Journal of Nanoscience and Nanotechnology,* vol. 12, pp. 4159-4162, 2012.

[24] O. Bisi, S. Ossicini, and L. Pavesi, "Porous silicon: a quantum sponge structure for silicon based optoelectronics," *Surface Science Reports,* vol. 38, pp. 1-126, 2000.

[25] R. J. Martin-Palma, "Biomedical applications of nanostructured porous silicon: a review," *Journal of Nanophotonics,* vol. 4, p. 042502, 2010.

[26] J. M. Buriak and M. J. Allen, "Lewis Acid Mediated Functionalization of Porous Silicon with Substituted Alkenes and Alkynes," *Journal of the American Chemical Society,* vol. 120, pp. 1339-1340, 1998.

[27] J. R. Stetter, W. R. Penrose, and S. Yao, "Sensors, Chemical Sensors, Electrochemical Sensors, and ECS," *Journal of The Electrochemical Society,* vol. 150, pp. S11-S16, 2003.

[28] L. C. Clark and C. Lyons, "Electrode Systems for Continuous Monitoring in Cardiovascular Surgery," *Annals of the New York Academy of Sciences,* vol. 102, pp. 29-45, 1962.

[29] S. P. Mohanty and E. Kougianos, "Biosensors: a tutorial review," *IEEE Potentials,* vol. 25, pp. 35-40, 2006.

[30] S. P. J. Higson, S. M. Reddy, and P. M. Vadgama, "Enzyme and other biosensors: evolution of a technology," *Engineering Science & Education Journal,* vol. 3, pp. 41-48, 1994.

[31] D. M. Fraser, "Glucose biosensors: The sweet smell of success," *Medical Device Technology,* vol. 5, pp. 44-47, 1994.

[32] J. Stocker, D. Balluch, M. Gsell, H. Harms, J. Feliciano, S. Daunert*, K. A. Malik and J. R. van der Meer*, "Development of a set of simple bacterial biosensors for quantitative and rapid measurements of arsenite and arsenate in potable water," *Environmental Science & Technology,* vol. 37, pp. 4743-4750, 2003.

[33] D. R. Thévenot, K. Toth, R. A. Durst, and G. S. Wilson, "Electrochemical biosensors: recommended definitions and classification," *Biosensors and Bioelectronics,* vol. 16, pp. 121-131, 2001.

[34] S. Okumoto, A. Jones, and W. B. Frommer, "Quantitative imaging with fluorescent biosensors," *Annual Reviews of Plant Biology,* vol. 63, pp. 663-706, 2012.

[35] L. Moreno-Hagelsieb, Y. Nizet, X. Tang, J. P. Raskin, D. Flandre, and L. A. Francis, "CMOS compatible anodic Al_2O_3 based sensors for bacteria detection," *Procedia Chemistry,* vol. 1, pp. 1283-1286, 2009.

[36] O. Lazcka, F. J. Del Campo, and F. X. Munoz, "Pathogen detection: a perspective of traditional methods and biosensors," *Biosensors and Bioelectronics,* vol. 22, pp. 1205-1217, 2007.

[37] J. Tschmelak, G. Proll, and G. Gauglitz, "Sub-nanogram per litre detection of the emerging contaminant progesterone with a fully automated immunosensor based on evanescent field techniques," *Analytica Chimica Acta,* vol. 519, pp. 143-146, 2004.

[38] Y. M. Bae, B.-K. Oh, W. Lee, W. H. Lee, and J.-W. Choi, "Detection of insulin–antibody binding on a solid surface using imaging ellipsometry," *Biosensors and Bioelectronics,* vol. 20, pp. 895-902, 2004.

[39] A. J. Baeumner, R. N. Cohen, V. Miksic, and J. Min, "RNA biosensor for the rapid detection of viable Escherichia coli in drinking water," *Biosensors and Bioelectronics,* vol. 18, pp. 405-413, 2003.

[40] V. M. Starodub, L. L. Fedorenko, A. P. Sisetskiy, and N. F. Starodub, "Control of myoglobin level in a solution by an immune sensor based on the photoluminescence of porous silicon," *Sensors and Actuators B: Chemical,* vol. 58, pp. 409-414, 1999.

[41] A. Jane, R. Dronov, A. Hodges, and N. H. Voelcker, "Porous silicon biosensors on the advance," *Trends in Biotechnology,* vol. 27, pp. 230-239, 2009.

[42] V. S. Lin, "A porous silicon-based optical interferometric biosensor," *Science,* vol. 278, pp. 840-843, 1997.

[43] M. P. Schwartz, C. Yu, S. D. Alvarez, B. Migliori, D. Godin, L. Chao, M. J.Sailor, "Using an oxidized porous silicon interferometer for determination of relative protein binding affinity through non-covalent capture probe immobilization," *physica status solidi (a),* vol. 204, pp. 1444-1448, 2007.

[44] B. Cho, S. Kim, H.-G. Woo, S. Kim, and H. Sohn, "Detection of human IgG using photoluminescent porous silicon interferometer," *Journal of Nanoscience and Nanotechnology,* vol. 15, pp. 1083-1087, 2015.

[45] W. Kutner, J. Wang, M. L'Her, and R. P. Buck, "Analytical aspects of chemically modified electrodes: Classification, critical evaluation and recommendations (IUPAC Recommendations 1998)," *Pure and Applied Chemistry,* vol. 70, pp. 1301-1318, 1998.

[46] B. A. Durst RA, Murray RW, Buck RP, Andrieux CP, "Chemically modified electrodes: recommended terminology and definitions. ," *Pure and Applied Chemistry,* vol. 69, pp. 1317-1323, 1997.

[47] M. Archer, M. Christophersen, and P. M. Fauchet, "Macroporous silicon electrical sensor for DNA hybridization detection," *Biomedical Microdevices,* vol. 6, pp. 203-211, Sep 2004.

[48] G. Recio-Sánchez, V. Torres-Costa, M. Manso, D. Gallach, J. López-García, and R. J. Martín-Palma, "Towards the development of electrical biosensors based on nanostructured porous silicon," *Materials,* vol. 3, pp. 755-763, 2010.

[49] M. J. Song, D. H. Yun, N. K. Min, and S. I. Hong, "Electrochemical biosensor array for liver diagnosis using silanization technique on nanoporous silicon electrode," *Journal of Bioscience and Bioengineering,* vol. 103, pp. 32-37, Jan 2007.

[50] S. Setzu, S. Salis, V. Demontis, A. Salis, M. Monduzzi, and G. Mula, "Porous silicon-based potentiometric biosensor for triglycerides," *Physica Status Solidi (a),* vol. 204, pp. 1434-1438, 2007.

[51] D. C. Cullen, R. S. Sethi, and C. R. Lowe, "Multi-analyte miniature conductance biosensor," *Analytica Chimica Acta,* vol. 231, pp. 33-40, 1990.

[52] M. Archer and P. M. Fauchet, "Electrical sensing of DNA hybridization in porous silicon layers," *Physica Status Solidi (a),* vol. 198, pp. 503-507, 2003.

[53] J. T. Connelly and A. J. Baeumner, "Biosensors for the detection of waterborne pathogens," *Analytical and Bioanalytical Chemistry,* vol. 402, pp. 117-127, 2012.

[54] B. Byrne, E. Stack, N. Gilmartin, and R. O'Kennedy, "Antibody-based sensors: principles, problems and potential for detection of pathogens and associated toxins," *Sensors (Basel),* vol. 9, pp. 4407-4445, 2009.

[55] D. H. Gelfand, "Taq DNA Polymerase " in *PCR Technology Principles and Applications for DNA Amplification*, H. A. Erlich, Ed., ed UK: Palgrave Macmillan UK, 1989, pp. 17-22.

[56] P. M. Fratamico, "Comparison of culture, polymerase chain reaction (PCR), TaqMan Salmonella, and Transia Card Salmonella assays for detection of Salmonella spp. in naturally-contaminated ground chicken, ground turkey, and ground beef," *Molecular and Cellular Probes,* vol. 17, pp. 215-221, 2003.

[57] E. Segal and N.Massad-Ivanir, "Porous silicon for bacteria detection," in *Porous silicon for biomedical application*, ed Israel: woodhead publishing limited, 2014, pp. 286-303.

[58] A. Berrier, M. C. Schaafsma, G. Nonglaton, J. Bergquist, and J. G. Rivas, "Selective detection of bacterial layers with terahertz plasmonic antennas," *Biomedical Optics Express,* vol. 3, pp. 2937-2949, 2012.

[59] L. A. DeLouise, P. M. Kou, and B. L. Miller, "Cross-correlation of optical microcavity biosensor response with immobilized enzyme activity. Insights into biosensor sensitivity," *Analytical Chemistry,* vol. 77, pp. 3222-3230, 2005.

[60] D. Zhang and E. C. Alocilja, "Characterization of nanoporous silicon-based DNA biosensor for the detection of salmonella enteritidis," *IEEE Sensors Journal,* vol. 8, pp. 775-780, 2008.

[61] F. P. Mathew and E. C. Alocilja, "Porous silicon-based biosensor for pathogen detection," *Biosensors and Bioelectronics,* vol. 20, pp. 1656-1661, 2005.

[62] S. Li, J. Huang, and L. Cai, "A porous silicon optical microcavity for sensitive bacteria detection," *Nanotechnology,* vol. 22, p. 425502, 2011.

[63] S. Chan, S. R. Horner, P. M. Fauchet, and B. L. Miller, "Identification of gram negative bacteria using nanoscale silicon microcavities," *Journal of the American Chemical Society,* vol. 123, pp. 11797-11798, 2001.

[64] S. D. Alvarez, M. P. Schwartz, B. Migliori, C. U. Rang, L. Chao, and M. J. Sailor, "Using a porous silicon photonic crystal for bacterial cell-based biosensing," *Physica Status Solidi (a),* vol. 204, pp. 1439-1443, 2007.

[65] C.-C. Wu, S. D. Alvarez, C. U. Rang, L. Chao, and M. J. Sailor, "Label-free optical detection of bacteria on a 1-D photonic crystal of porous silicon," presented at the Proc. of SPIE Vol. 7167 United States, 2009.

[66] N. Massad-Ivanir, Y. Mirsky, A. Nahor, E. Edrei, L. M. Bonanno-Young, N. Ben Dov, A. Sa'ar and E. Segal, "Trap and track: designing self-reporting porous Si photonic crystals for rapid bacteria detection," *Analyst,* vol. 139, pp. 3885-3894, 2014.

[67] K. A. Kilian, T. Bocking, and J. J. Gooding, "The importance of surface chemistry in mesoporous materials: lessons from porous silicon biosensors," *Chemical Communications,* vol. 30, pp. 630-640, 2009.

[68] N. Massad-Ivanir, G. Shtenberg, A. Tzur, M. A. Krepker, and E. Segal, "Engineering nanostructured porous SiO_2 surfaces for bacteria detection via "direct cell capture"," *Analytical Chemistry,* vol. 83, pp. 3282-3289, 2011.

[69] N. Massad-Ivanir, G. Shtenberg, and E. Segal, "Advancing nanostructured porous si-based optical transducers for label free bacteria detection," *Adv Exp Med Biol,* vol. 733, pp. 37-45, 2012.

[70] G. Shtenberg, N. Massad-Ivanir, L. Fruk, and E. Segal, "Nanostructured porous Si optical biosensors: effect of thermal oxidation on their performance and properties," *ACS Appl Mater Interfaces,* vol. 6, pp. 16049-16055, Sep 24 2014.

[71] A. E. Pap, K. Kordás, T. F. George, and S. Leppävuori, "Thermal Oxidation of Porous Silicon: Study on Reaction Kinetics," *The Journal of Physical Chemistry B,* vol. 108, pp. 12744-12747, 2004.

[72] L. T. Canham, M. P. Stewart, J. M. Buriak, C. L. Reeves, M. Anderson, E. K. Squire*, et al.*, "Derivatized Porous Silicon Mirrors: Implantable Optical Components with Slow Resorbability," *physica status solidi (a),* vol. 182, pp. 521-525, 2000.

[73] E. J. Anglin, M. P. Schwartz, V. P. Ng, L. A. Perelman, and M. J. Sailor, "Engineering the chemistry and nanostructure of porous silicon Fabry-Perot films for loading and release of a steroid," *Langmuir,* vol. 20, pp. 11264-11269, Dec 7 2004.

[74] http://www.ammrf.org.au/myscope/sem/ practice /principles/layout.php, 2016-03-05

[75] M. H. Nada, "Scanning Electron Microscopy," *BAOJ Microbiology,* vol. 1, pp. 005：1-8, 2015.

[76] N. Couniot, T. Vanzieleghem, J. Rasson, N. Van Overstraeten-Schlogel, O. Poncelet, J. Mahillon, L. A. Francis, D. Flandre, "Lytic enzymes as selectivity means for label-free, microfluidic and impedimetric detection of whole-cell bacteria using ALD-Al_2O_3 passivated microelectrodes," *Biosensors and Bioelectronics*, vol. 67, pp. 154-161, 2015